
Data use policy

We request that the present study be specifically and clearly acknowledged when data sets or data samples are used for data analyses and visualizations in publications, posters, oral presentations, reports, Web pages, and any other types of scientific media. Please cite also the relevant original studies of each used specific data samples

1. Supplementary material summary

1.1. Information detailed in the description of the experimental data sets

To facilitate the use of the soft tissue artifact (STA) data sets provided in the supplementary material, the following information are summarized in paragraph 2 for each data set sample.

- a) *Data samples name and scientific article\s of reference;*
- a) *Subject or specimen characteristics* - available information aimed at describing subject characteristics (age, mass, height, body mass index, etc.);
- b) *Motor task description* - available information aimed at describing the motor task analyzed (e.g. type of motion, gait speed, range of joint motion, tread and rise when step or seat are used, type of footwear, etc.);
- c) *Experimental data description* - list of the body segments under analysis, skin marker locations, anatomical landmarks (ALs) used (their acronyms are listed in section 3.3, Table {anat_landmk}),
- d) *Anatomical coordinate system definitions (ACS)*
- e) *Measurement specifications* - description of the measurement systems and techniques used to process the position data (number of cameras, capture volume, sample frequency, measurement accuracy, etc.);
- f) *Ground truth* - description of the technique used to determine the ground truth bone pose (measurement accuracy, procedures for calibration, registration, and synchronization between instruments, etc.).
- g) *STA characterization* - for each marker, a statistical description of the relevant STA is provided according to the proposed metrics. The dispersion of each STA parameter over all

available markers is described using a five-number summary technique (minimum, lower quartile, median, upper quartile, and maximum).

A total of 31 data sets are described and made available in the supplementary material. When more than a motor task is obtained from the same experimental set-up, the relevant data sets are grouped in a single database and information relative to points *c*, *d*, and *e* are provided only once. If all data sets in a database are relative to the same specimen/subject, also point *a* is reported only once.

1.2. Data storing and exchange: the lexicon

A lexicon is described in paragraph 2 that was used as format for the benchmark data sets shared as supplementary material. It has its roots in a previous lexicon based on the syntactic lexicon, CAMARC DST (Data Storage and Transfer), first proposed for storing and data exchange between laboratories involved in the CAMARC II project (Paul and Morris, 1992; Cappozzo and Della Croce, 1994) and developed within the IST Project (IST-1999-10954), Virtual Animation of the Kinematics of the Human for Industrial, Educational and Research Purposes.

The lexicon was devised to store the data in a common data format, relative to position and orientation of upper or lower limb body segments while aiming at a complete description of the kinematics of a motor task. The lexicon is detailed in terms of:

- Data set storing description (Dataset name; Data information; Measurement Units).
- Subject description (Subject name; Subject information; Warning; Subject data).
- Legend tables (owner, motor task, footwear, pathology, side, segment, anatomical landmarks)

Data are stored at a pre-elaboration level, to acknowledge the fact that each laboratory used its own experimental protocol to acquire and process the data, described in the following section, and to allow different possible further processing procedures. This format was designed so that data could be exchanged and compared without forcing different laboratories to uniform all protocols and procedures for data processing. This choice does not preclude a user to obtain a final data representation according to his/her interests, without knowing the experimental set-up of the laboratory where data were acquired. A software that reads and processes data coming from different set-ups can be developed and used without any change. For some variables and parameters, to be included in the file, standard names were used (listed in *ad hoc* tables, reported at the end of this document). For further uses of this lexicon, these values can of course be modified or added, if required.

2. Description of the experimental data sets

2.1. Ex-vivo data from FOROIT

Scientific articles of reference - A detailed description of the original data set can be found in Cereatti et al. (2009), Camomilla et al. (2013) and Bonci et al. (2014).

Experimental data description - Twelve markers were glued on the thigh skin along two longitudinal lines in antero-lateral and antero-medial positions avoiding the quadriceps muscle bellies. (Fig. 1). The following ALs were calibrated using a pointer equipped with a cluster of four markers: ASIS, PSIS, LE and ME. The hip joint centre (HJC) was determined using a functional approach as described in Cereatti et al. (2009).

Anatomical coordinate system definitions - Both the pelvic and femoral ACSs were determined according to the definitions proposed in Cappozzo et al. (1995).

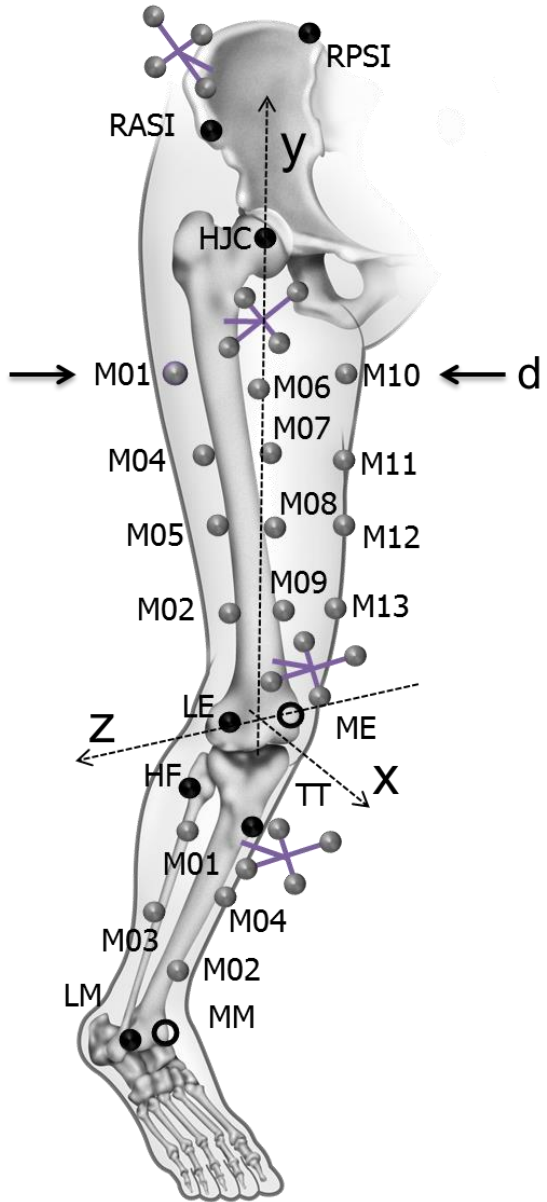


Figure 1 – Thigh markers were positioned along three longitudinal lines in antero-lateral (M01-M04), anterior (M06-M09), and antero-medial positions (M10-M013). Shank markers were positioned in frontal (M01, M03) and medial positions (M04, M02). The following ALs (dark circles) were calibrated using a pointer equipped with a cluster of four markers: RASIS, LASIS, RPSIS, LPSIS, LE, ME, HF, TT, LM, MM (see definitions in Table 3.3). d is the thigh diameter at the proximal level. The HJC was determined using a functional approach as described in Cereatti et al. (2009) and the pin markers.

Measurement specifications - The instantaneous markers position was reconstructed using a 9-camera stereophotogrammetric system (VICON MX) acquiring at 120 sample/s. The measurement volume was a 1.5-m-sided cube. A spot-check was performed to assess the accuracy of the stereophotogrammetric system according to Della Croce and Cappozzo

(2000). The marker cluster coordinate system poses relative to the global system of reference were estimated using a SVD technique (Soderkvist and Wedin, 1993).

Ground truth - Two pins equipped with a four marker cluster were implanted into the femur and two into the pelvis. Cruciform incisions were made through the skin and soft issue to reduce forces applied to the pins. Relative angular and linear displacements between pin clusters inserted in the same bone exhibited root mean square values lower than 0.31 deg and 0.1mm, respectively.

2.1.1. Data sample 1: Hip joint centre functional movement (Star-Arc)

Specimen characteristics - A whole body 75 y.o. adult female cadaver. The diameters of the proximal and distal sections of the thigh were 190 mm and 123 mm, respectively.

Motor task description - While the cadaver was lying supine on a table, an operator rotated the right femur with respect to the pelvis. The movements consisted of rotations in the sagittal plane, and in three planes externally rotated about the crano-caudal axis by about 20 deg. This was followed by a half circumduction.

STA characteristics - Skin-marker trajectories in the thigh ACS are depicted in Fig. 2. Trajectories were filtered with a 2nd-order lowpass Butterworth filter with a cutoff frequency of 10 Hz. Statistical data describing the relevant STAs are shown in Fig. 3. Magnitude of the instantaneous displacement of thigh skin-markers along with the hip joint angular kinematics are depicted in Fig. 4.

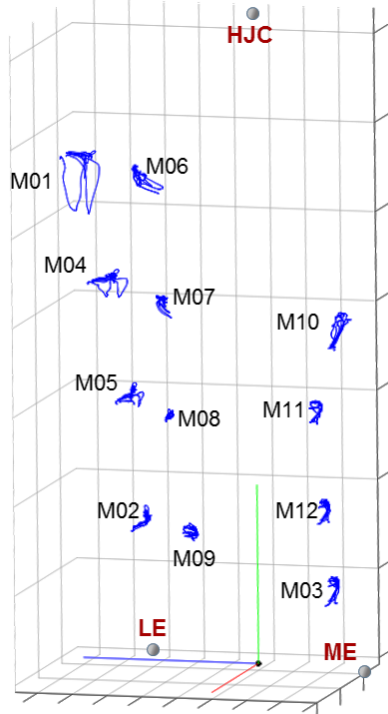


Figure 2 – HIP JOINT CENTRE FUNCTIONAL MOVEMENT Femur ACS, relevant ALs, and skin-marker trajectories (represented in blue). The axes of the ACS are represented in red, green, and blue

for the x (antero/posterior, div = 50 mm), y (superior/inferior, div = 50 mm), and z (right/left, div = 20 mm) directions, respectively.

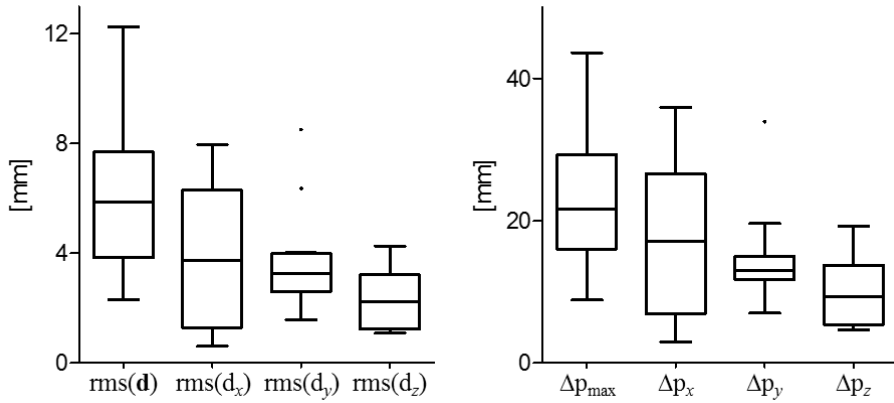


Figure 3 – HIP JOINT CENTRE FUNCTIONAL MOVEMENT Box-plots of the eight parameters ($\text{rms}(\mathbf{d})$, $\text{rms}(\mathbf{d}_x)$, $\text{rms}(\mathbf{d}_y)$, and $\text{rms}(\mathbf{d}_z)$, in the left panel; Δp_{\max} , Δp_x , Δp_y , and Δp_z , in the right panel) that describe the STA affecting the twelve skin-markers on the thigh during the movement. Outliers are also depicted.

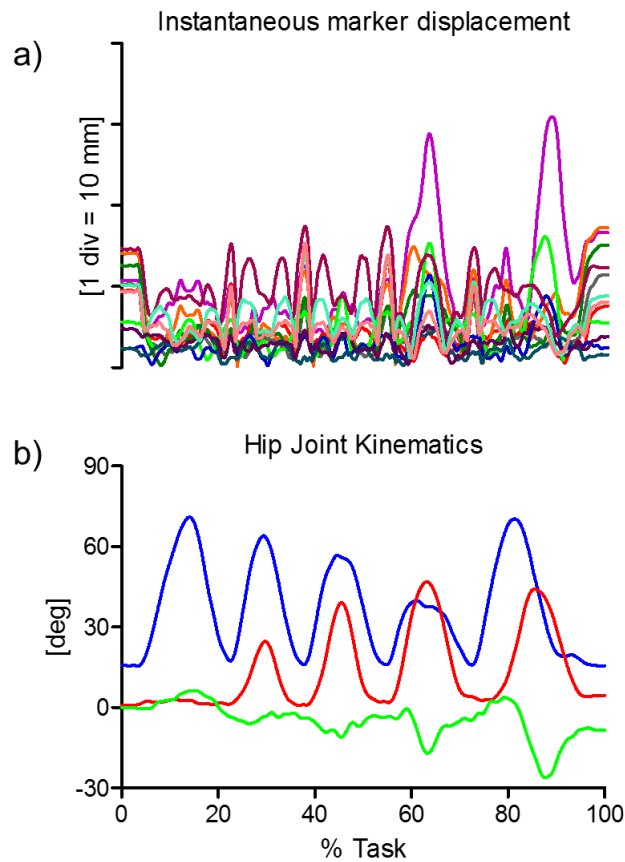


Figure 4 – HIP JOINT CENTRE FUNCTIONAL MOVEMENT a) Magnitude of the instantaneous displacement of the twelve skin-markers glued on the thigh and represented in the femur ACS. b) Relevant hip joint kinematics computed according to the convention proposed by Grood and Suntay (1983) (flexion/extension, ab/adduction and internal/external rotation in blue, red and green, respectively; flexion, abduction and internal rotation are positive).

2.1.2. Data sample 3: Hip and knee flexion/extension

Specimen characteristics - A whole body 80 y.o. adult male cadaver. The diameters of the proximal and distal sections of the thigh were 161 mm and 105 mm, respectively.

Motor task description - While the cadaver was lying supine on a table, an operator moved the foot with respect to the pelvis, making the hip and knee to flex and the extend back.

STA characteristics - Skin-marker trajectories in the thigh and shank ACSs are depicted in Fig. 5. Trajectories were filtered with a 2nd-order lowpass Butterworth filter with a cutoff frequency of 10 Hz. Statistical data describing the relevant STAs are shown in Fig. 6. Magnitude of the instantaneous displacement of thigh and shank skin-markers along with the hip and knee joint angular kinematics are depicted in Fig. 7.

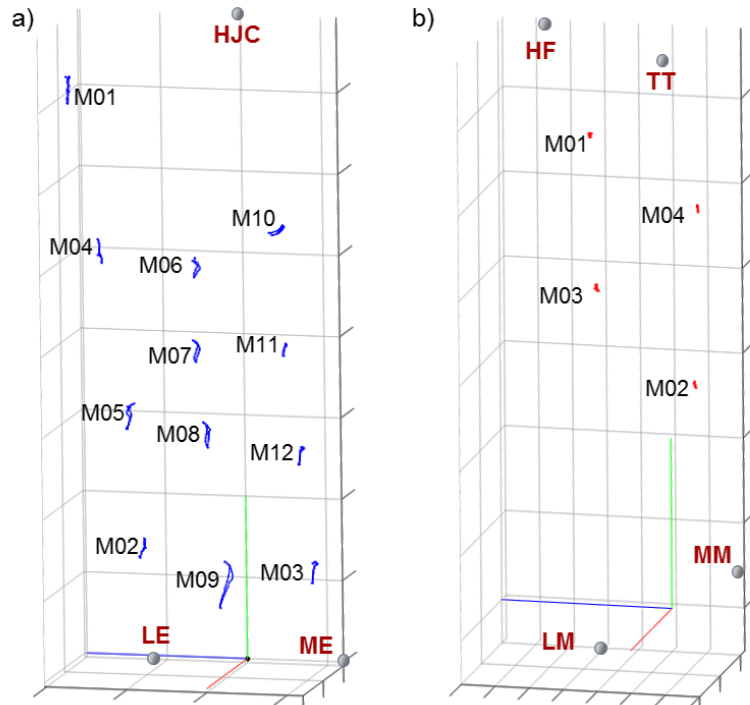


Figure 5 – HIP AND KNEE FLEXION/EXTENSION Femur (a) and tibial (b) ACSs, relevant ALs, and thigh and shank skin-marker trajectories (represented in blue and red, respectively). The axes of the ACSs are represented in red, green, and blue for the x (antero/posterior, div = 50 mm), y (superior/inferior, div = 50 mm), and z (right/left, a) div = 50 mm; b) div = 20 mm) directions, respectively.

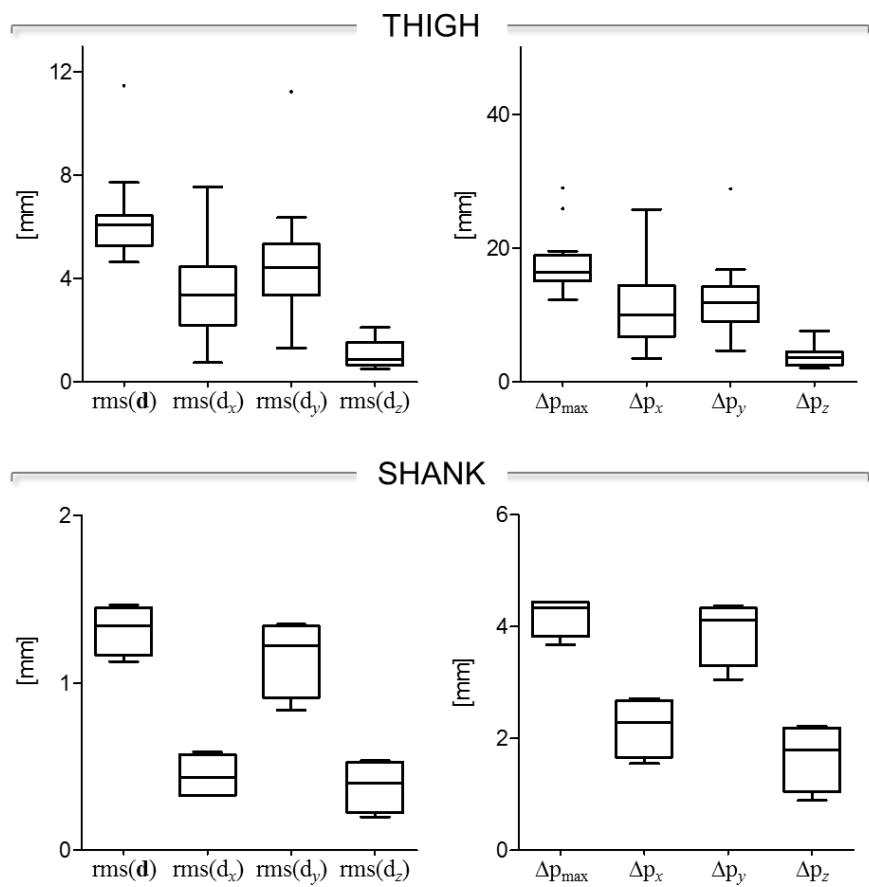


Figure 6 – HIP AND KNEE FLEXION/EXTENSION Box-plots of the eight parameters ($\text{rms}(\mathbf{d})$, $\text{rms}(\mathbf{d}_x)$, $\text{rms}(\mathbf{d}_y)$, and $\text{rms}(\mathbf{d}_z)$, in the left panel; Δp_{max} , Δp_x , Δp_y , and Δp_z , in the right panel) that describe the STA affecting the twelve and four skin-markers on the thigh and the shank, respectively, during the movement. Outliers are also depicted.

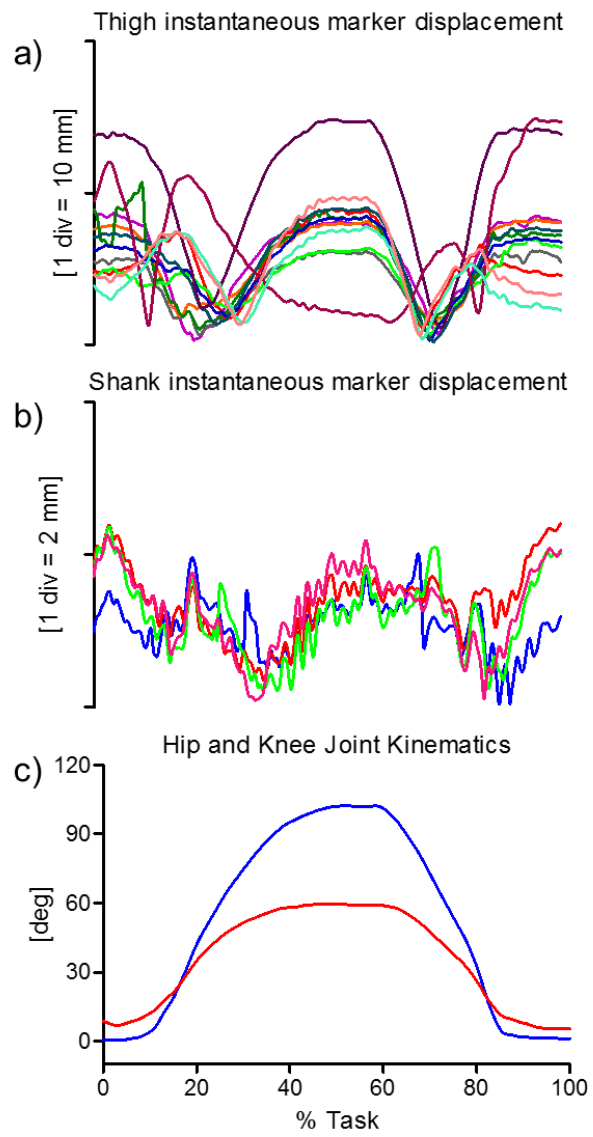


Figure 7 – HIP AND KNEE FLEXION/EXTENSION Magnitude of the instantaneous displacement of the twelve and four skin-markers glued on the thigh (a) and shank (b) represented in the relevant ACS. c) Relevant hip and knee joint kinematics computed according to the convention proposed by Grood and Suntay (1983) (hip and knee flexion/extension in red and blue, respectively; flexion is positive).

2.2. *In-vivo data from LMAM*

Scientific articles of reference - A detailed description of the original data set can be found in Barré et al. (2013) and Barré et al. (2015).

Experimental data description - 80 markers were attached to thigh and shank, with at least 35 markers for each body segment. The reciprocal distance between markers (diameter = 4 mm) varied between 25–40 mm (Fig. 8).

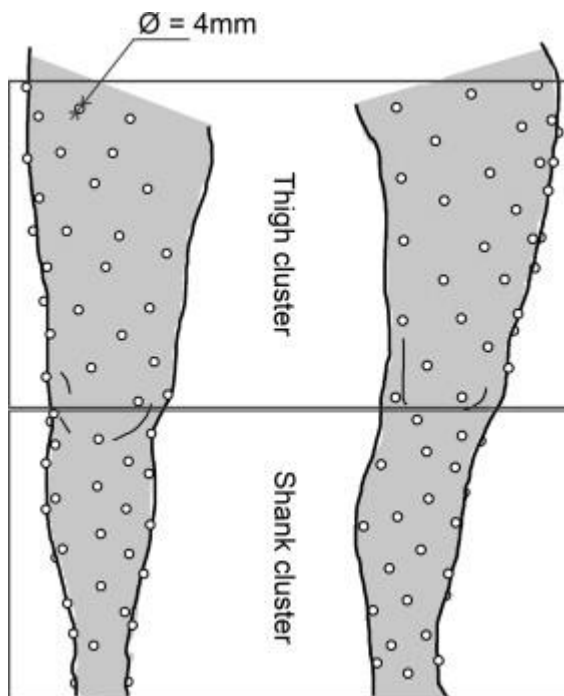


Figure 8 – Frontal (left) and sagittal (right) representation of the marker distribution for one specific subject. Some shank markers were also apposed on the medial part.

Anatomical coordinate system definitions - ACSs were defined using the prosthesis coordinate systems of the femoral and tibial components: the horizontal lateral axis of the femoral component, the vertical axis of the tibial component, designed to support the polyethylene rotating platform (Barré et al., 2013).

Measurement specifications - The instantaneous markers position was reconstructed using a 7-camera stereophotogrammetric system (VICON MX3+) acquiring at 240 sample/s. The measurement volume was a 2-m-sided cube. A spot-check was performed to assess the accuracy of the stereophotogrammetric system according to Della Croce and Cappozzo, 2000.

Ground truth - Two fluoroscopes (BV Pulsera 300, Philips, NL) were configured to acquire X-ray images at a maximal frame rate of 30 sample/s. To correct for distortions in the X-ray images, a calibration was performed using a calibration plate. Synchronization between fluoroscopes and stereo-photogrammetric systems was performed a posteriori using an

additional X-ray detector providing a synchronous signal (delay of less than 0.4 ms between samples for both systems). To compute the transformation between both systems, calibration was performed with three reflective markers attached to a box located at the centre of the system and visible by each system using a least squares method. Applied on the dataset of this study, the average residual for this method is less than 0.08 mm with a SD below 0.03 mm.

2.2.1. Data sample 8: Treadmill waking

Subject characteristics - A 75 y.o. male subject with a total knee prosthesis. Height = 1.67 m, mass = 65 kg.

Motor task description - Static acquisition in the upright position was followed by a treadmill gait acquisition at a self-defined comfortable speed (5.8 m/s) over 15 seconds.

STA characteristics - Skin-marker trajectories in the thigh and shank ACSs are depicted in Fig. 9. A recursive digital filter was used which corresponded to a low-pass filter with a cutoff frequency of 9Hz. Statistical data describing the relevant STAs are shown in Fig. 10. Magnitude of the instantaneous displacement of thigh and shank skin-markers along with the knee joint angular kinematics are depicted in Fig. 11.

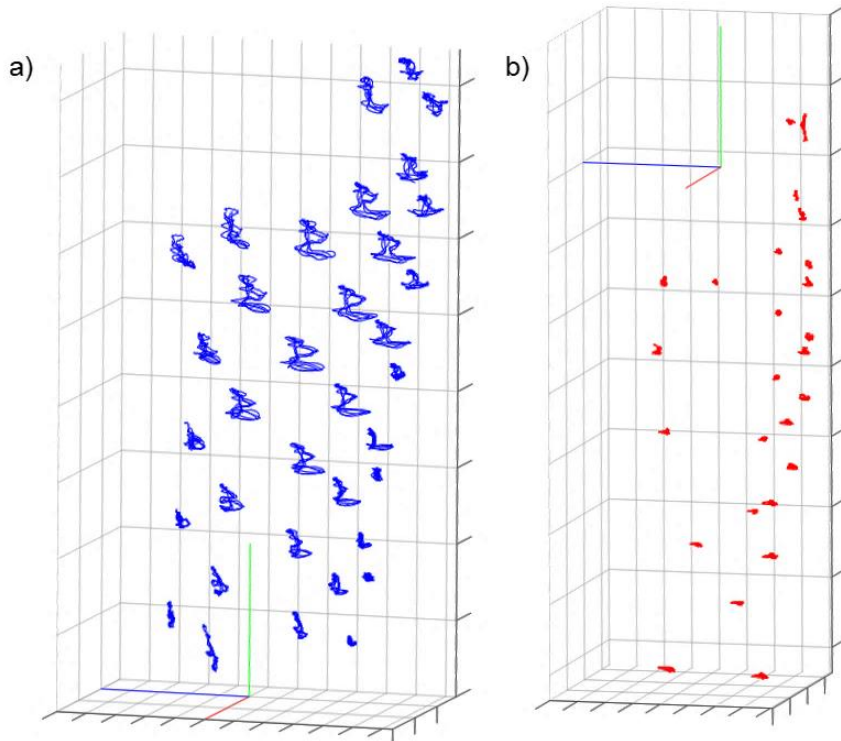


Figure 9 – TREADMILL WAKING Femur (a) and tibial (b) ACSs, and thigh and shank skin-marker trajectories (represented in blue and red, respectively). The axes of the ACSs are represented in red, green, and blue for the x (antero/posterior, div = 50 mm), y (superior/inferior, div = 50 mm), and z (right/left, div = 20 mm) directions, respectively.

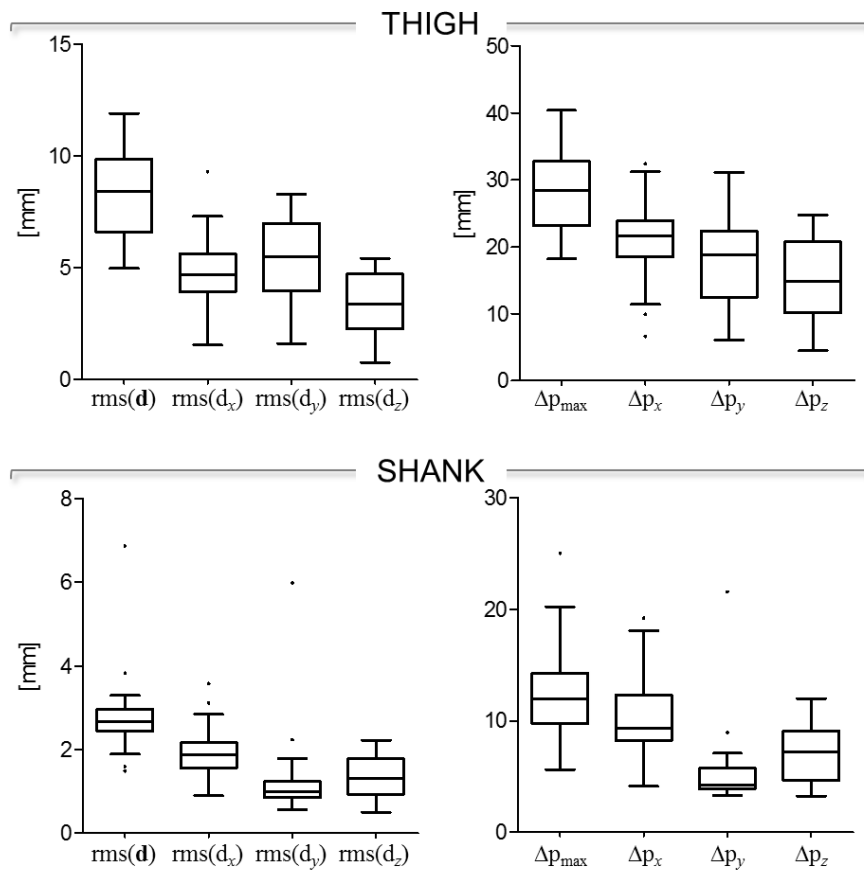


Figure 10 – TREADMILL WAKING Box-plots of the eight parameters ($\text{rms}(\mathbf{d})$, $\text{rms}(\mathbf{d}_x)$, $\text{rms}(\mathbf{d}_y)$, and $\text{rms}(\mathbf{d}_z)$, in the left panel; Δp_{\max} , Δp_x , Δp_y , and Δp_z , in the right panel) that describe the STA affecting the thirty-five and twenty-six skin-markers on the thigh and the shank, respectively, during the movement. Outliers are also depicted.

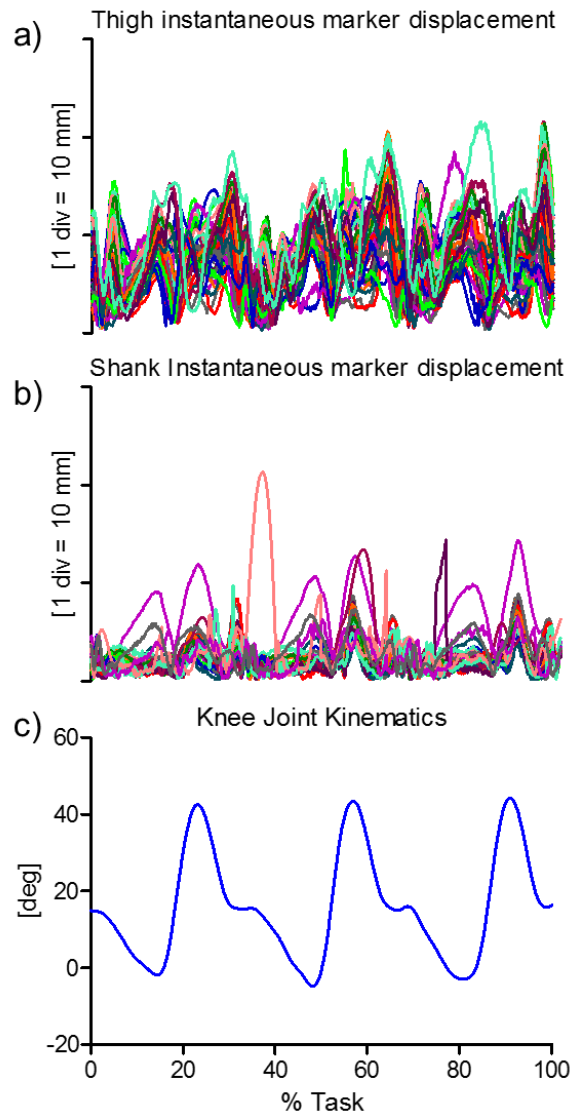


Figure 11 – TREADMILL WAKING Magnitude of the instantaneous displacement of the thirty-five and twenty-six skin-markers glued on the thigh (a) and shank (b) represented in the relevant ACS. c) Relevant knee joint kinematics computed according to the convention proposed by Grood and Suntay (1983) (flexion/extension in blue, with flexion as positive).

2.3. In-vivo data from UNIBO

Scientific articles of reference - A detailed description of the original data set can be found in Stagni et al. (2005).

Experimental data description - A cluster of reflecting skin markers was attached to the lateral aspect of thigh and shank (19 and 10, respectively). The clusters were 4–5 cm spaced grids of markers with a diameter of 0.6 cm. One rigid plate with four markers was attached to the pelvis using a modified Milwaukee orthosis (Fig. 12). A static up-right posture was acquired. The position of 10 anatomical landmarks (right and left anterior iliac spines, sacrum, greater trochanter, lateral and medial epicondyles, tibial tuberosity, head of fibula, lateral and medial malleoli) was calibrated with respect to the relevant cluster of markers. Two repetitions were collected for each of the listed motor tasks.

Anatomical coordinate system definitions – ACSs were defined according to the CAST protocol (Benedetti et al., 1998).

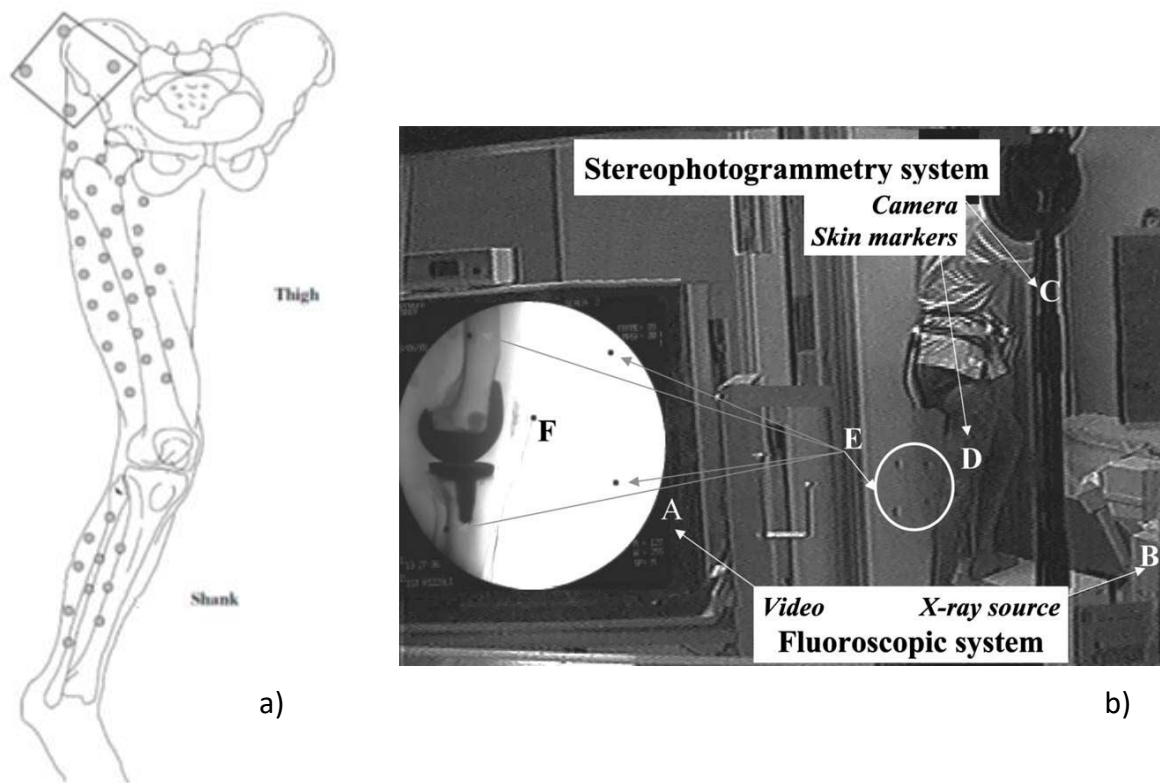


Figure 12 a) skin marker distribution on thigh and shank, marker numbers are reported in Figure 13; b) Experimental set-up: A. real-time visible feed-back of the fluoroscopic images acquired. B. X-rays sourced of the fluoroscope. C. one of the five cameras of the stereophotogrammetric system. D. skin markers on the lateral aspect of the thigh and shank. E. the four specialized radiopaque/reflecting markers for spatial registration. F. the four specialized radiopaque/reflecting marker for temporal registration

Measurement specifications - The marker trajectories were collected at 50 frames per second by means of a stereophotogrammetric system with 5 TV cameras (Smart, e-Motion, Padova, Italy). The stereophotogrammetric calibrated field of view was 1.5 x 1.5 x 1 m.

Ground truth - The subjects performed each motor task with the knee under analysis inside the fluoroscopic 32 cm field of view. Five additional specialized reflecting and radiopaque markers, visible to stereophotogrammetric and fluoroscopic systems, with a diameter of 1.2 cm were used. Four of these were placed on a plane parallel to the image plane of the fluoroscope for spatial registration of the two measurement systems. The fifth was attached to the skin over the patella for temporal synchronization. The 3D pose (position and orientation) of the prosthesis components was reconstructed by means of the 2D fluoroscopic projections and CAD models of the prosthesis components. Series of images were acquired at nominal 6 samples per second with a standard fluoroscope (DRS, System 1694 D, General Electric CGR, Issy-les-Moulineaux, France). The images were printed out on films and digitised by means of a scanner (Scanmaster DX, Howtek, Hudson, NH, USA). Moreover, images of a 3D cage of plexiglas with 18 tantalum balls in known positions and of a rectangular grid of lead balls 10 mm apart were collected in order to calculate respectively the position of the camera focus and the parameters necessary for image distortion correction. This was obtained using a global spatial warping technique (Gronenschild, 1997). An established technique for 3D kinematics analysis of a known object from a single view was implemented (Banks and Hodge, 1996). Prosthesis component poses in space were obtained from each fluoroscopic image by an iterative procedure using a technique based on CAD-model shape matching. To test for the process accuracy, the femoral and tibial components of the same prosthesis implanted in the subjects of the present study (Optetrak PS-cemented, Exactech Inc., Gainesville, FL, USA) were fixed in an unknown relative pose using bone-cement. Fluoroscopic images were taken in five different positions within the field of view. The relative pose of the two components in each image was estimated using the method described. These estimates were compared with the ones obtained by a 3D digitizer (MicroScribe, Immersion, San Jose, CA, USA), with nominal accuracy of 0.2 mm. The femoral component was held fixed to a workbench and the coordinates of about 38000 and 23000 points were collected on both the femoral and tibial component surfaces, respectively. The Iterative Closest Point technique (Besl and McKay, 1992) was used for surface rigid registration between the points digitized and the relevant prosthesis component CAD model. Then, the relative pose between the two registered CAD models was calculated. The results showed that the accuracy with which relative orientation and position of the components can be estimated

is better than 1.5 and 1.5 mm respectively, as good as those previously obtained (Banks and Hodge, 1996). Spatial registration between the stereophotogrammetric and fluoroscopic measurement systems was obtained by defining a common absolute reference coordinate system by means of the four radiopaque and reflecting markers. The temporal synchronization was obtained by matching the fluoroscopic trajectories with the resampled stereophotogrammetric ones of the fifth specialized marker. The matching was obtained by calculating the maximum cross-correlation between the two trajectories, considering the resampling frequency and the starting frame as the parameters to be determined. The possible misalignment of the prosthesis components with respect to the relevant anatomical coordinate system was calculated in the static up-right posture, considered as reference position. This misalignment, if present, is due to surgery. The fluoroscopy-based 3D pose of the anatomical coordinate system was calculated accordingly.

2.3.1. Data samples 6,14,17: knee extension against gravity, sit-to-stand/stand-to-sit, step up/down

Subject characteristics - A 67 y.o. female subject with total knee replacement. Height = 1.55 m, mass = 58 kg.

Motor task description - Knee extension against gravity performed in up-right posture with the hip held flexed at approximately 45 deg, sit-to-stand/stand-to-sit, step up/down.

STA characteristics - Skin-marker trajectories in the thigh and shank ACSs are depicted in Figs. 13, 16, 19, for knee extension against gravity, sit-to-stand/stand-to-sit and, step up/down, respectively. Stereophotogrammetric data were acquired at 50 Hz and fluoroscopic data at 6Hz, thus synchronized data were all down-sampled at 6 Hz. Statistical data describing the relevant STAs are shown in Figs. 14, 17, 20, for knee extension against gravity, sit-to-stand/stand-to-sit and, step up/down, respectively. For each motor task, the magnitude of the instantaneous displacement of thigh and shank skin-markers along with the knee joint angular kinematics are depicted in Figs. 15, 18, 21, for knee extension against gravity, sit-to-stand/stand-to-sit and, step up/down, respectively.

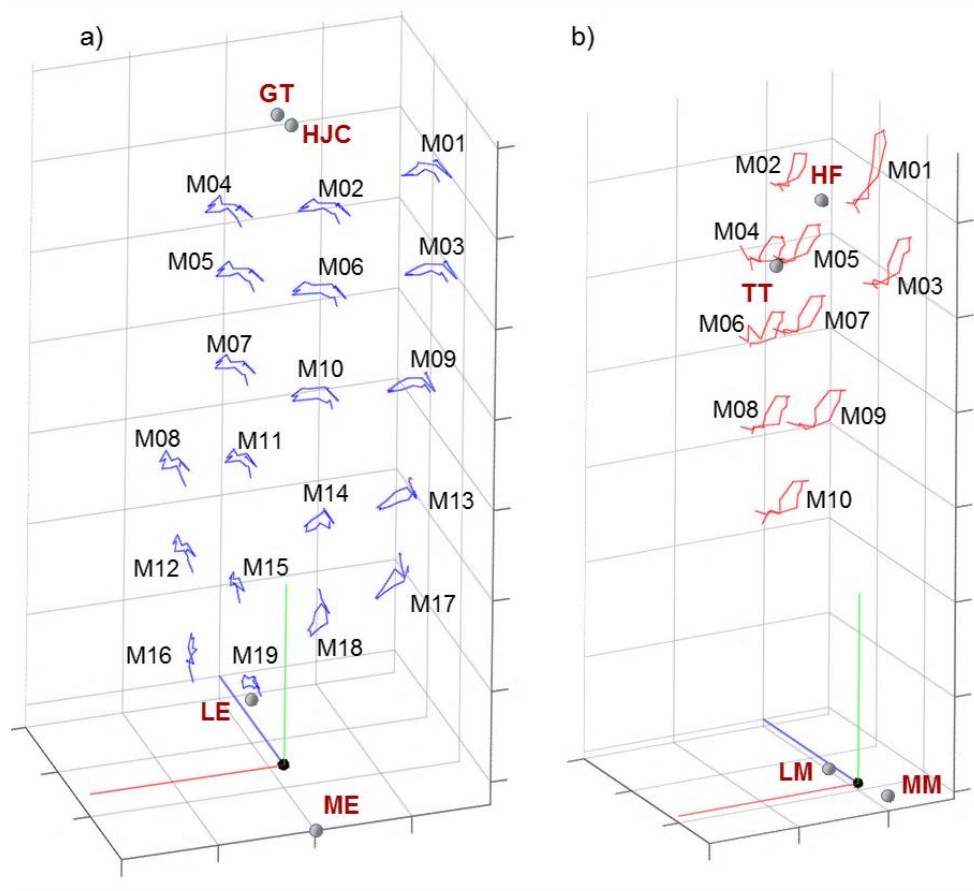


Figure 13 – KNEE EXTENSION AGAINST GRAVITY. Femur (a) and tibial (b) ACSs, relevant ALs, and thigh and shank skin-marker trajectories (represented in blue and red, respectively). The axes of the ACSs are represented in red, green, and blue for the x (antero/posterior, div = 50 mm), y (superior/inferior, div = 50 mm), and z (right/left, div = 50 mm) directions, respectively.

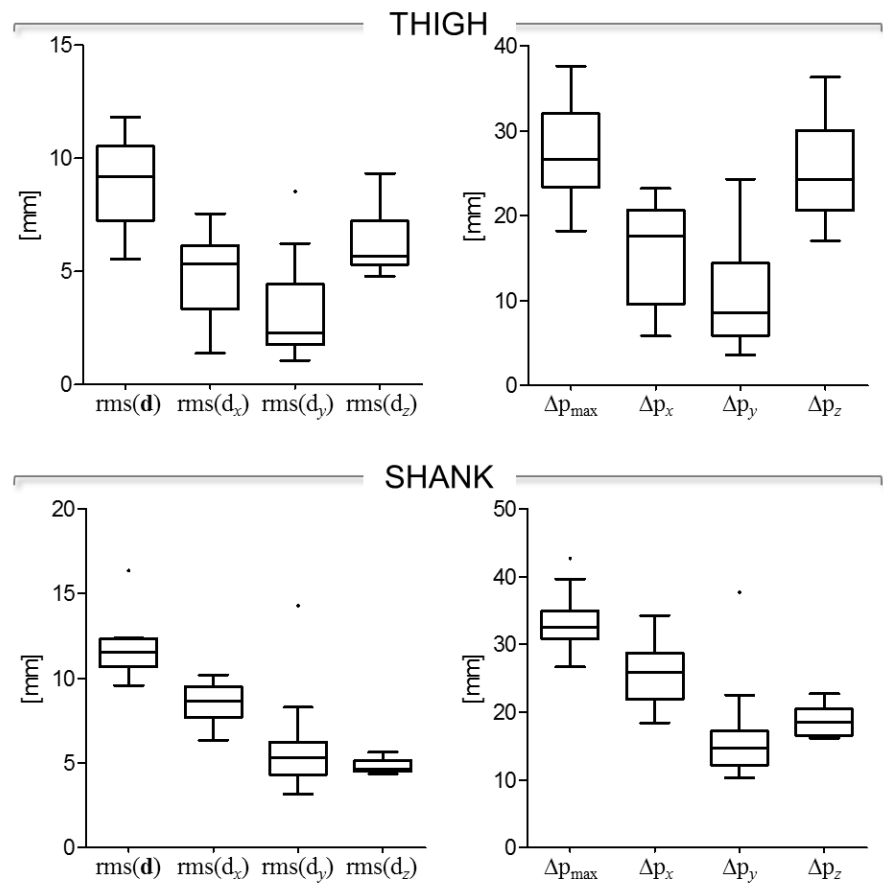


Figure 14 – KNEE EXTENSION AGAINST GRAVITY. Box-plots of the eight parameters ($\text{rms}(\mathbf{d})$, $\text{rms}(\mathbf{d}_x)$, $\text{rms}(\mathbf{d}_y)$, and $\text{rms}(\mathbf{d}_z)$, in the left panel; Δp_{\max} , Δp_x , Δp_y , and Δp_z , in the right panel) that describe the STA affecting the nineteen and ten skin-markers on the thigh and the shank, respectively, during the movement. Outliers are also depicted.

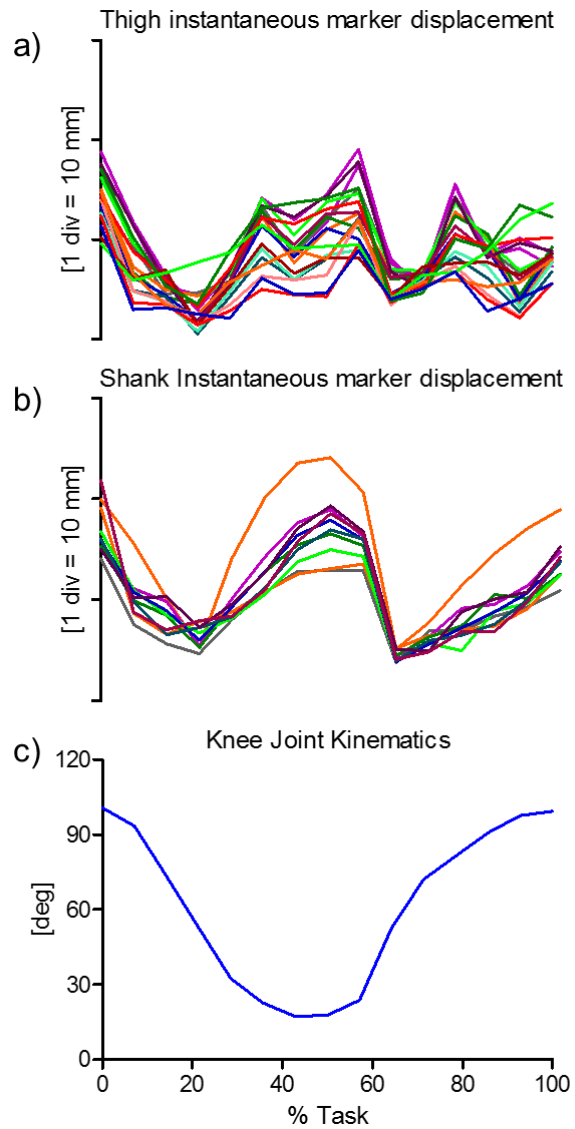


Figure 15 – KNEE EXTENSION AGAINST GRAVITY. Magnitude of the instantaneous displacement of the nineteen and ten skin-markers glued on the thigh (a) and shank (b) represented in the relevant ACS. c) Relevant knee joint kinematics computed according to the convention proposed by Grood and Suntay (1983) (flexion/extension in blue, with flexion as positive).

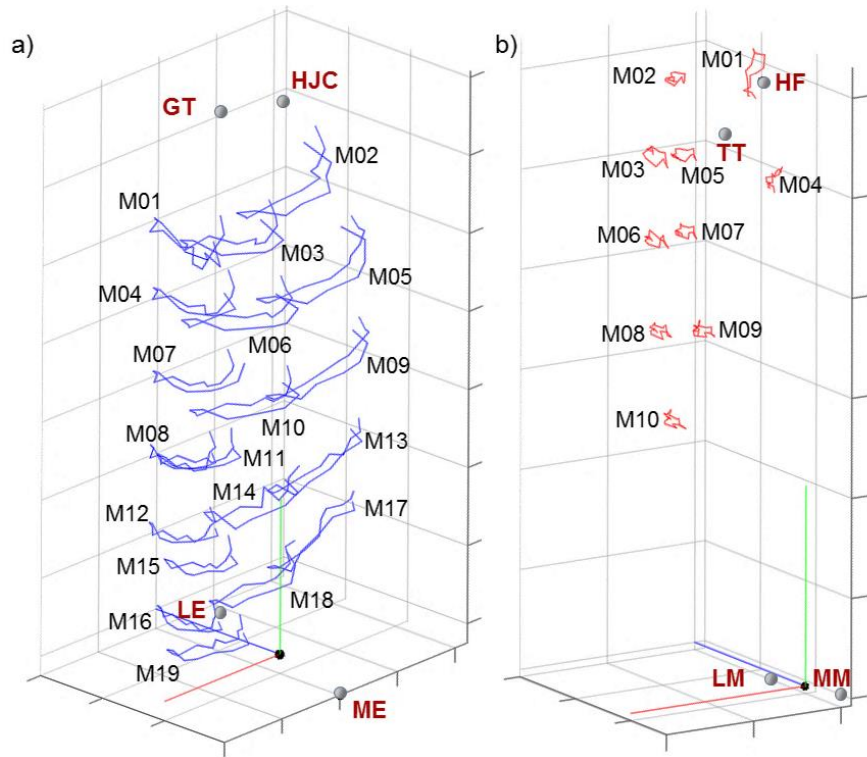


Figure 16 – SIT-TO-STAND/STAND-TO-SIT. Femur (a) and tibial (b) ACSs, relevant ALs, and thigh and shank skin-marker trajectories (represented in blue and red, respectively). The axes of the ACSs are represented in red, green, and blue for the x (antero/posterior, div = 50 mm), y (superior/inferior, div = 50 mm), and z (right/left, div = 50 mm) directions, respectively.

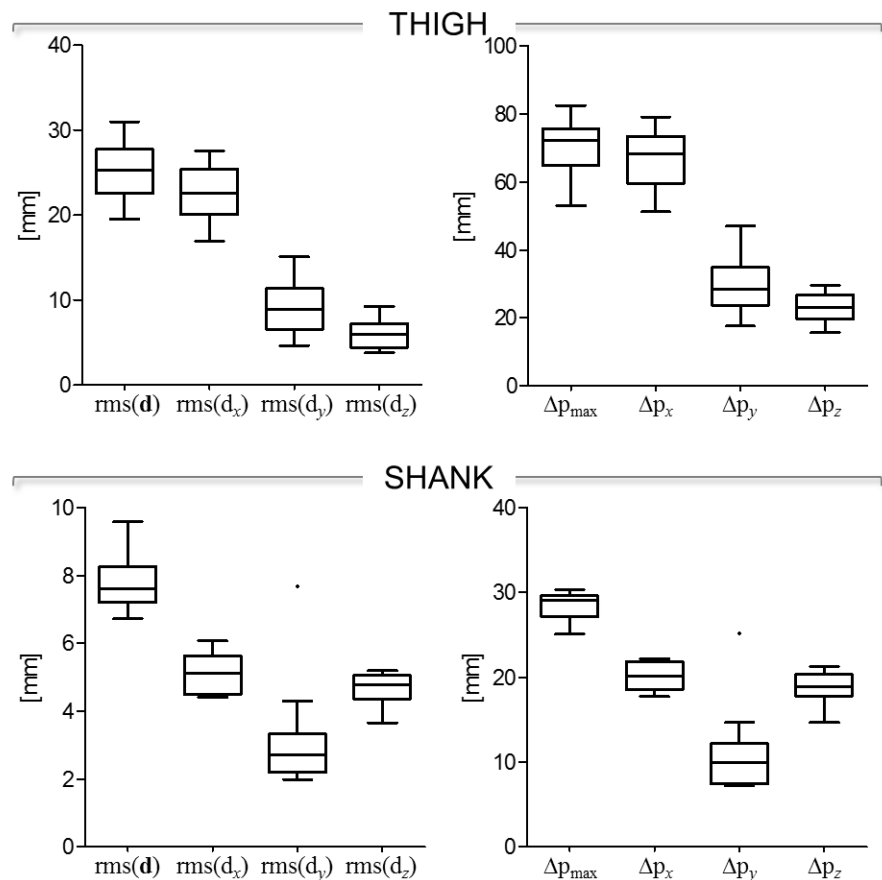


Figure 17 – SIT-TO-STAND/STAND-TO-SIT. Box-plots of the eight parameters ($\text{rms}(\mathbf{d})$, $\text{rms}(\mathbf{d}_x)$, $\text{rms}(\mathbf{d}_y)$, and $\text{rms}(\mathbf{d}_z)$, in the left panel; Δp_{\max} , Δp_x , Δp_y , and Δp_z , in the right panel) that describe the STA affecting the nineteen and ten skin-markers on the thigh and the shank, respectively, during the movement. Outliers are also depicted.

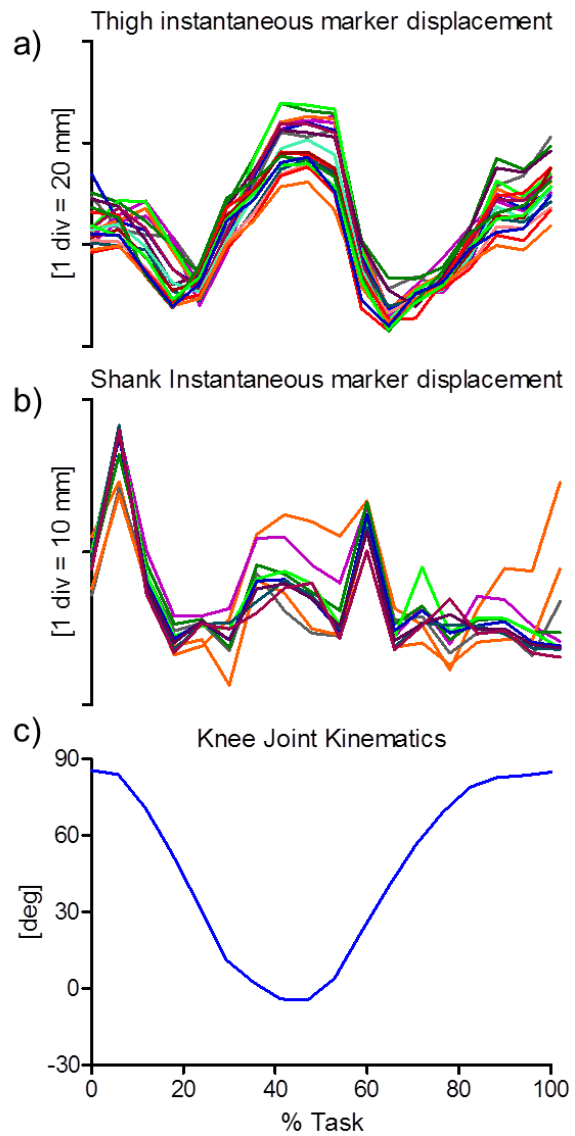


Figure 18 – SIT-TO-STAND/STAND-TO-SIT. Magnitude of the instantaneous displacement of the nineteen and ten skin-markers glued on the thigh (a) and shank (b) represented in the relevant ACS. c) Relevant knee joint kinematics computed according to the convention proposed by Grood and Suntay (1983) (flexion/extension in blue, with flexion as positive).

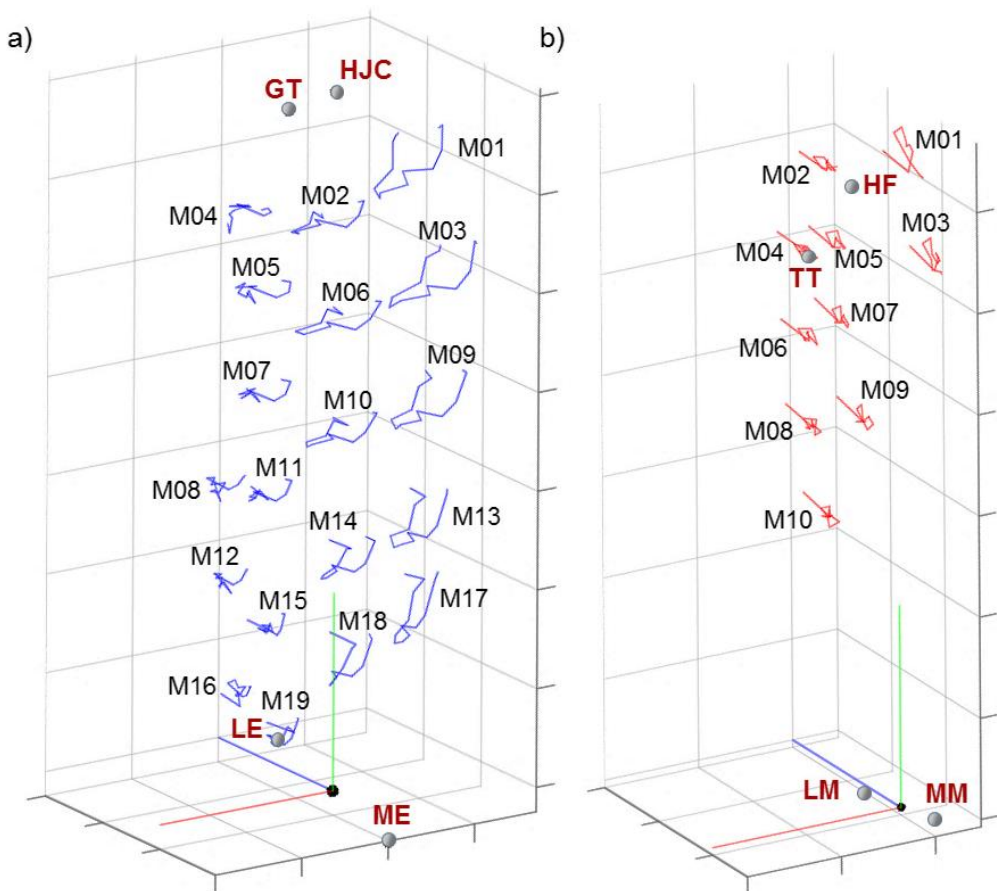


Figure 19 – STEP UP/DOWN. Femur (a) and tibial (b) ACSs, relevant ALs, and thigh and shank skin-marker trajectories (represented in blue and red, respectively). The axes of the ACSs are represented in red, green, and blue for the x (antero/posterior, div = 50 mm), y (superior/inferior, div = 50 mm), and z (right/left, div = 50 mm) directions, respectively.

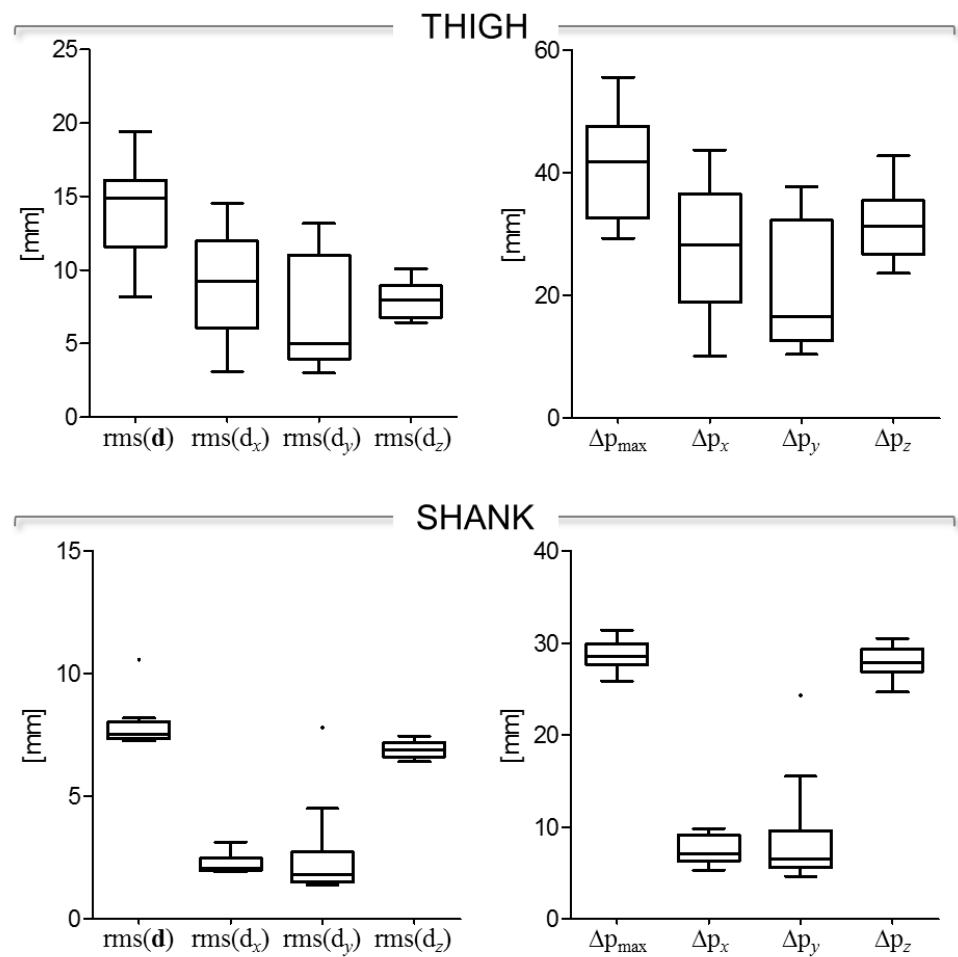


Figure 20 – STEP UP/DOWN. Box-plots of the eight parameters ($\text{rms}(\mathbf{d})$, $\text{rms}(\mathbf{d}_x)$, $\text{rms}(\mathbf{d}_y)$, and $\text{rms}(\mathbf{d}_z)$, in the left panel; Δp_{\max} , Δp_x , Δp_y , and Δp_z , in the right panel) that describe the STA affecting the nineteen and ten skin-markers on the thigh and the shank, respectively, during the movement. Outliers are also depicted.

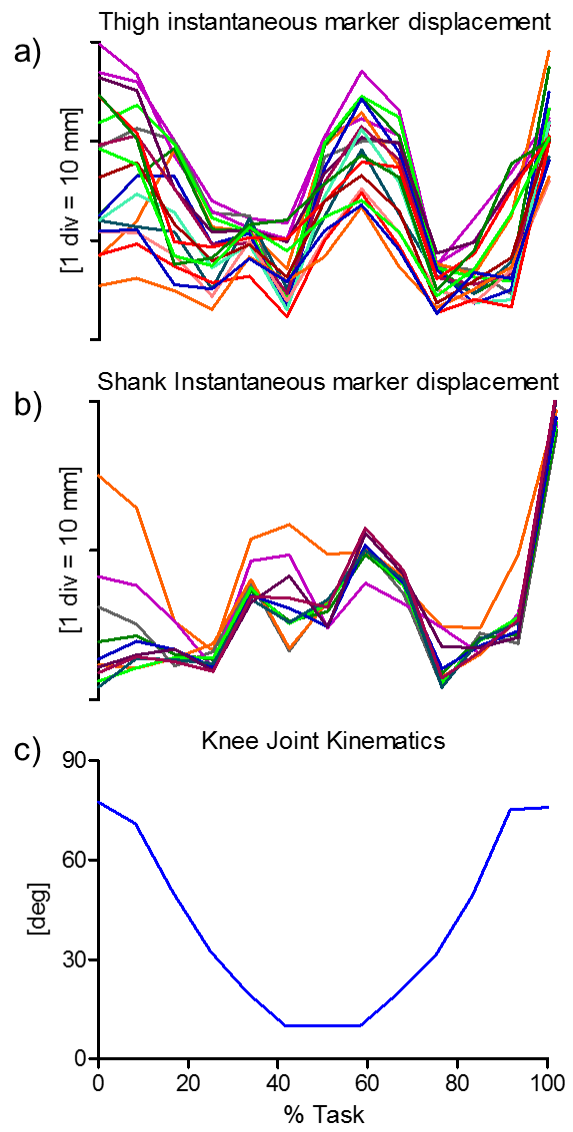


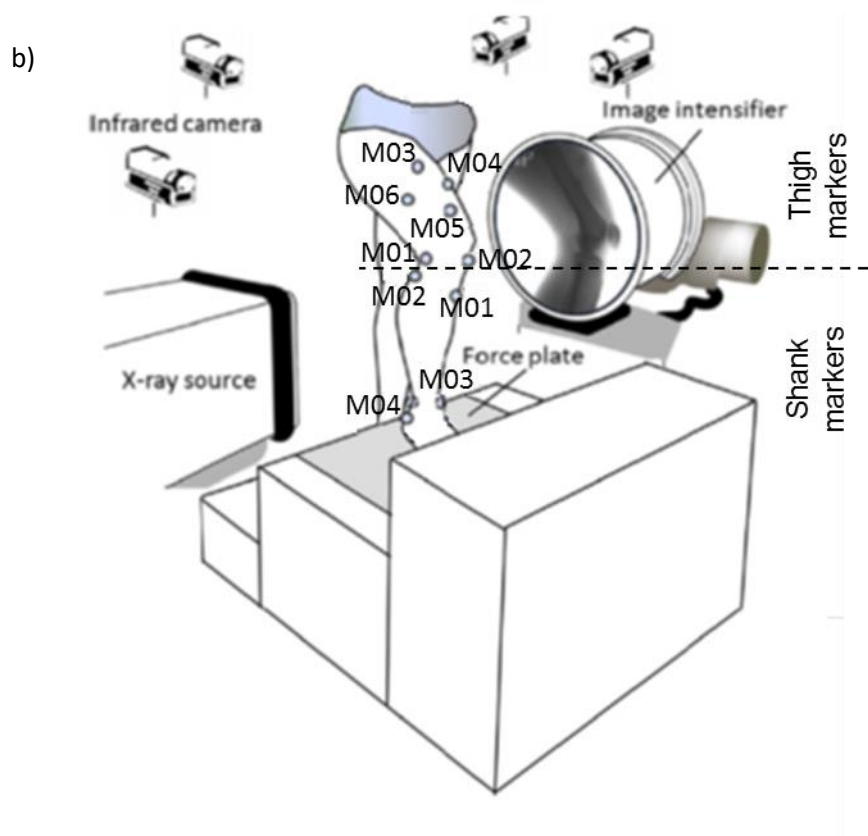
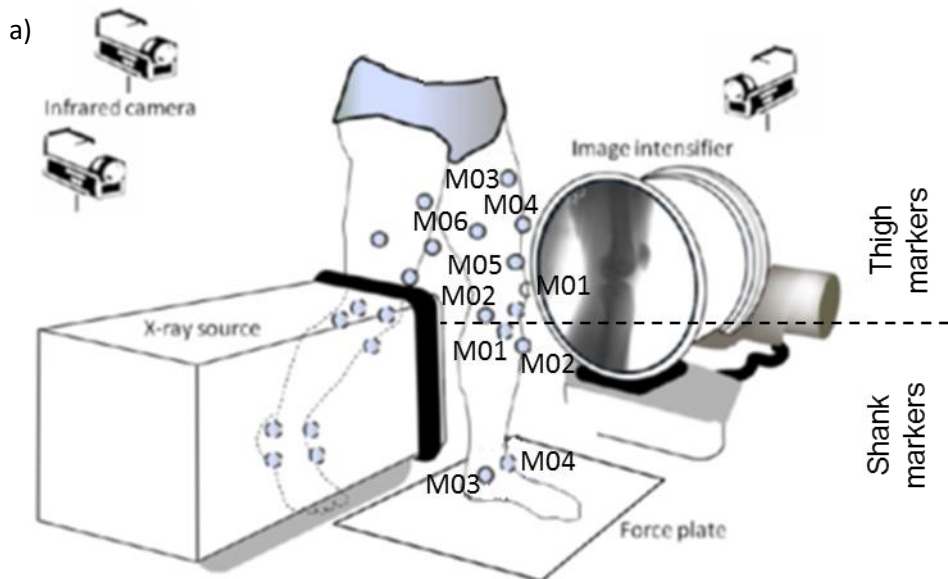
Figure 21 – STEP UP/DOWN. Magnitude of the instantaneous displacement of the nineteen and ten skin-markers glued on the thigh (a) and shank (b) represented in the relevant ACS. c) Relevant knee joint kinematics computed according to the convention proposed by Grood and Suntay (1983) (flexion/extension in blue, with flexion as positive).

2.4. *In-vivo data from NTU*

Scientific articles of reference - A detailed description of the original data set can be found in Tsai et al. (2009, 2011) and in Kuo et al. (2011).

Experimental data description - Ten markers were used to track the motion of the thigh (MFC and LFC were renamed as ME and LE in the available data for coherence with the adopted lexicon; thigh markers: T1, T2, T3, and T4) and shank (TT, FH, MMA, and LMA; the latter two were renamed as MM and LM in the available data for coherence with the adopted lexicon); markers are depicted in Fig. 22 for the different motor tasks. Data for the subjects standing at the anatomical position were also collected.

Anatomical coordinate system definitions – ACSs for the bones were defined based on the anatomical features of the bones following the literature (Miranda et al., 2010).



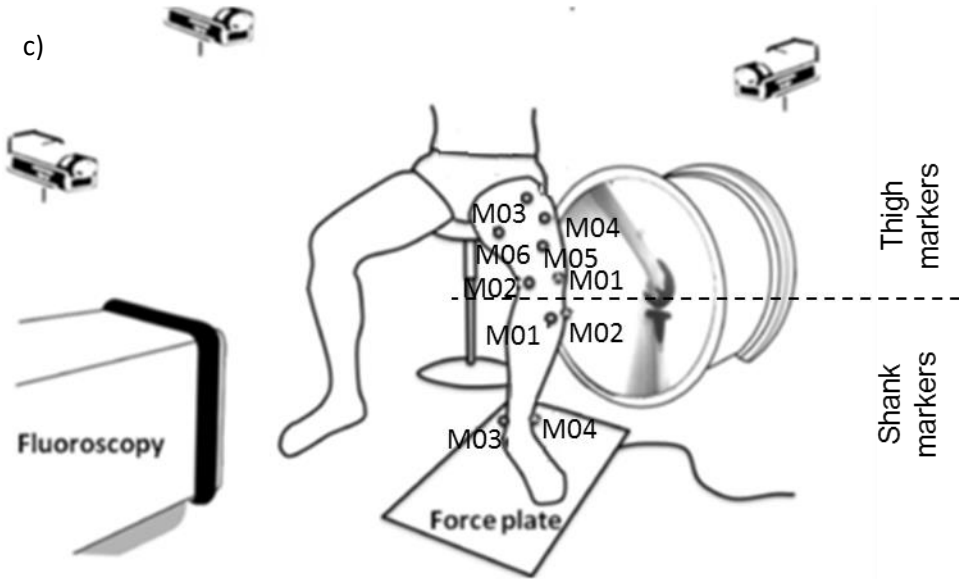


Figure 22 A subject performing (a) overground walking (b) stair ascending and (c) sit-to-stand tasks while kinematic data were measured using a 7-camera stereophotogrammetry system and a fluoroscopy system and kinetic data using a force plate. The cameras shown are schematic representation whereas in the real life situations, the cameras were placed around the subjects without interfering with the activities. The following ALs were manually identified and equipped with markers: RASIS, LASIS, RPSIS, LPSIS, ME, LE, HF, TT, LM, MM (see definitions in Table 3.3). Some markers were affixed onto anatomical landmarks (thigh: M01-LE, M02-ME; shank: TT-M01, HF-M02, LM-M03, MM-M04).

Measurement specifications - The sampling rate of the two 7-camera Vicon systems (VICON 370, VICON 512, Oxford Metrics, UK) was set at 60 sample/s.

Ground truth - Each subject received a computed tomography scan of the knee joint (CT, PQ-5000, Picker International, USA), from 15 cm superior to the joint line to 15 cm inferior, with a slice thickness of 1 mm and a pixel size of 0.625×0.625 mm. The CT data were segmented using a threshold filter to obtain volumetric models of the individual bones, namely the femur, tibia, fibula and patella. These subject-specific volumetric bone models, including their external surfaces and internal structures, were then used for subsequent registration with fluoroscopic images. The fluoroscopy system was calibrated using a 30×30 cm transparent calibration box, two parallel sides of which were marked with lead markers at given positions. The box was placed with one of the marked sides on the image intensifier of the fluoroscopy and its image obtained. The image was used to correct image distortions via a modified polynomial method (Baltzopoulos, 1995) and to estimate the position of the point Xray source. For the spatial registration between the fluoroscopy and Vicon systems, five infrared retro-reflective markers were attached at known positions on the calibration box.

During tests, the fluoroscopic images were obtained at a sampling rate of 30 sample/s using an image grabber card (PCI bus frame grabber, Foresight, USA). During STS, the projection beam of the fluoroscopy system was adjusted so that the image plane was slightly oblique with respect to the sagittal plane of the tested knee to avoid overlapping of the bilateral knee joints on the fluoroscopic image, Fig. 22c. Temporal synchronization of the two systems was achieved using an electrical trigger. The registration of the CT-derived volumetric bone models and fluoroscopy images was performed by comparing systematically the fluoroscopic image with the digitally reconstructed radiograph (DRR) of the volumetric bone model (Lu et al., 2008). A DRR was generated by casting X-rays through the volumetric CT data of a bone model and projecting onto the image plane to form an image resembling a radiograph with detailed internal information of the bony structures (Penney et al., 1998). The 3D pose of the bone at each image frame was obtained by searching for the pose of the bone model using an optimization procedure to produce the DRR which best matched the fluoroscopic image. A computer graphics user interface (GUI) was developed to assist with the visualization of the registration and reconstruction of the 3D bone poses. The registration method has previously been evaluated for its accuracy using a cadaveric knee, giving means and standard deviations of the knee pose errors of 0.24 ± 0.77 mm, 0.41 ± 3.06 mm and 0.59 ± 1.13 deg for in-plane translation, out-of-plane translation, and all rotations, respectively (Lu et al., 2008).

2.4.1. Data sample 5: knee flexion/extension

Subject characteristics - An adult male subject free from musculoskeletal diseases. Height = 1.76 m, mass = 74 kg.

Motor task description – The subject sat on an armless, height-adjustable chair to perform a complete cycle of active knee flexion/extension at an average speed of about 30 deg/s with the assistance of a metronome.

STA characteristics - Skin-marker trajectories in the thigh and shank ACSs are depicted in Fig. 23. Stereophotogrammetric data were acquired at 60 Hz and then down-sampled to 30 Hz. Statistical data describing the relevant STAs are shown in Fig. 24 for knee flexion/extension. Magnitude of the instantaneous displacement of thigh and shank skin-markers along with the knee joint angular kinematics is depicted in Fig. 25 for knee flexion/extension.

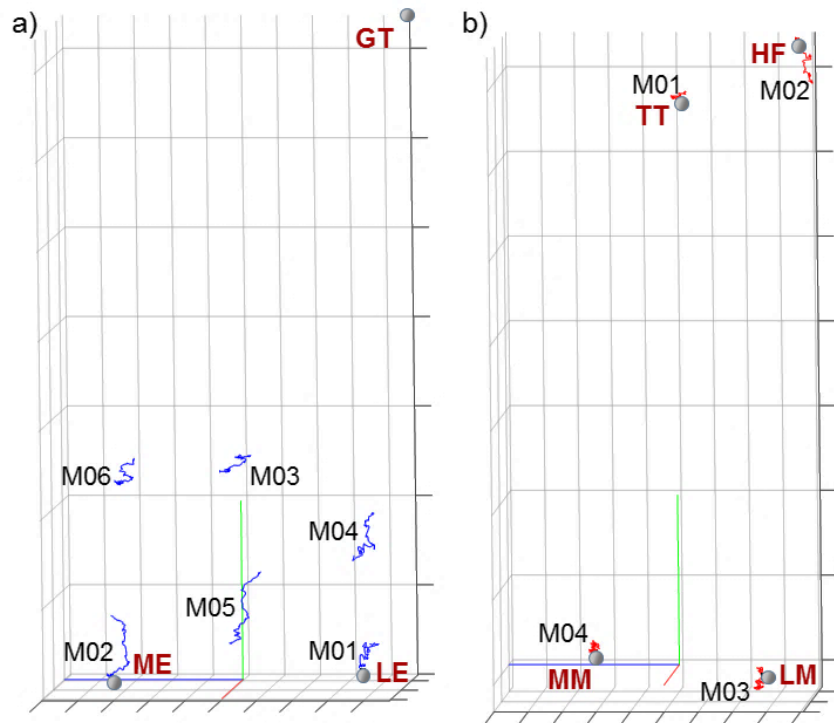


Figure 23 – Femur (a) and tibial (b) ACSs, relevant ALs, and thigh and shank skin-marker trajectories (represented in blue and red, respectively). The axes of the ACSs are represented in red, green, and blue for the x (antero/posterior, div = 50 mm), y (superior/inferior, div = 50 mm), and z (right/left, div = 20 mm) directions, respectively.

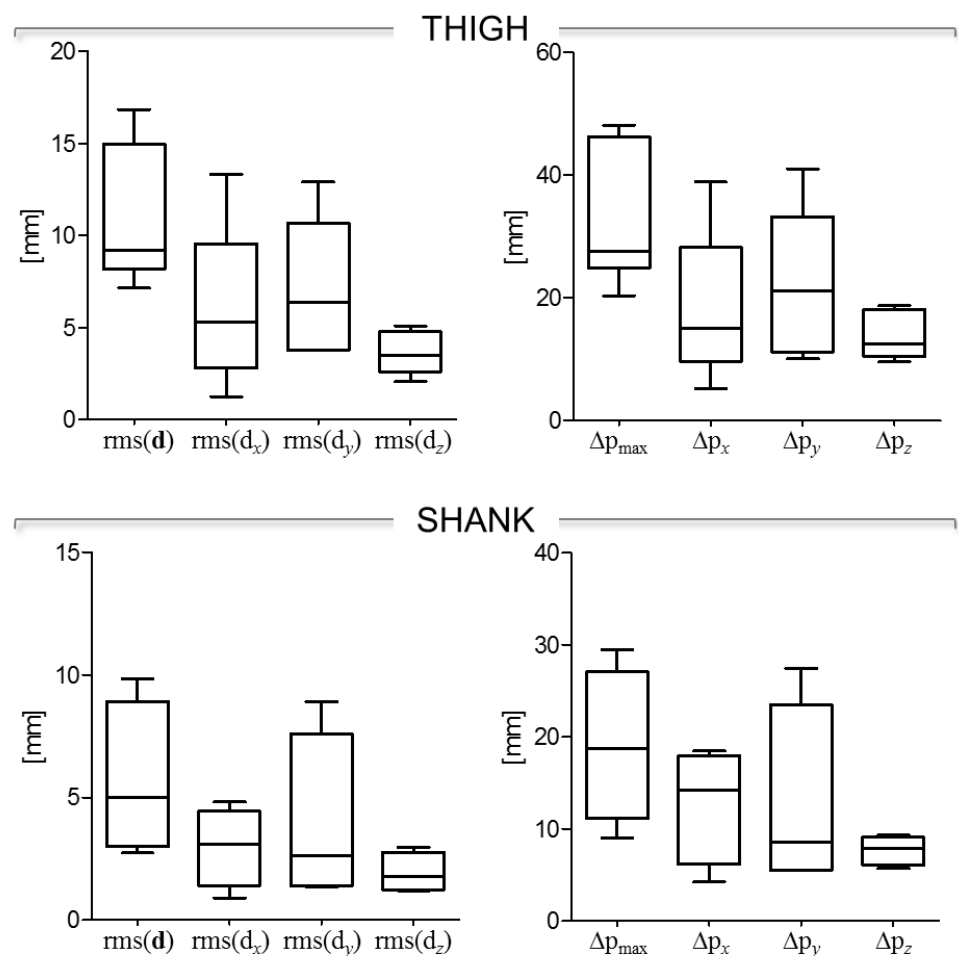


Figure 24 – Box-plots of the eight parameters ($\text{rms}(\mathbf{d})$, $\text{rms}(\mathbf{d}_x)$, $\text{rms}(\mathbf{d}_y)$, and $\text{rms}(\mathbf{d}_z)$, in the left panel; Δp_{\max} , Δp_x , Δp_y , and Δp_z , in the right panel) that describe the STA affecting the six and four skin-markers on the thigh and the shank, respectively, during the movement. Outliers are also depicted.

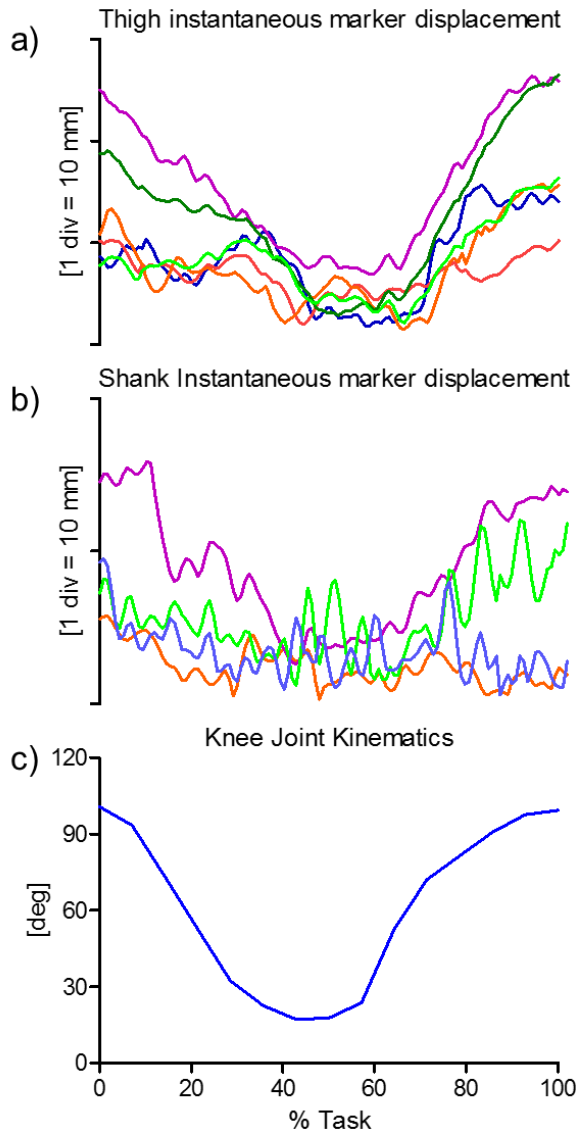


Figure 25 –Magnitude of the instantaneous displacement of the six and four skin-markers glued on the thigh (a) and shank (b) represented in the relevant ACS. c) Relevant knee joint kinematics computed according to the convention proposed by Grood and Suntay (1983) (flexion/extension in blue, with flexion as positive).

2.4.2. Data samples 9, 12, 16: overground walking, sit to stand, step-up

Subject characteristics - An adult male subject free from musculoskeletal diseases. Height = 1.74 m, mass = 83 kg.

Motor task description - Overground walking at the subject's self-selected speed was measured only during the stance phase, as depicted in Fig. 22a. For the sit-to-stand task, each subject was asked to sit with the hips abducted at about 30 deg on an armless, height-adjustable chair and stand up at a self-selected speed (Fig. 22b). The height of the chair was set at 115% of the knee-heel distance for each subject. Step-up was performed on a three-step stair (height: 18 cm; depth: 46 cm) at a self-selected speed (Fig. 22c).

STA characteristics - Skin-marker trajectories in the thigh and shank ACSs are depicted in Figs. 26, 29, 32, for stance phase overground walking, sit to stand, and step-up, respectively. Stereophotogrammetric data were acquired at 60Hz and then down-sampled to 30Hz. Statistical data describing the STAs are shown in Figs. 27, 30, 33, for overground walking, sit to stand, and step-up, respectively. For each motor task, the magnitude of the instantaneous displacement of thigh and shank skin-markers along with the knee joint angular kinematics is depicted in Figs. 28, 31, 34, for stance phase overground walking, sit to stand, and step-up, respectively.

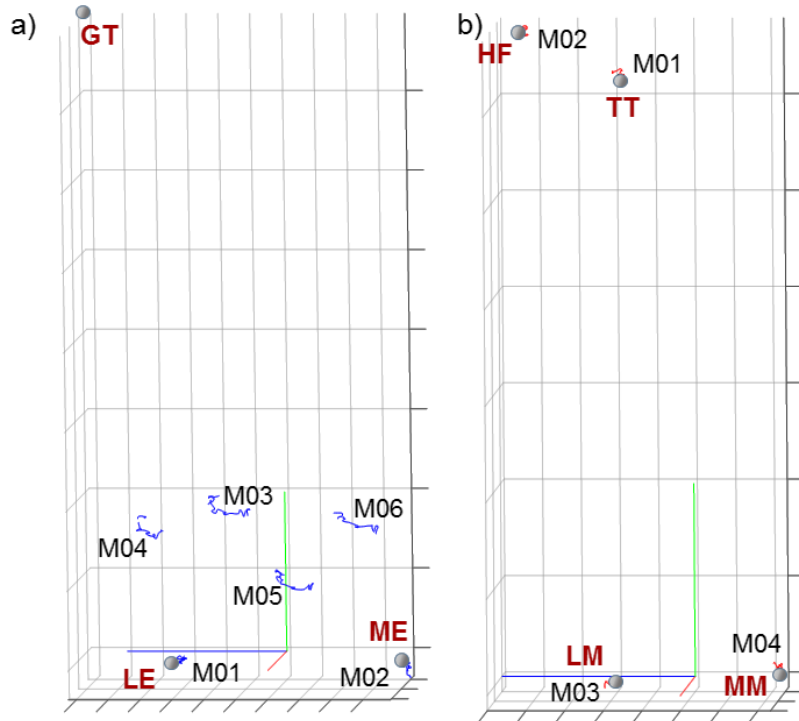


Figure 26 – STANCE PHASE OVERGROUND WALKING. Femur (a) and tibial (b) ACSs, relevant ALs, and thigh and shank skin-marker trajectories (represented in blue and red, respectively). The axes of the ACSs are represented in red, green, and blue for the x (antero/posterior, div = 50 mm), y (superior/inferior, div = 50 mm), and z (right/left, div = 20 mm) directions, respectively.

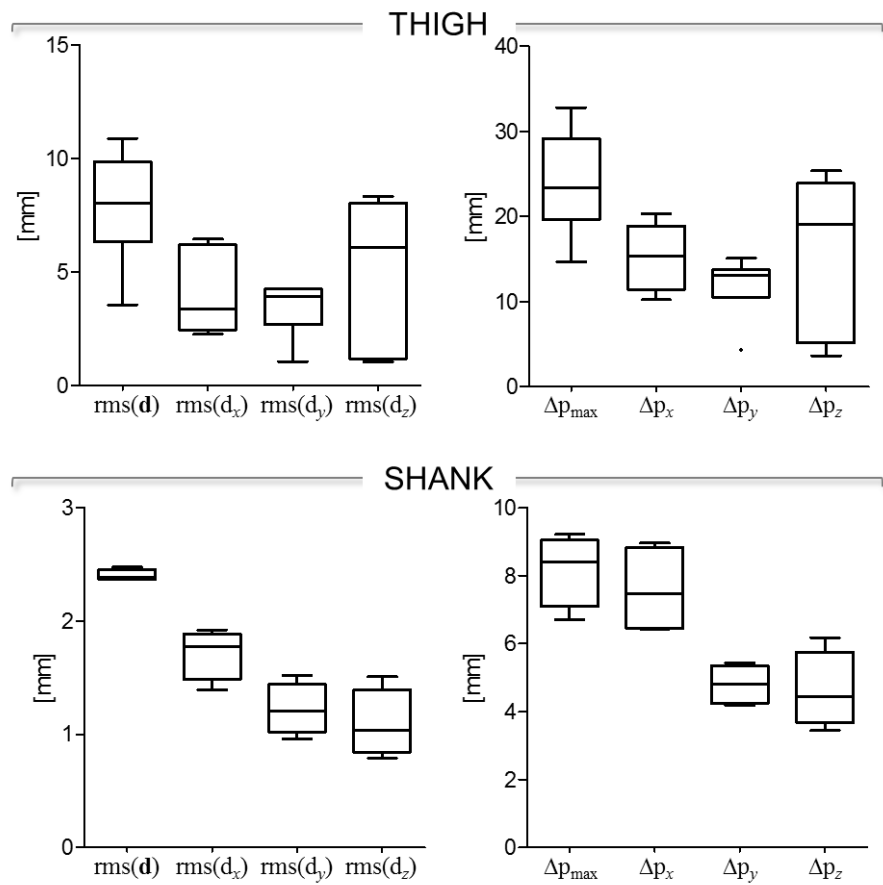


Figure 27 – STANCE PHASE OVERGROUND WALKING. Box-plots of the eight parameters ($\text{rms}(\mathbf{d})$, $\text{rms}(\mathbf{d}_x)$, $\text{rms}(\mathbf{d}_y)$, and $\text{rms}(\mathbf{d}_z)$, in the left panel; Δp_{max} , Δp_x , Δp_y , and Δp_z , in the right panel) that describe the STA affecting the six and four skin-markers on the thigh and the shank, respectively, during the movement. Outliers are also depicted.

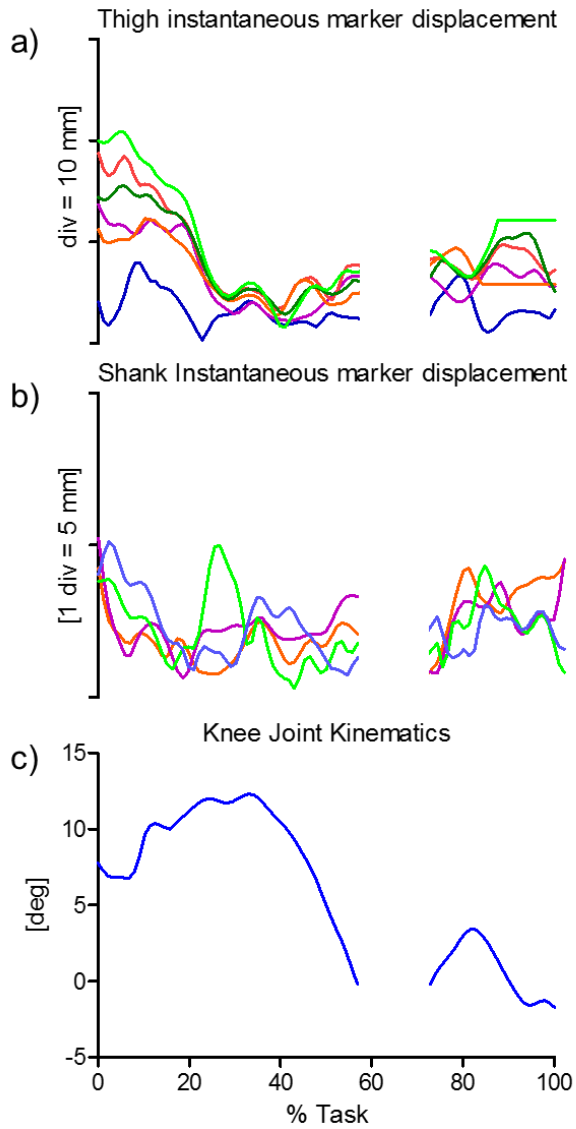


Figure 28 – STANCE PHASE OVERGROUND WALKING. Magnitude of the instantaneous displacement of the six and four skin-markers glued on the thigh (a) and shank (b) represented in the relevant ACS. c) Relevant knee joint kinematics computed according to the convention proposed by Grood and Suntay (1983) (flexion/extension in blue, with flexion as positive). The data between 60%-70% were not shown because the knee joints were overlapped on the fluoroscopic images.

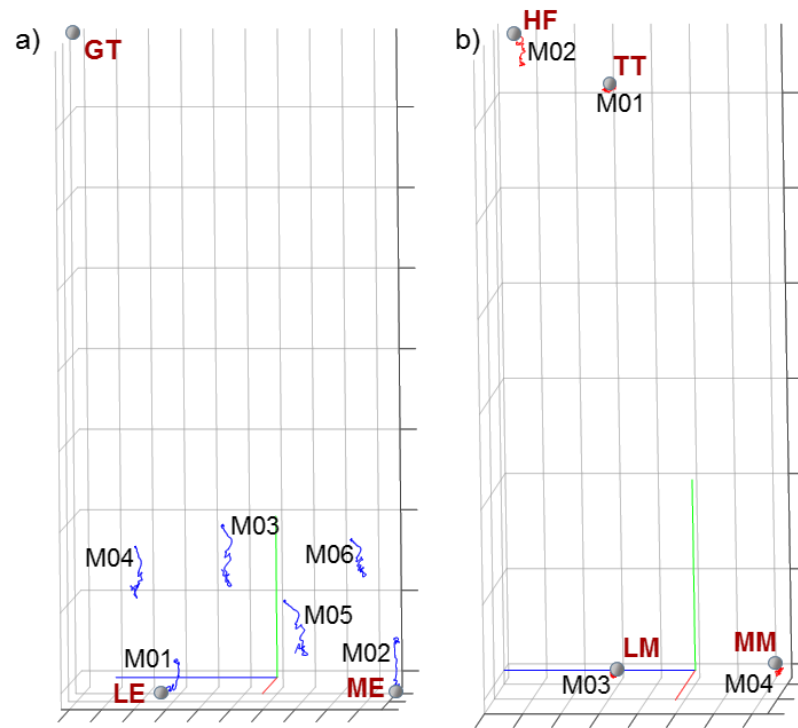


Figure 29 – SIT TO STAND. Femur (a) and tibial (b) ACSs, relevant ALs, and thigh and shank skin-marker trajectories (represented in blue and red, respectively). The axes of the ACSs are represented in red, green, and blue for the x (antero/posterior, div = 50 mm), y (superior/inferior, div = 50 mm), and z (right/left, div = 20 mm) directions, respectively.

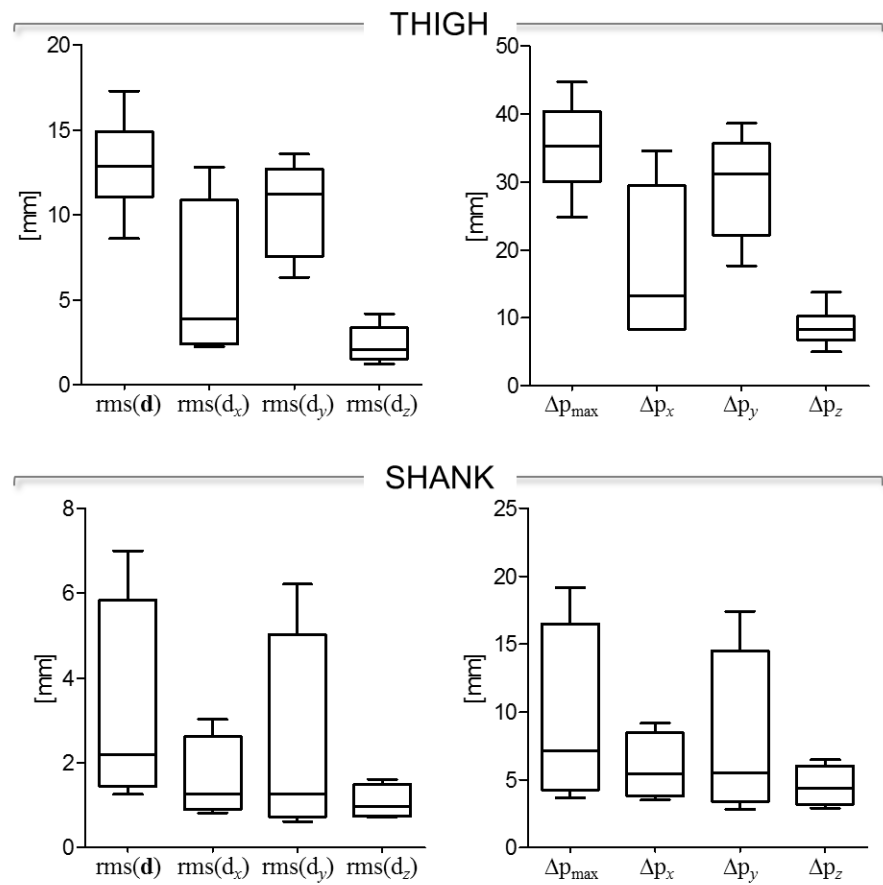


Figure 30 – SIT TO STAND. Box-plots of the eight parameters ($\text{rms}(\mathbf{d})$, $\text{rms}(\mathbf{d}_x)$, $\text{rms}(\mathbf{d}_y)$, and $\text{rms}(\mathbf{d}_z)$, in the left panel; Δp_{max} , Δp_x , Δp_y , and Δp_z , in the right panel) that describe the STA affecting the six and four skin-markers on the thigh and the shank, respectively, during the movement. Outliers are also depicted.

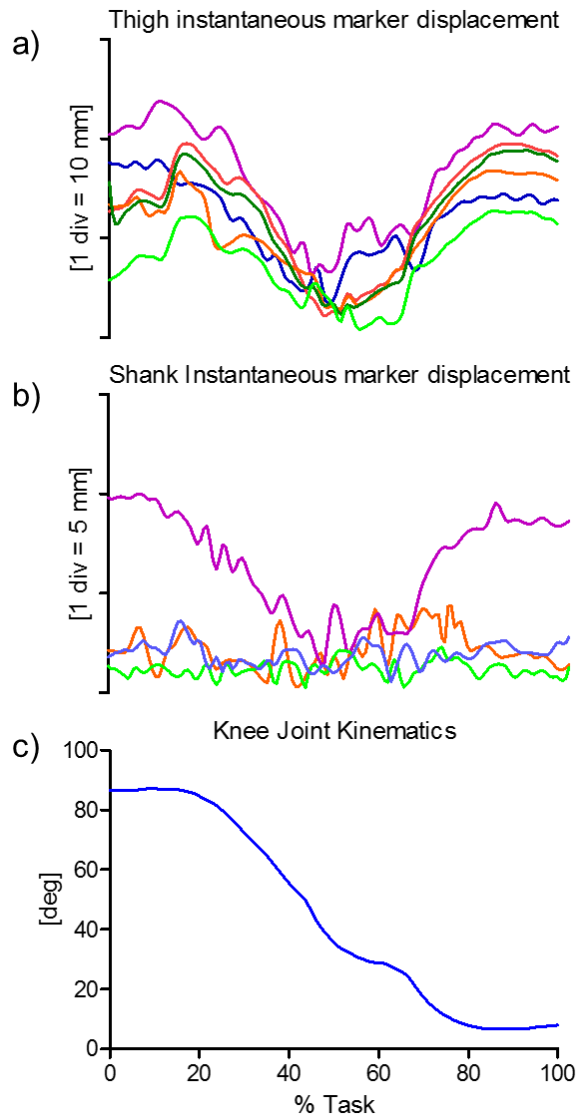


Figure 31 – SIT TO STAND. Magnitude of the instantaneous displacement of the six and four skin-markers glued on the thigh (a) and shank (b) represented in the relevant ACS. c) Relevant knee joint kinematics computed according to the convention proposed by Grood and Suntay (1983) (flexion/extension in blue, with flexion as positive).

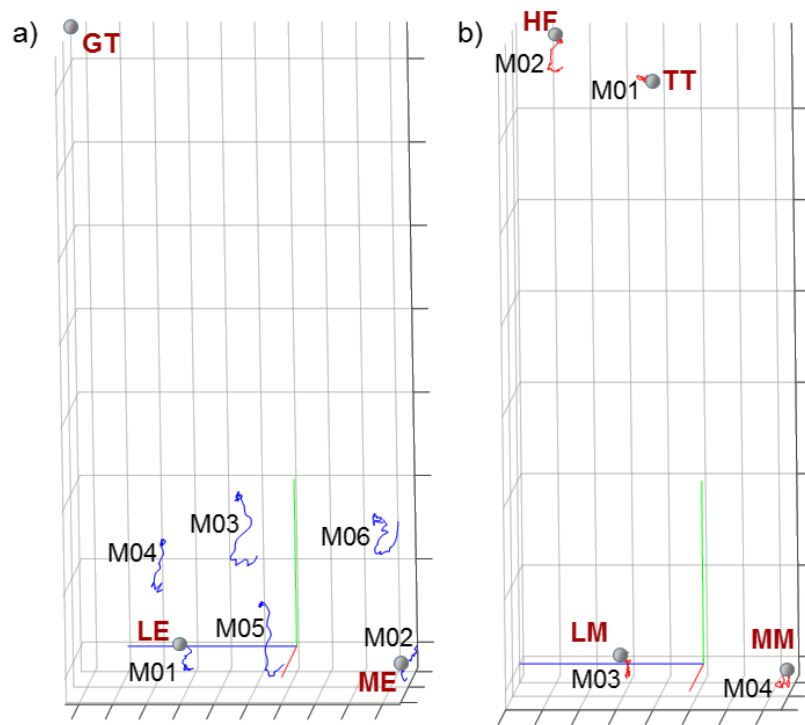


Figure 32 – STEP-UP. Femur (a) and tibial (b) ACSs, relevant ALs, and thigh and shank skin-marker trajectories (represented in blue and red, respectively). The axes of the ACSs are represented in red, green, and blue for the x (antero/posterior, div = 50 mm), y (superior/inferior, div = 50 mm), and z (right/left, div = 20 mm) directions, respectively.

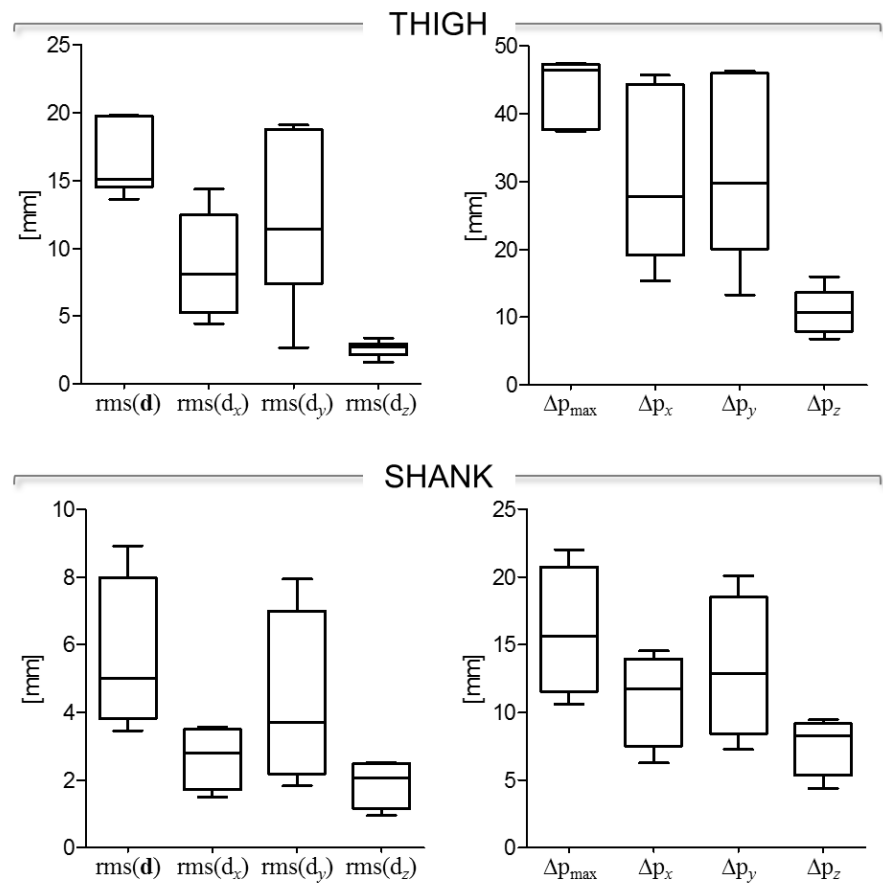


Figure 33 – STEP-UP. Box-plots of the eight parameters ($\text{rms}(\mathbf{d})$, $\text{rms}(\mathbf{d}_x)$, $\text{rms}(\mathbf{d}_y)$, and $\text{rms}(\mathbf{d}_z)$, in the left panel; Δp_{\max} , Δp_x , Δp_y , and Δp_z , in the right panel) that describe the STA affecting the six and four skin-markers on the thigh and the shank, respectively, during the movement. Outliers are also depicted.

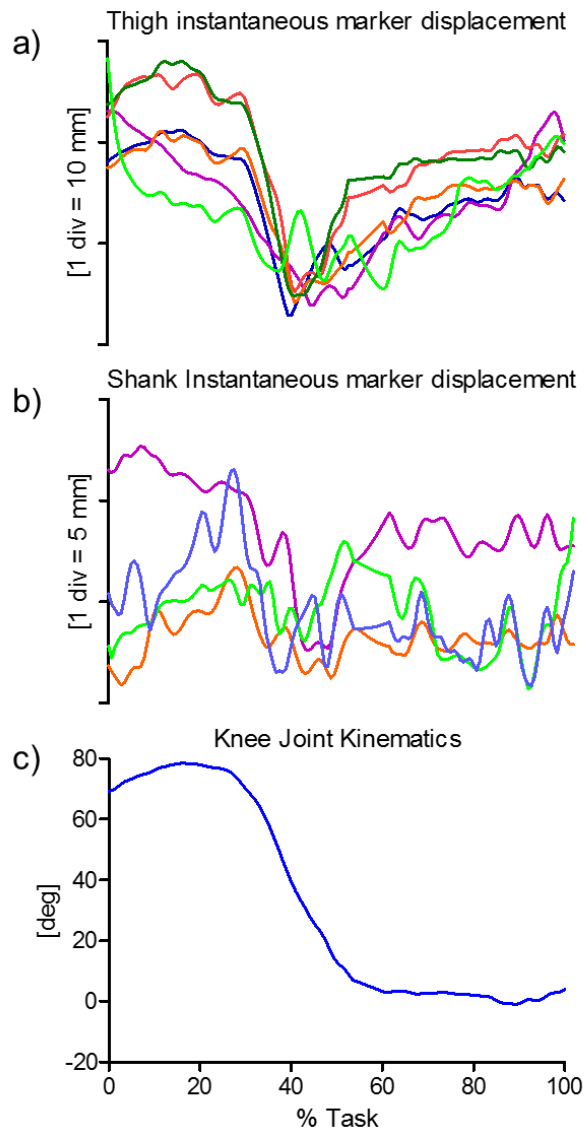


Figure 34 – STEP-UP. Magnitude of the instantaneous displacement of the six and four skin-markers glued on the thigh (a) and shank (b) represented in the relevant ACS. c) Relevant knee joint kinematics computed according to the convention proposed by Grood and Suntay (1983) (flexion/extension in blue, with flexion as positive).

2.4.3. Data sample 13: sit to stand

Subject characteristics - An adult female subject with posterior cruciate ligament retaining mobile bearing total knee replacement. Height = 1.61 m, mass = 87 kg.

Motor task description - Each subject sat with the hips abducted at about 30 degrees on an armless, height-adjustable chair and stood up at a self-selected speed. The projection beam of the fluoroscopy system was adjusted so that the image plane was slightly oblique with respect to the sagittal plane of the tested knee to avoid overlapping of the bilateral knee joints on the fluoroscopic image.

STA characteristics - Skin-marker trajectories in the thigh and shank ACSs are depicted in Fig. 35. Stereophotogrammetric data were acquired at 60 Hz and then down-sampled to 30 Hz. Statistical data describing the relevant STAs are shown in Fig. 36. Magnitude of the instantaneous displacement of thigh and shank skin-markers along with the knee joint angular kinematics is depicted in Fig. 37.

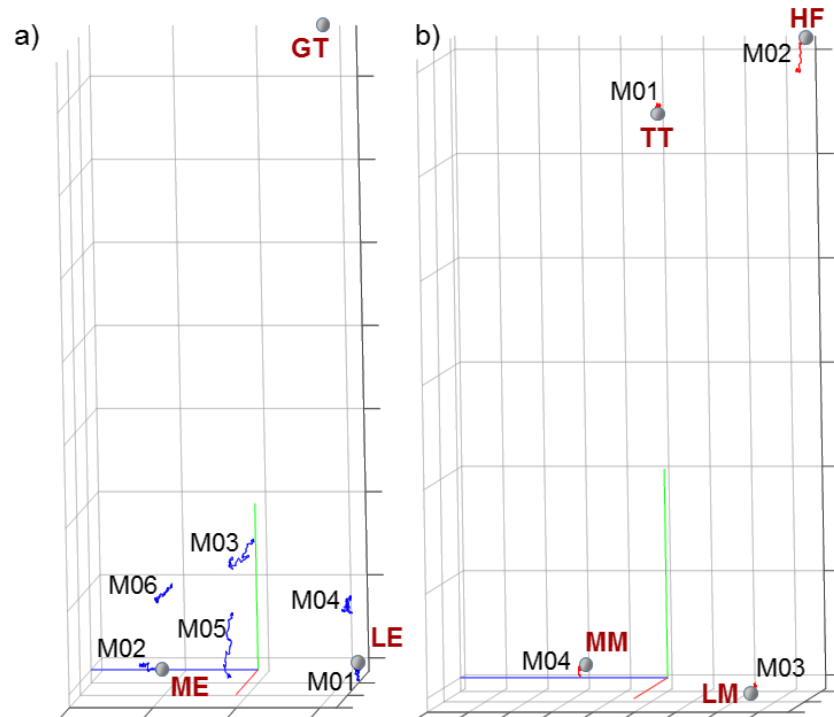


Figure 35 – Femur (a) and tibial (b) ACSs, relevant ALs, and thigh and shank skin-marker trajectories (represented in blue and red, respectively). The axes of the ACSs are represented in red, green, and blue for the x (antero/posterior, div = 50 mm), y (superior/inferior, div = 50 mm), and z (right/left, a) div = 50 mm; b) div = 20 mm directions, respectively.

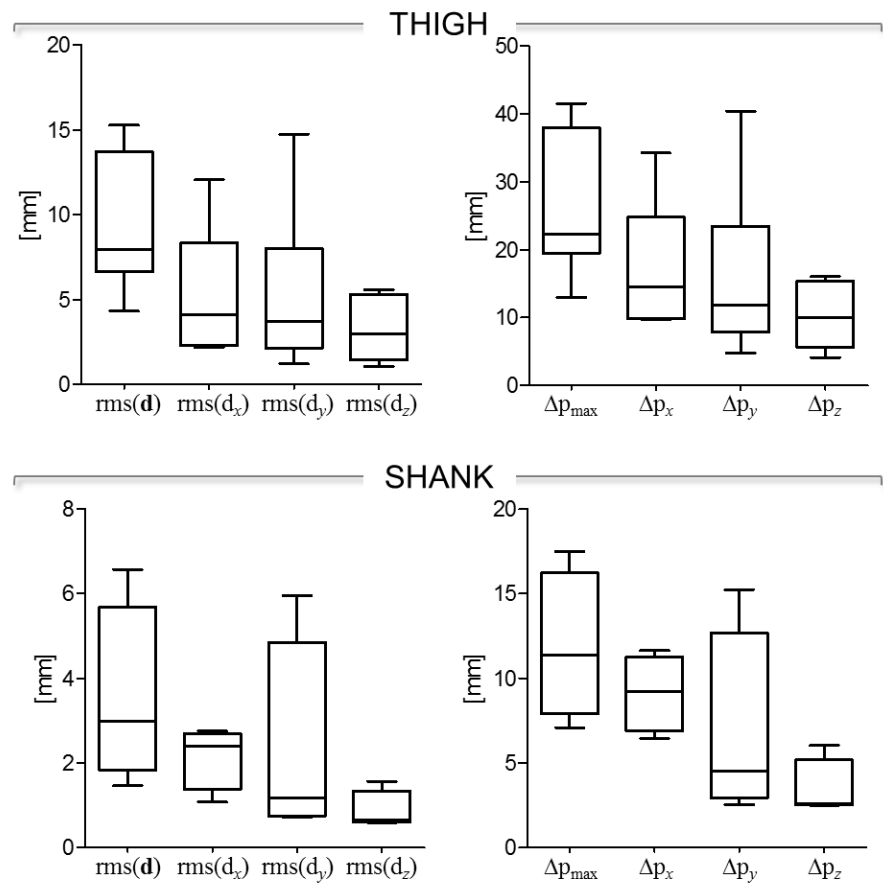


Figure 36 – Box-plots of the eight parameters ($\text{rms}(\mathbf{d})$, $\text{rms}(\mathbf{d}_x)$, $\text{rms}(\mathbf{d}_y)$, and $\text{rms}(\mathbf{d}_z)$, in the left panel; Δp_{\max} , Δp_x , Δp_y , and Δp_z , in the right panel) that describe the STA affecting the six and four skin-markers on the thigh and the shank, respectively, during the movement. Outliers are also depicted.

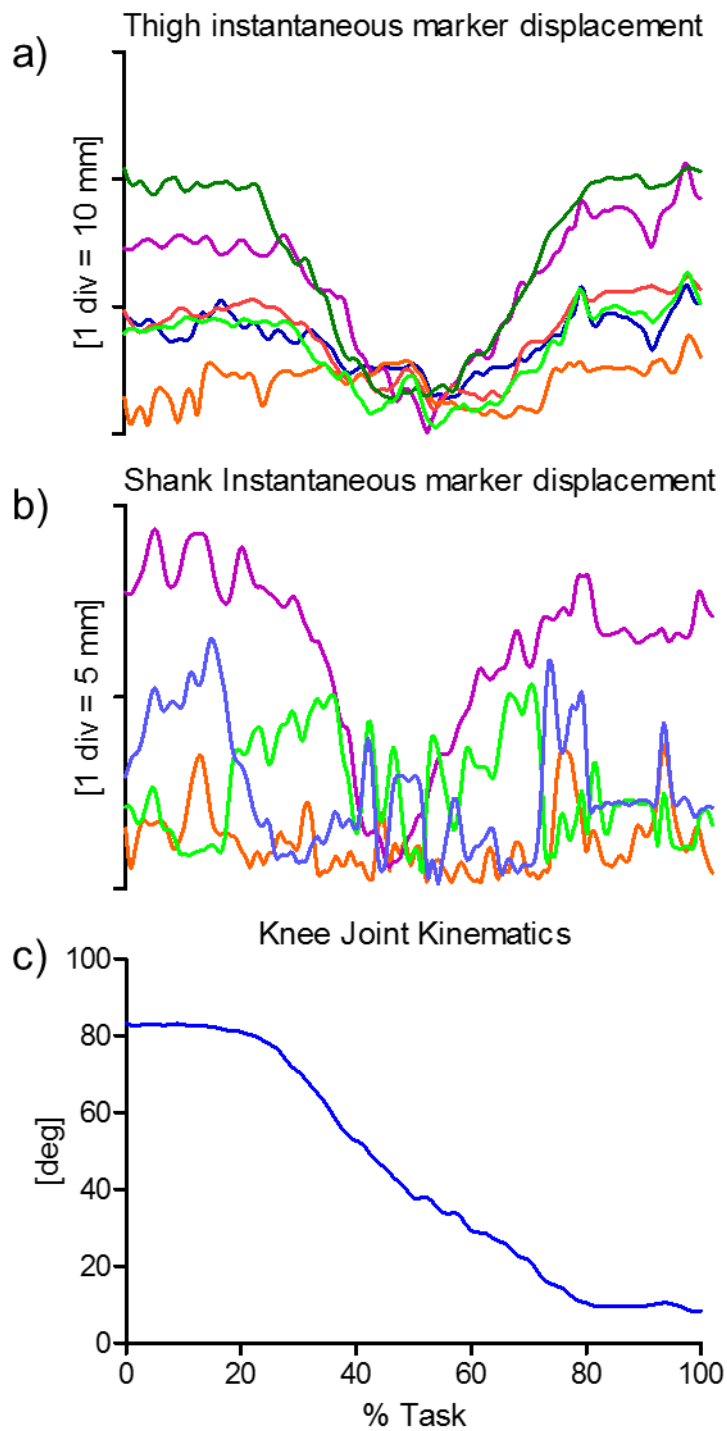


Figure 37 –Magnitude of the instantaneous displacement of the six and four skin-markers glued on the thigh (a) and shank (b) represented in the relevant ACS. c) Relevant knee joint kinematics computed according to the convention proposed by Grood and Suntay (1983) (flexion/extension in blue, with flexion as positive).

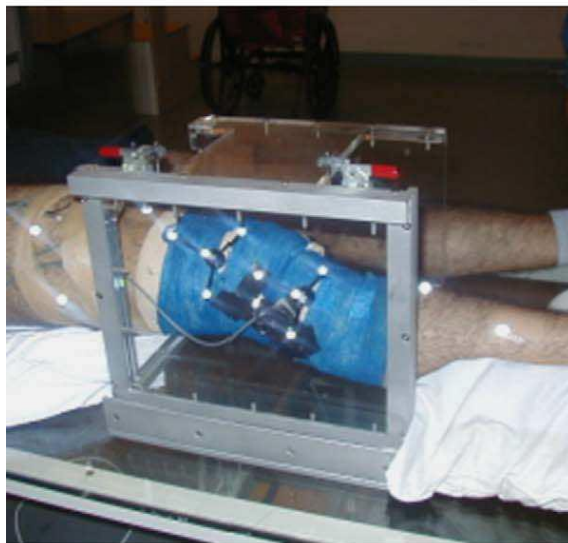
2.5. *In-vivo data from OTTAWA*

Scientific articles of reference - A detailed description of the original data set can be found in Benoit et al., 2006 and in Andersen et al., 2012 for hopping.

Experimental data description - Triads of three non-collinear 7 mm reflective markers (pin-markers) were affixed to the pins. Additional clusters of four 10 mm surface markers (skin-markers) were affixed onto the lateral and frontal aspects of both the right thigh and shank (Fig. 38a and 38b). Skin-markers were spaced 10–15 cm from adjacent markers within their respective cluster and their arrangement was chosen to ensure they remained non-coplanar in at least two camera views throughout the range of motion. Reflective markers were also placed on the right heel, 5th metatarsal and lateral malleolus.



(a)



(b)

Figure 38 a) Picture of the bone-pin and surface markers configurations for a representative subject. The pins are inserted in the tibia and femur, respectively. Each pin is equipped with a 4 marker-cluster. The skin is equipped with 4 retroreflective markers for the thigh and 4 for the shank. Skin-marker names as shown in Figures 39, 42, 45. b) RSA procedure and calibration box. The right leg is extended.

Measurement specifications - Bone-pin and skin-marker trajectories were tracked within 0.8 m³ measurement volume (1.1 m x 0.8 m x 0.9 m) using four infrared cameras (ProReflex, Qualisys AB, Sweden), sampling at 120 sample/s. Marker coordinates were transformed using the direct linear transform (DLT) and the raw 3D coordinates exported and saved to a local computer for analysis.

Anatomical coordinate system definitions – To define femur and tibia ACSs, the following 19 anatomical landmarks were identified on RSA radiographs (described below):

- 1–4. Tibial pin-markers.
5. Proximal medial tibial eminence (tibial reference point).
6. The most distal point along a line through point 5 and parallel to the long axis of the tibia.
- 7–8. Medial and lateral edges of proximal tibia respectively.
9. A distal point along a line drawn perpendicular to the long axis of the tibia and running originating at the tibial reference point.
- 10–14. Femoral pin-markers.
15. Proximal (deepest) point of the condylar groove (notch)
(femoral reference point).
16. The most distal point along a line through point
15 and parallel to the long axis of the femur.
- 17–18. Medial and lateral edges of the distal femur, respectively.
19. A distal point along a line drawn perpendicular to the long axis of the femur and originating at the femoral reference point.

The origin of the femoral coordinate system was located at the deepest point of the intercondylar groove (point 15). The origin of the tibial coordinate system was located at the highest point of the medial intercondylar eminence (point 5). Local coordinate systems of the femur and tibia were defined as follows:

X_f cross product of vectors Z_f and Y_f; from the femoral origin, directed laterally.

Y_f cross product of Z_f and vector joining points 17 and 18; from the femoral origin, directed anteriorly.

Z_f vector joining points 15 and 16; from the femoral origin directed longitudinally along the femoral axis in the frontal plane.

X_t cross product of vectors Z_t and Y_t; from the tibial origin, directed laterally.

Y_t cross product of Z_t and vector joining points 7 and 8; from the tibial origin, directed anteriorly.

Zt vector joining points 5 and 6; from the tibial origin directed longitudinally along the tibial axis in the frontal plane.

Ground truth – Stainless steel Apex self-drilling/self-tapping pins (Stryker Howmedica AB Sweden, 3.0 mm diameter, #5038-2-110) were inserted under local anaesthetic into the distal femur and proximal tibia of the right leg (Ramsey et al., 2003) at the Karolinska University Hospital (Stockholm, Sweden). The femoral pin was inserted between the iliotibial band and the quadriceps tendon superior of the vastus lateralis to minimise impingement problems. Following surgery subjects performed active flexion and extension movements while standing to identify whether movement restrictions were evident. Subjects were then transported by wheelchair to the motion analysis laboratory for data collection. To test for eventual pin bending, standing reference trial were performed before and after each block of movement trials and the orientation of the target clusters from the first reference trial was matched against the second to verify the pins did not bend and the triad did not rotate during testing. Following the motion analysis recordings, the leg was extended through a biplanar calibration box (Cage 10, RSA Biomedical Innovations, Umea°, Sweden) and biplanar radiographs (RSA) were recorded (Fig. 38b). All radiographs were taken with the subject supine and the knee flexed between 0 deg and 10 deg. From these radiographs, two local anatomical reference points were identified and digitized with the aid of an experienced RSA technician (Sahlgrenska University Hospital Gothenburg, Sweden). In total, the 19 points described in the ACS section were digitised to derive the anatomical coordinate system using UMRSA software (version 5, Biomedical Innovations-AB, Umea, Sweden).

2.5.1. Data samples 10,11,19: Overground walking, lateral cutting manoeuvres, hopping

Subject characteristics - A 22 y.o. subject. Height = 1.75 m, mass = 63 kg.

Motor task description - The participant perform a series of overground walking trials and lateral cutting manoeuvres, after a several practice trials. For gait testing, subjects walked along a 12 m walkway at a self-selected pace, and the stance phase was analysed. Before performing the lateral cutting manoeuvre, subjects jumped for maximal horizontal distance. Their longest measurement was recorded and marked on the floor to determine the proper takeoff distance to the force platform. From an initial standing position the subject pushed off using the left leg and, upon landing onto their right foot, immediately pushed off the platform, cutting to the left at an angle of approximately 45 deg.

STA characteristics - Skin-marker trajectories in the thigh and shank ACSs are depicted in Figs. 39, 42, 45, for stance phase overground walking, lateral cutting manoeuvres, hopping, respectively. Unfiltered data were used. Statistical data describing the STAs are shown in Figs. 40, 43, 46, for stance phase overground walking, lateral cutting manoeuvres, hopping, respectively. Magnitude of the instantaneous displacement of thigh and shank skin-markers along with the knee joint angular kinematics is depicted in Figs. 41, 44, 47, for stance phase overground walking, lateral cutting manoeuvres, hopping, respectively.

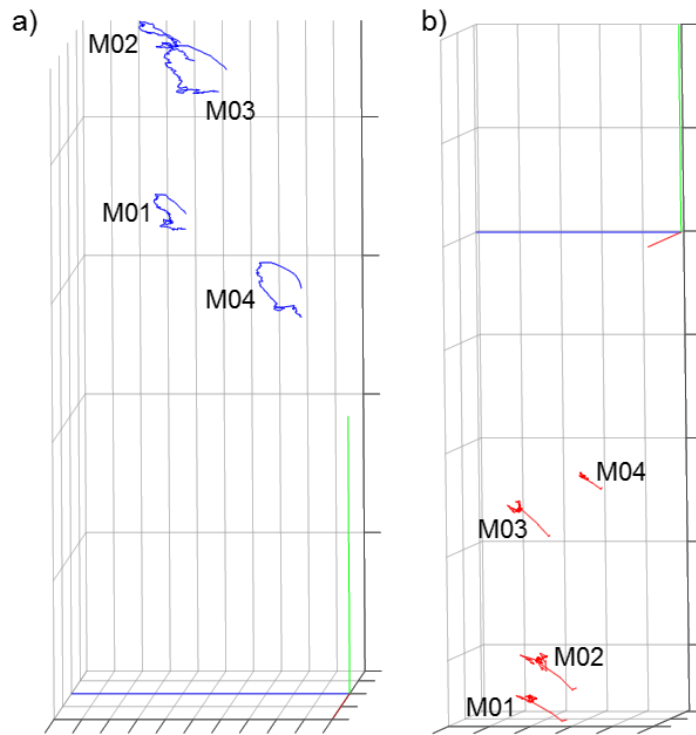


Figure 39 – STANCE PHASE OVERGROUND WALKING. Femur (a) and tibial (b) ACSs, and thigh and shank skin-marker trajectories (represented in blue and red, respectively). The axes of the ACSs are represented in red, green, and blue for the x (antero/posterior, div = 50 mm), y (superior/inferior, div = 50 mm), and z (right/left, div = 20 mm) directions, respectively.

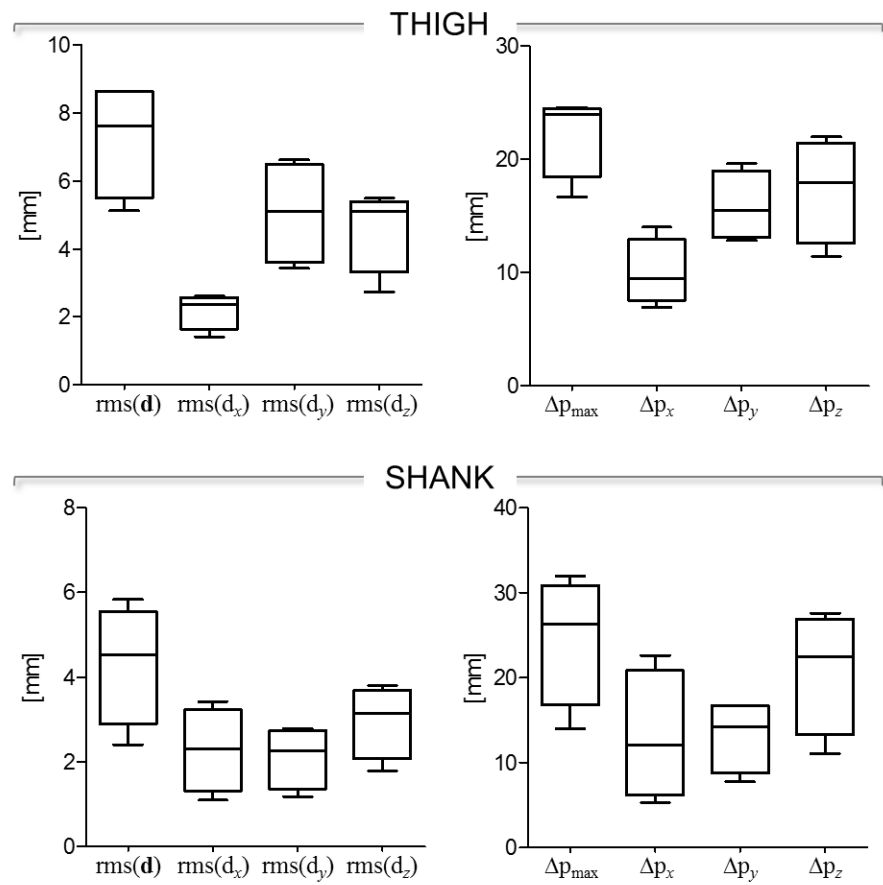


Figure 40 – STANCE PHASE OVERGROUND WALKING. Box-plots of the eight parameters ($\text{rms}(\mathbf{d})$, $\text{rms}(\mathbf{d}_x)$, $\text{rms}(\mathbf{d}_y)$, and $\text{rms}(\mathbf{d}_z)$, in the left panel; Δp_{\max} , Δp_x , Δp_y , and Δp_z , in the right panel) that describe the STA affecting the four skin-markers on the thigh and shank, respectively, during the movement. Outliers are also depicted.

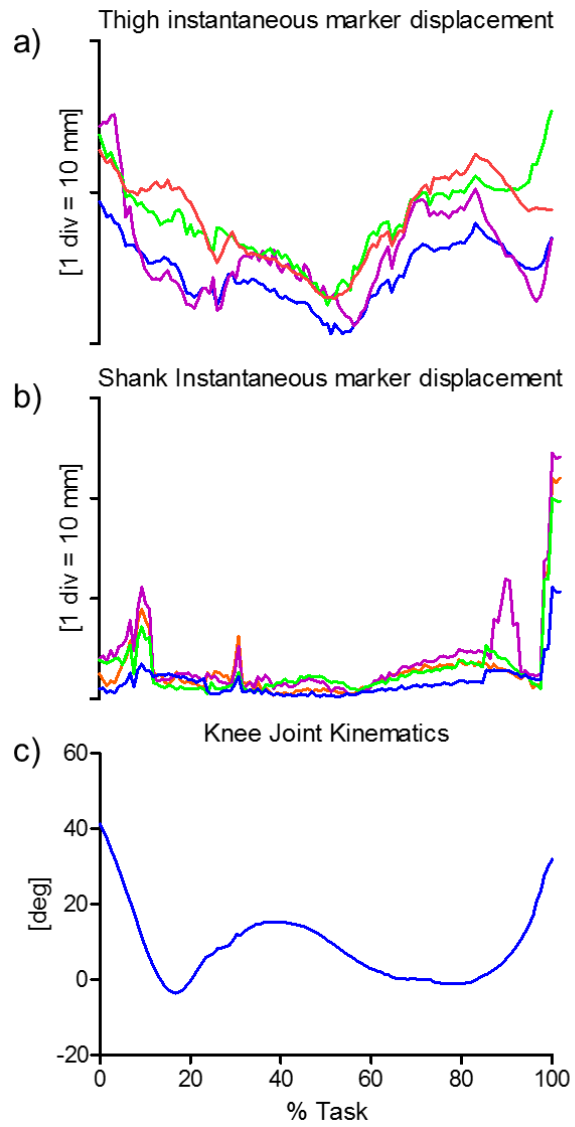


Figure 41 – STANCE PHASE OVERGROUND WALKING. Magnitude of the instantaneous displacement of the four skin-markers glued on the thigh (a) and shank (b) represented in the relevant ACS. c) Relevant knee joint kinematics computed according to the convention proposed by Grood and Suntay (1983) (flexion/extension in blue, with flexion as positive).

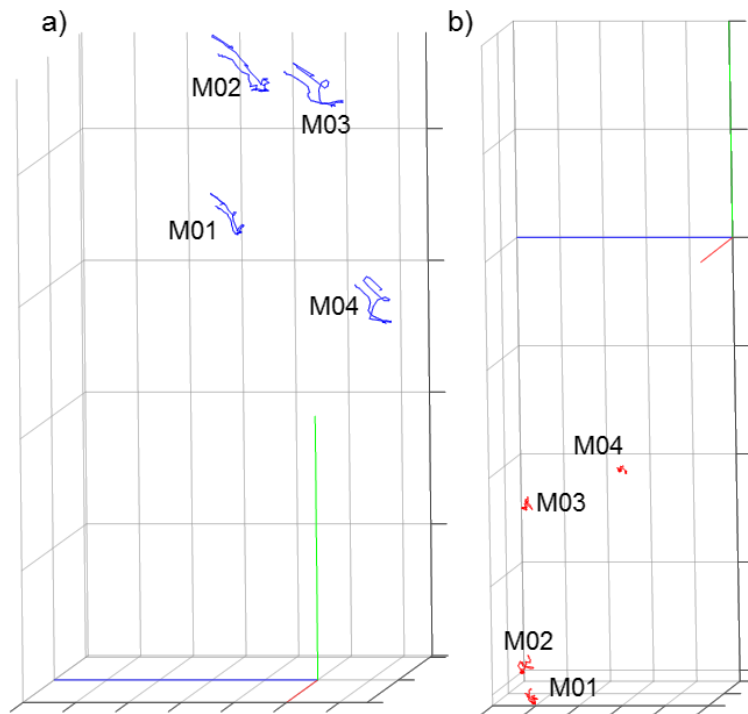


Figure 42 – LATERAL CUTTING MANOEUVRES. Femur (a) and tibial (b) ACSs, and thigh and shank skin-marker trajectories (represented in blue and red, respectively). The axes of the ACSs are represented in red, green, and blue for the x (antero/posterior, div = 50 mm), y (superior/inferior, div = 50 mm), and z (right/left, div = 20 mm) directions, respectively.

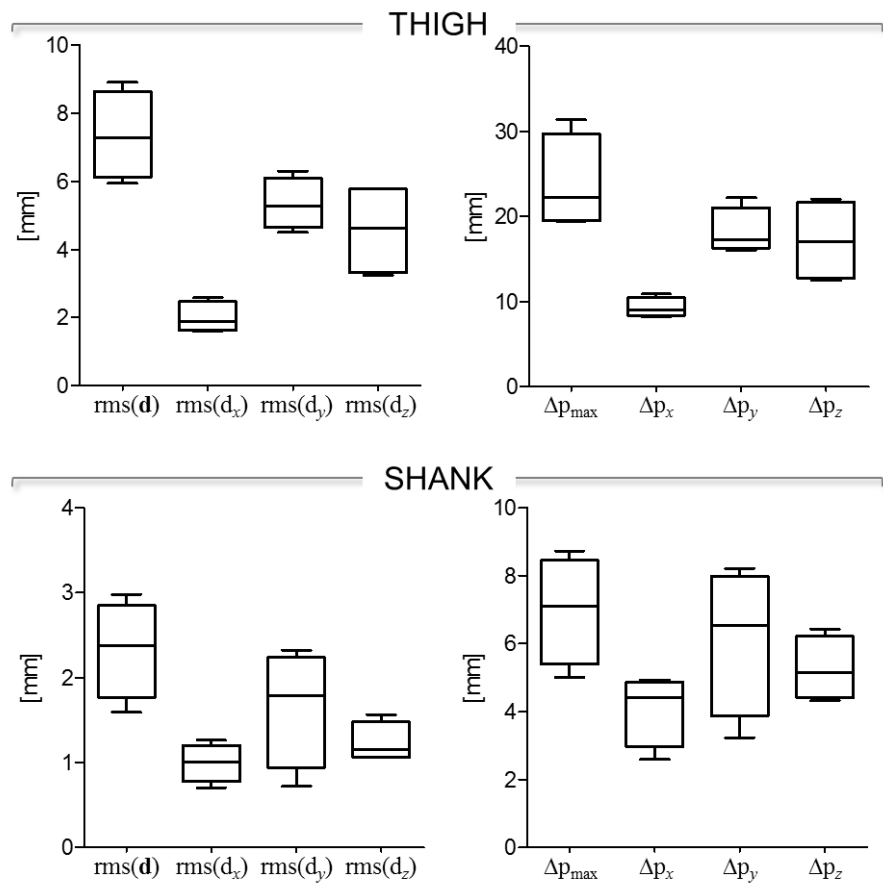


Figure 43 – LATERAL CUTTING MANOEUVRES. Box-plots of the eight parameters ($\text{rms}(\mathbf{d})$, $\text{rms}(d_x)$, $\text{rms}(d_y)$, and $\text{rms}(d_z)$, in the left panel; Δp_{\max} , Δp_x , Δp_y , and Δp_z , in the right panel) that describe the STA affecting the four skin-markers on the thigh and shank, respectively, during the movement. Outliers are also depicted.

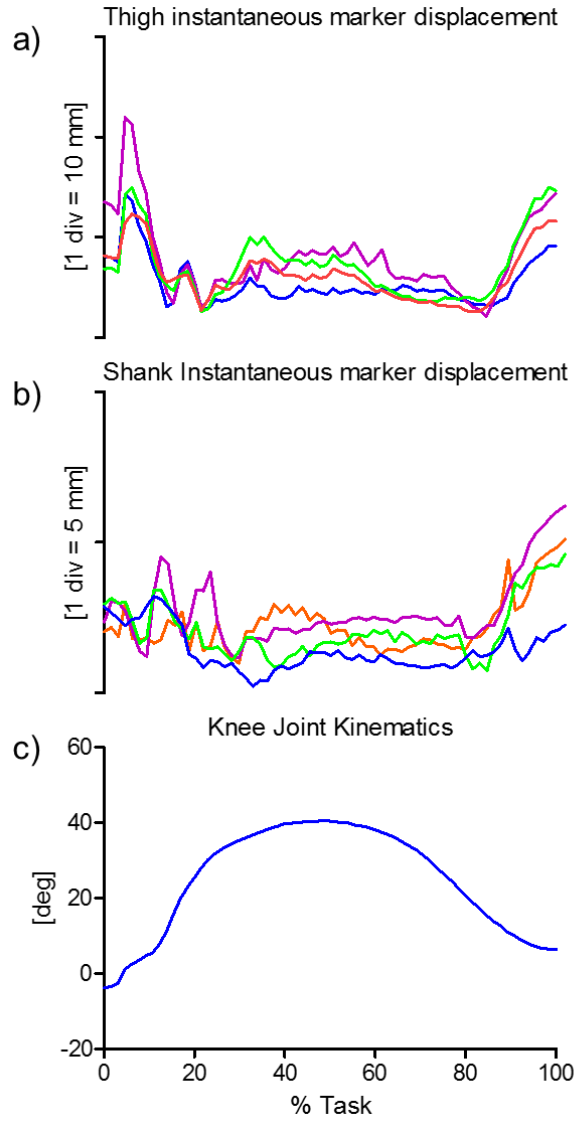


Figure 44 – LATERAL CUTTING MANOEUVRES. Magnitude of the instantaneous displacement of the four skin-markers glued on the thigh (a) and shank (b) represented in the relevant ACS. c) Relevant knee joint kinematics computed according to the convention proposed by Grood and Suntay (1983) (flexion/extension in blue, with flexion as positive).

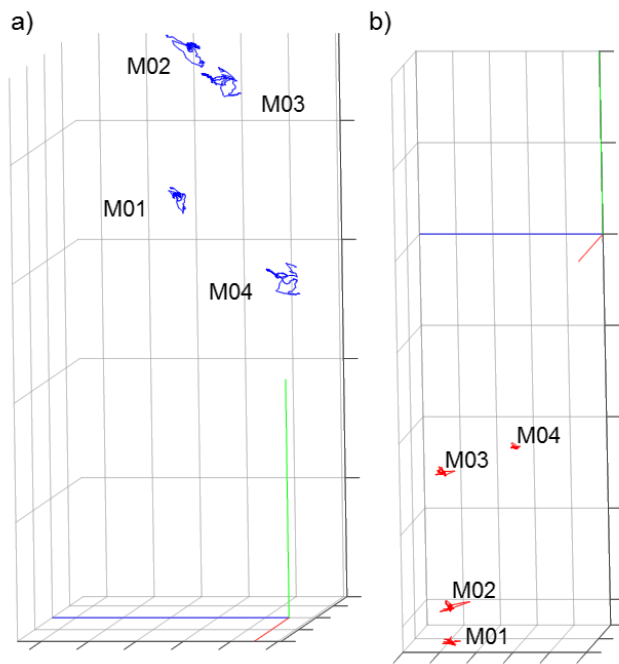


Figure 45 – HOPPING. Femur (a) and tibial (b) ACSs, and thigh and shank skin-marker trajectories (represented in blue and red, respectively). The axes of the ACSs are represented in red, green, and blue for the x (antero/posterior, div = 50 mm), y (superior/inferior, div = 50 mm), and z (right/left, a) div = 50 mm; b) div = 20 mm) directions, respectively.

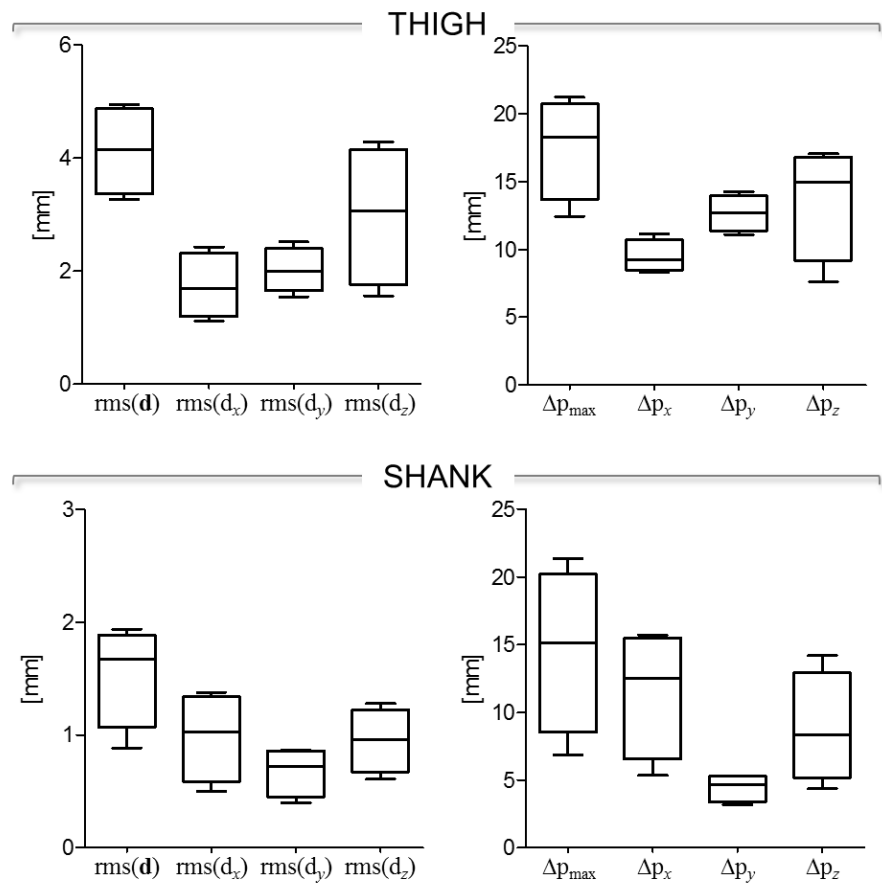


Figure 46 – HOPPING. Box-plots of the eight parameters ($\text{rms}(\mathbf{d})$, $\text{rms}(d_x)$, $\text{rms}(d_y)$, and $\text{rms}(d_z)$, in the left panel; Δp_{max} , Δp_x , Δp_y , and Δp_z , in the right panel) that describe the STA affecting the four skin-markers on the thigh and shank, respectively, during the movement. Outliers are also depicted.

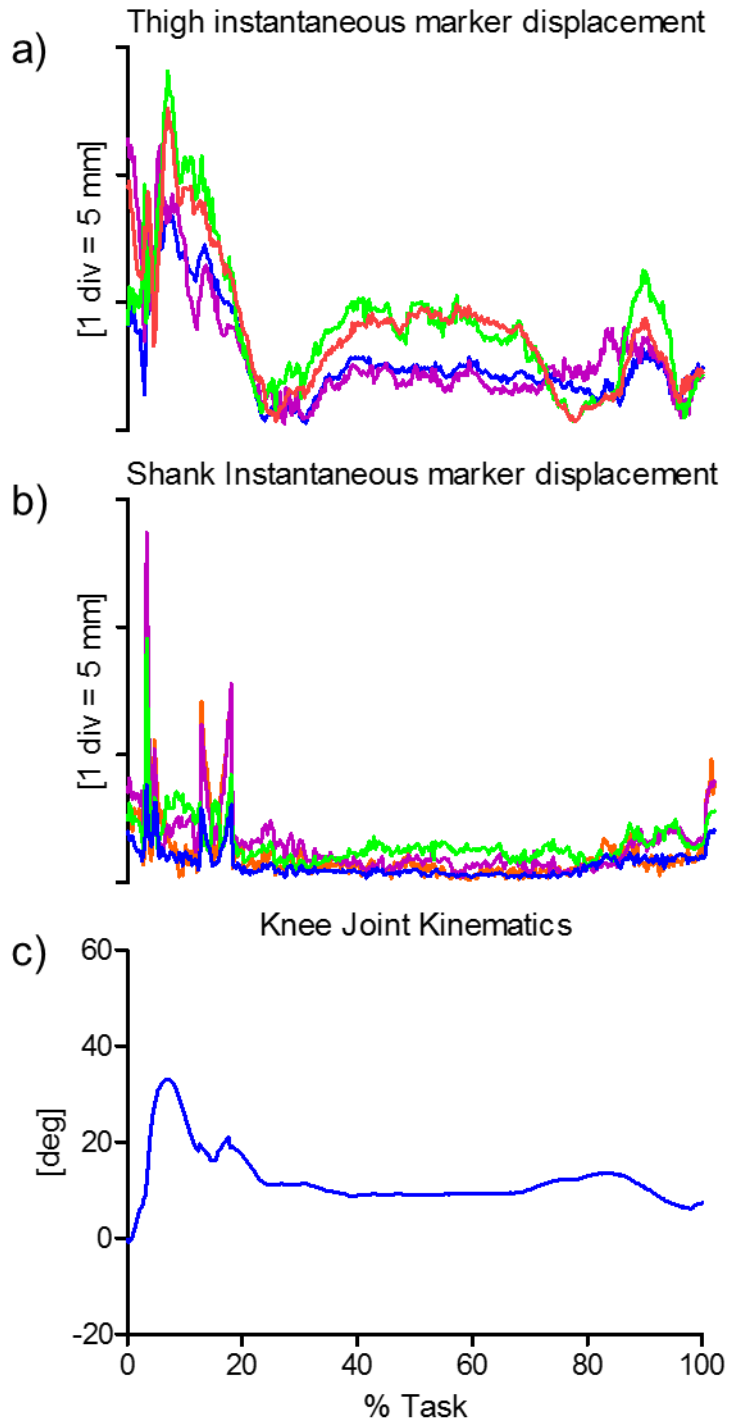


Figure 47 – HOPPING. Magnitude of the instantaneous displacement of the four skin-markers glued on the thigh (a) and shank (b) represented in the relevant ACS. c) Relevant knee joint kinematics computed according to the convention proposed by Grood and Suntay (1983) (flexion/extension in blue, with flexion as positive).

2.6. *In-vivo data from CSUOHIO*

Scientific articles of reference - A detailed description of the original data set can be found in Reinschmidt et al.,1997.

Experimental data description - Six skin markers were attached to each shank and thigh at standardized locations determined by anatomical landmarks (thigh: M01-M05 placed at 0, 40, and 80% of the distance between greater trochanter and distal end of the lateral femoral condyle; M03-M05 placed along 45, 70, and 95% of the distance between the anterior superior iliac spine and proximal patella. Shank: M01-M03 positioned at 20, 60, and 100% of the distance between the proximal end of the lateral tibial condyle and lateral malleolus; M04-M06 were attached at 0, 40, and 80% of the distance between the mid-tibial plateau and the distal end of the tibia. Three bone markers were also attached (femur: F1-F3; tibia: T1-T3), Fig. 48.

Anatomical coordinate system definitions – The tibial and femoral ACS were defined based on a standing trial where the subject stood in a neutral hip-wide fully extended knee position with the segments aligned with the force plate representing the laboratory coordinate system (LCS). During this standing trial, the ACS were assumed to be identical to the LCS, to allow for a consistent definition for both the skin and skeletal marker based ACS. A singular-value decomposition method (Soderkvist and Wedin, 1993) was used to calculate the transformation matrices (for each instant in time) between the femur and the tibia ACSs.

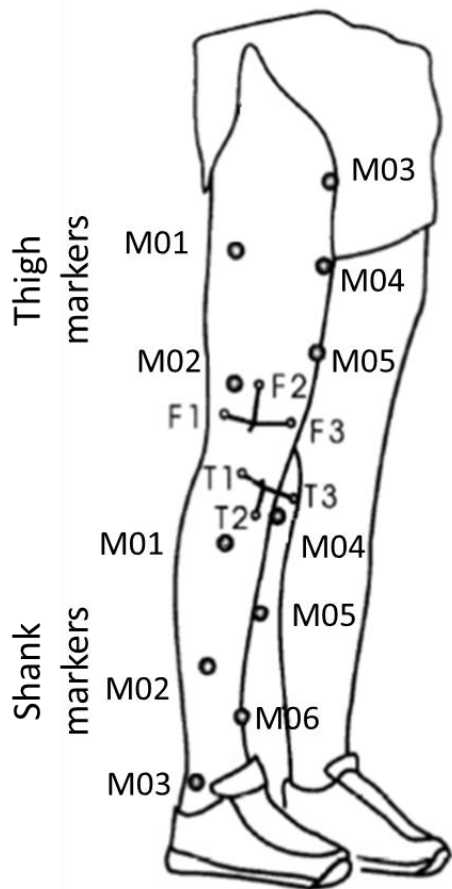


Figure 48 Bone marker (femur: F1-F3; tibia: T1-T3) and skin markers (thigh: M01-M05; shank: M01-M06) placement. M01-M05 were placed at 0,40, and 80% of the distance between greater trochanter and distal end of the lateral femoral condyle. M03-M05 were placed along 45, 70, and 95% of the distance between greater trochanter and distal end of the lateral femoral condyle. M01-M03 were positioned at 20, 60, and 100% of the distance between the proximal end of the lateral tibial condyle and lateral malleolus. M04-M06 were attached at 0, 40, and 80% of the distance between the mid-tibial plateau and the distal end of the tibia.

Measurement specifications - Right leg was filmed with three high-speed tine cameras (200 sample/s). The cameras were synchronized using LEDs triggered by a threshold detector connected to the force plate. Fluctuations in camera speed were corrected with timing information from internal LEDs. Each frame was manually digitized, and camera coordinates were filtered with a bi-directional fourth order low-pass Butterworth filter with a 10 Hz cut-off frequency determined from a residual analysis (Winter, 1990). Marker coordinates were time normalized with respect to stance phase and the spatial marker positions were calculated using DLT (Abdel-Aziz and Karara, 1971). The calibration frame available was not optimal due to the small number of calibration points (Hatze, 1988) and due to the small size of the frame (Wood and Marshall, 1986). This was of particular concern for the proximal thigh markers which were typically outside the calibrated volume. To assess the appropriateness of

the DLT model for each marker and to estimate the accuracy in determining the knee rotations, lens distortion errors were estimated from residuals of the three-dimensional reconstruction. Errors (residuals) for the markers were typically 2.5 mm. In the worst case, a 2.5 mm lens distortion could lead to about a 2 deg error in orientation of the skeletal segments, and a 1 deg error for the external segments. However, lens distortion tends to be in the same direction on the same segment, and therefore has a considerably smaller effect on joint rotations. Additionally, the 2.5 mm residuals also include errors due to the imperfect synchronization of the cameras affecting similarly the skin and skeletal marker based segments. Differences between skin and skeletal knee rotations well in excess of 2 deg cannot be attributed to inaccuracies of the motion analysis system. Random digitization errors were, after filtering, negligible.

Ground truth - Intracortical Hofmann bone pins (2.5 mm diameter) with triads of reflective markers were inserted under local anesthesia into the lateral tibia1 and femoral condyles of the subject's right leg. For one subject, skin marker based knee kinematics were also recorded prior to surgery to identify possible changes in running style due to the pin insertion. Knee kinematics showed a small (< 3 deg) shift from pre- to post-surgery condition for all rotations, attributed to slightly different standing trials used to define the anatomical coordinate systems. None of the subjects stated that his ability to run was affected by the pins.

2.6.1. Data sample 18: running

Subject characteristics - A male subject whose specific characteristics are not known was randomly selected out of three male subjects (age = 25.7 ± 2.1 y.o., height = 1.87 ± 0.10 m, mass = 85.5 ± 9.6 kg).

Motor task description - Stance phase of five heel-toe running trials (2.9 ± 0.2 m/s). The subjects wore slightly altered running shoes (Adidas Equipment Cushioning, 1994).

STA characteristics - Skin-marker trajectories in the thigh and shank ACSs are depicted in Fig. 49. Trajectories were filtered with a bi-directional fourth order low-pass Butterworth filter with a 10 Hz cutoff frequency. Statistical data describing the relevant STAs are shown in Fig. 50. Magnitude of the instantaneous displacement of thigh and shank skin-markers along with the knee joint angular kinematics is depicted in Fig.51.

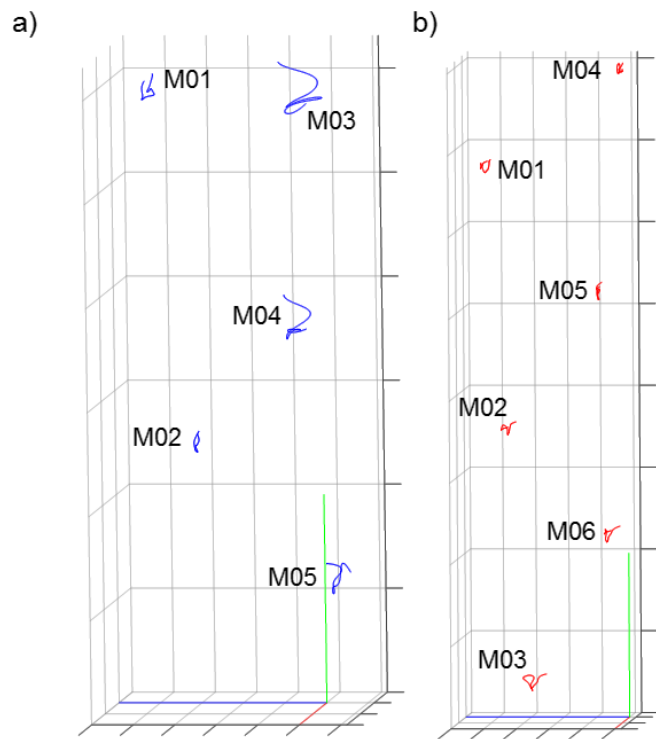


Figure 49 – Femur (a) and tibial (b) ACSs, and thigh and shank skin-marker trajectories (represented in blue and red, respectively). The axes of the ACSs are represented in red, green, and blue for the x (antero/posterior, div = 50 mm), y (superior/inferior, div = 50 mm), and z (right/left, div = 20 mm) directions, respectively.

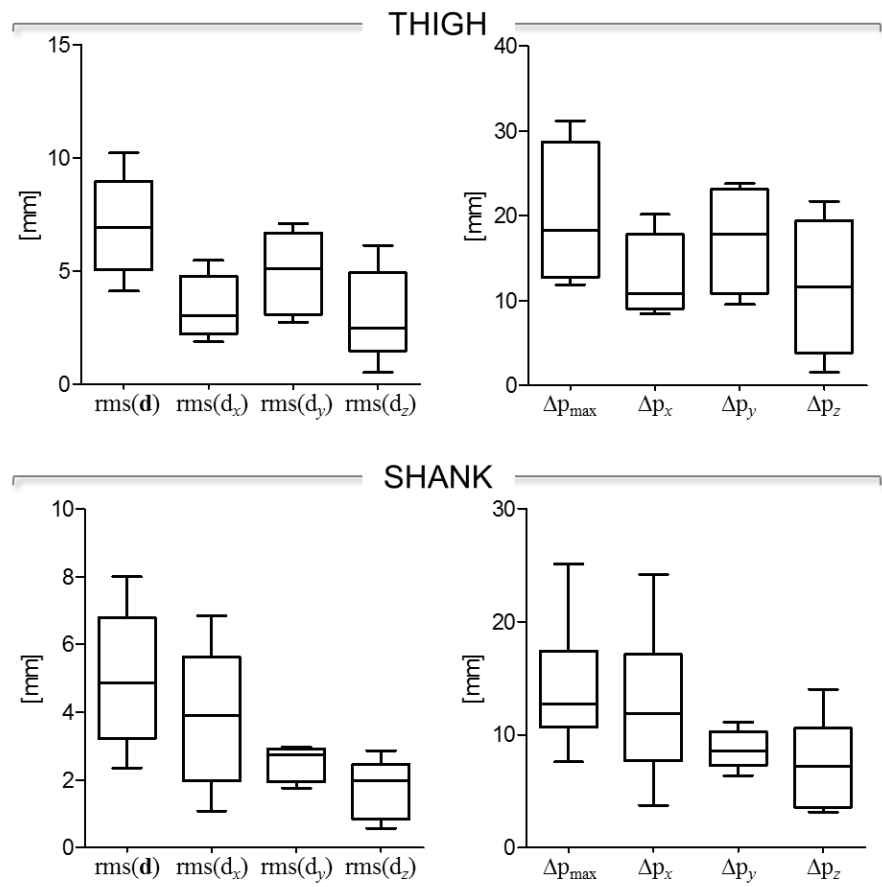


Figure 50 –Box-plots of the eight parameters ($\text{rms}(\mathbf{d})$, $\text{rms}(\mathbf{d}_x)$, $\text{rms}(\mathbf{d}_y)$, and $\text{rms}(\mathbf{d}_z)$, in the left panel; Δp_{\max} , Δp_x , Δp_y , and Δp_z , in the right panel) that describe the STA affecting the five and six skin-markers on the thigh and shank, respectively, during the movement. Outliers are also depicted.

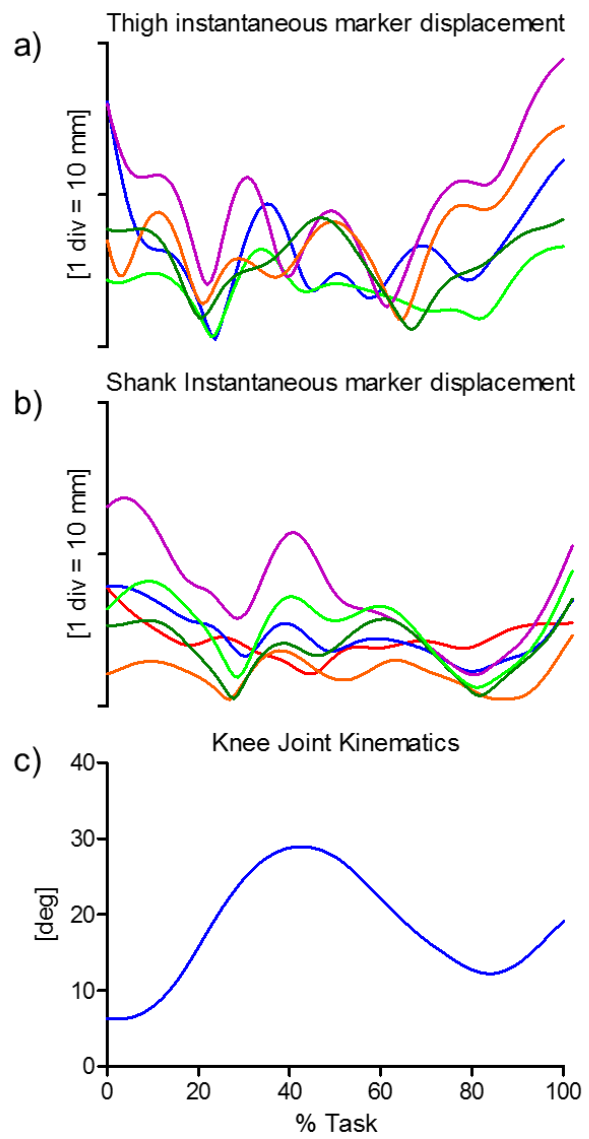


Figure 51 –Magnitude of the instantaneous displacement of the five and six skin-markers glued on the thigh (a) and shank (b) represented in the relevant ACS. c) Relevant knee joint kinematics computed according to the convention proposed by Grood and Suntay (1983) (flexion/extension in blue, with flexion as positive).

2.7. In-vivo data from UNIMELB

Scientific articles of reference - A detailed description of the original data set can be found in Akbarshahi et al. (2010).

Experimental data description - Ten reflective markers were placed on each subject's left leg (Fig. 52). Markers were positioned on the anterior and lateral aspects of the mid and distal third of the thigh (M02–M06), the mid anterior and lateral aspects of the shank (M01–M03), the lateral femoral epicondyle (M01) and the patella (M07).

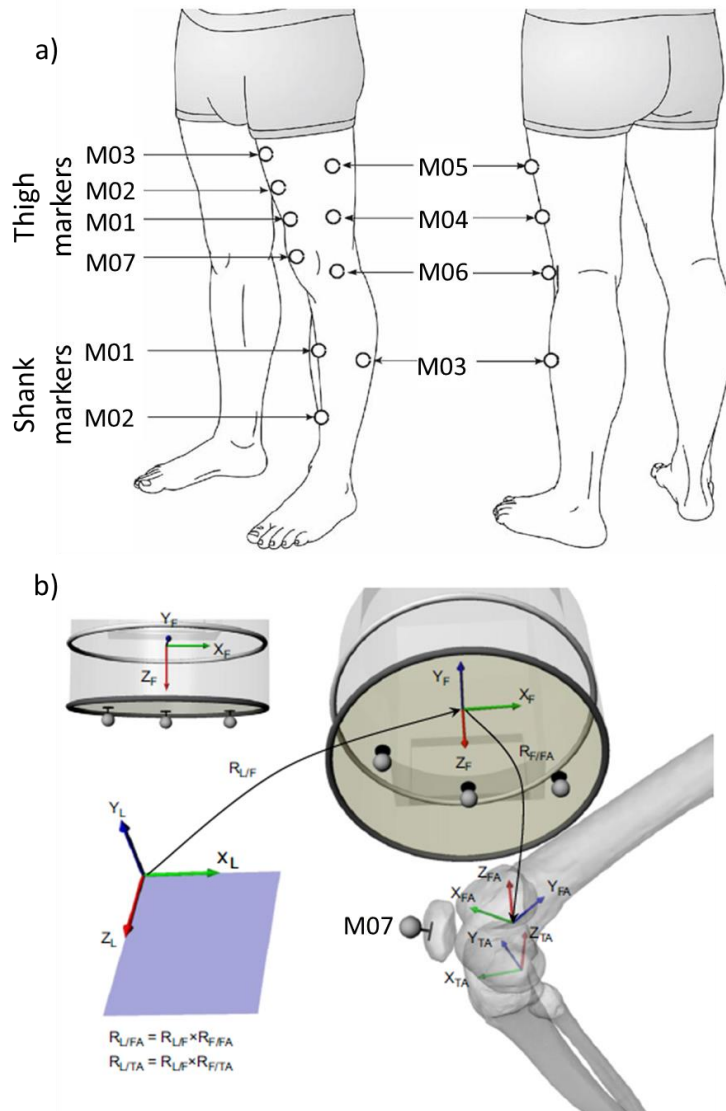


Figure 52 a) Schematic diagram showing the location of the skin-markers. Marker numbers are given as in the data samples 2, 4, 7, 15. B) three retro-reflective/radio-opaque markers were used to derive the transformation matrix ($R_{L/F}$) between the laboratory coordinate system (X_L , Y_L , Z_L) and the fluoroscopy coordinate system (X_F , Y_F , Z_F). Following the registration of the 3D bone models to the 2D X-ray images, the transformation matrices ($R_{F/FA}$ and $R_{F/TA}$) between the anatomical coordinate systems of the femur and tibia and the fluoroscopy coordinate system were calculated. (L: laboratory coordinate system; F: fluoroscopy coordinate system; TA: lower leg (tibia/fibula) anatomical coordinate system, M07: patellar marker used for synchronization).

Anatomical coordinate system definitions - ACSs were defined using the 3D MRI-based femur and tibia models. Bone-embedded as described in Fernandez et al. (2008) and Eckhoff et al. (2005).

Measurement specifications - The instantaneous markers position was reconstructed using a 9-camera stereophotogrammetric system (VICON 512 with M1 cameras) acquiring at 120 sample/s. The measurement volume was smaller than a 2-m-sided cube.

Ground truth - An X-ray fluoroscopy unit (Pulsera, Philips) operating in pulsed mode at 30 sample/s was used. were configured to acquire X-ray images at a maximal frame rate of 30 sample/s. Three radio-opaque reflective markers, visible in both stereophotogrammetric and fluoroscopy systems, were placed on a plane parallel to the image plane of the X-ray unit. These markers were used to synchronize data between the two systems using the distance between these and the marker on the patella and to perform relevant coordinate systems transformations. The X-ray images were corrected for image distortion, and the projective parameters of the X-ray system were determined using a calibration routine (Banks and Hodge, 1996). The 3D MRI-based model of the femur and of the tibia were acquired from a 3T Siemens MRI device and they were registered to the two dimensional X-ray images using custom software that iteratively matched the model pose to the X-ray images. Maximum errors obtained for the fluoroscopy measurements were 1.5mm for in-plane translations, 3mm for translations normal to the image plane, and 0.61 for rotations in all planes.

2.7.1. Data samples 2,4,7,15: hip axial rotation, open-chain knee flexion, treadmill walking, and step-up

Subject characteristics - A 34 y.o. male healthy subject. Height = 1.76 m, mass = 74 kg.

Motor task description - hip axial rotation with the knee extended and the foot resting in the centre of a swivel disc; open-chain knee flexion; walking on a treadmill (data were visible only from mid-swing to mid-stance due to the limited imaging field of view and occlusion from the contralateral leg); and a step-up.

STA characteristics - Skin-marker trajectories in the thigh and shank ACSs are depicted in Figs. 53, 56, 59, 62, for hip axial rotation, open-chain knee flexion, treadmill walking, and step-up, respectively. Stereophotogrammetric data were acquired at 120 Hz and then down-sampled to 30 Hz. Statistical data describing the STAs are shown in Figs. 54, 57, 60, 63, for hip axial rotation, open-chain knee flexion, treadmill walking, and step-up, respectively. For each motor task, the magnitude of the instantaneous displacement of thigh and shank skin-markers along with the knee joint angular kinematics are depicted in Figs. 55, 58, 61, 64, for hip axial rotation, open-chain knee flexion, treadmill walking, and step-up, respectively.

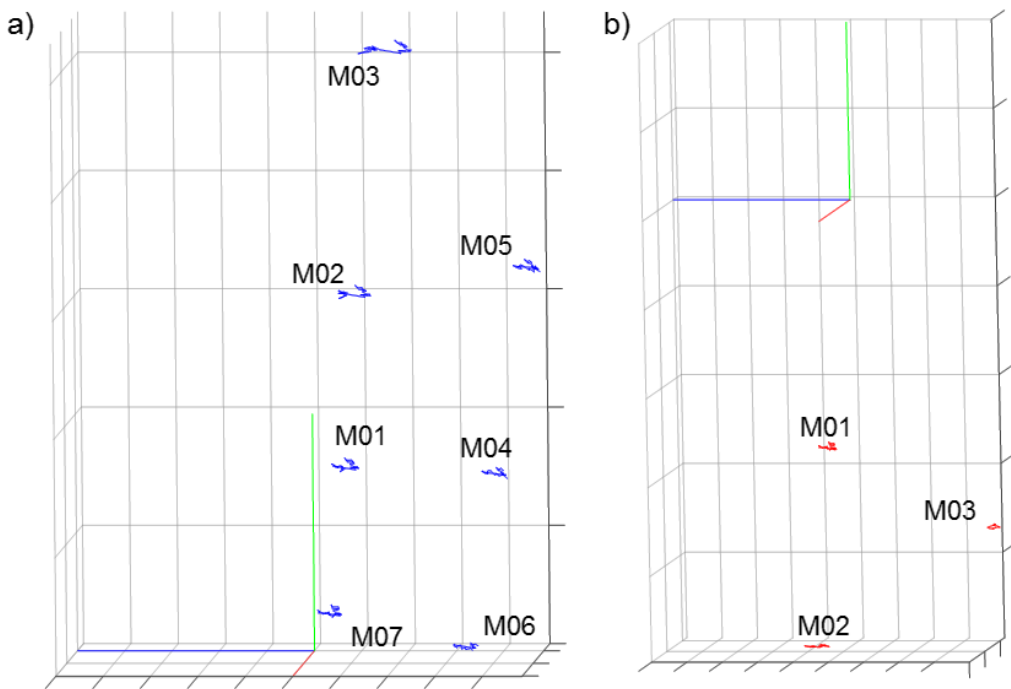


Figure 53 – HIP AXIAL ROTATION. Femur (a) and tibial (b) ACSs, and thigh and shank skin-marker trajectories (represented in blue and red, respectively). The axes of the ACSs are represented in red, green, and blue for the x (antero/posterior, div = 50 mm), y (superior/inferior, div = 50 mm), and z (right/left, div = 20 mm) directions, respectively.

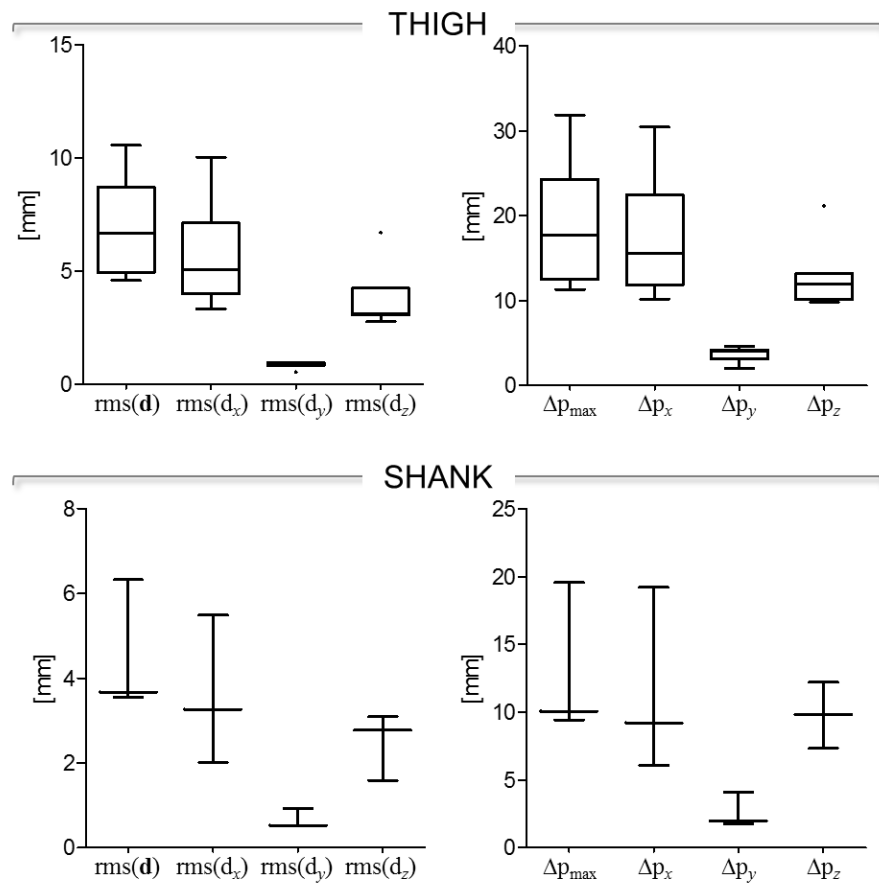


Figure 54 – HIP AXIAL ROTATION. Box-plots of the eight parameters ($\text{rms}(\mathbf{d})$, $\text{rms}(d_x)$, $\text{rms}(d_y)$, and $\text{rms}(d_z)$, in the left panel; Δp_{\max} , Δp_x , Δp_y , and Δp_z , in the right panel) that describe the STA affecting the six and three skin-markers on the thigh and shank, respectively, during the movement. Outliers are also depicted.

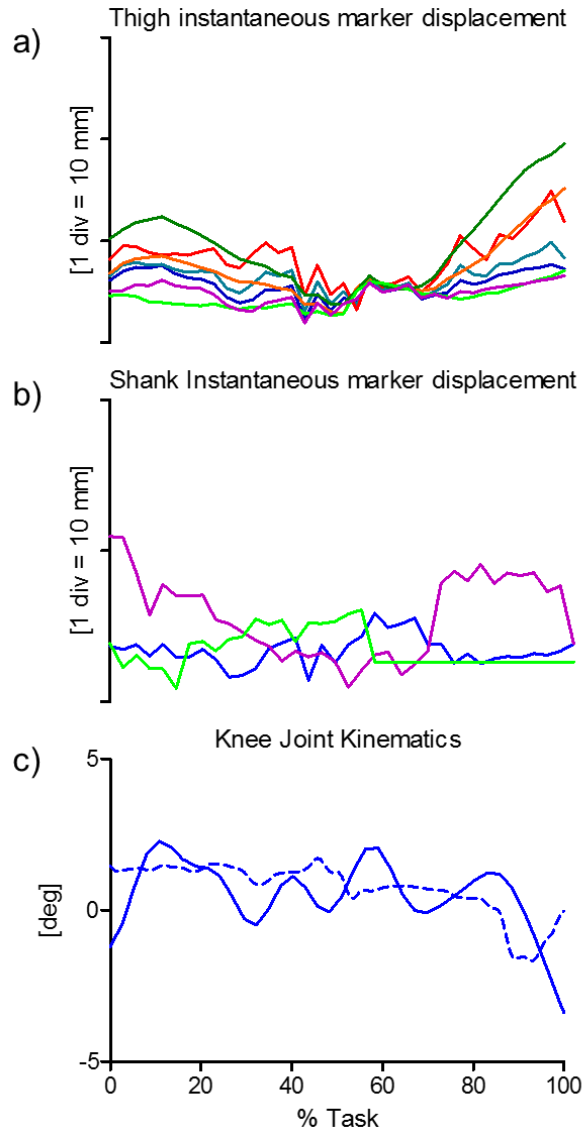


Figure 55 – HIP AXIAL ROTATION. Magnitude of the instantaneous displacement of the six and three skin-markers glued on the thigh (a) and shank (b) represented in the relevant ACS. c) Relevant knee joint kinematics computed according to the convention proposed by Grood and Suntay (1983) (flexion/extension in blue, with flexion as positive – fluorokinematics in continuous line and the best performing marker-based kinematic in dotted line).

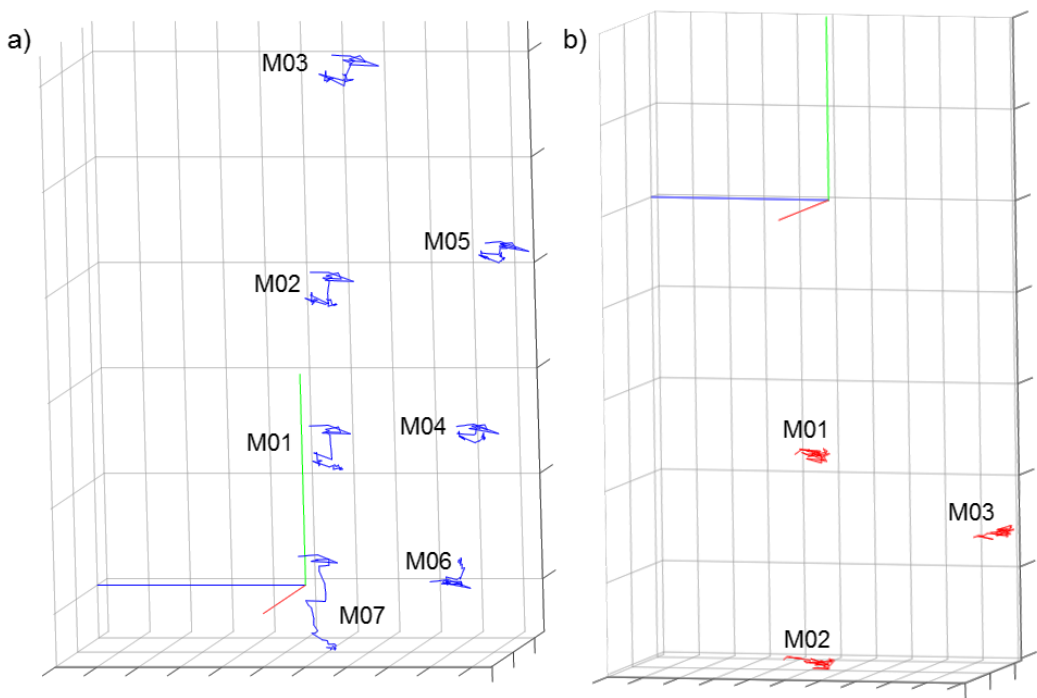


Figure 56 – OPEN-CHAIN KNEE FLEXION. Femur (a) and tibial (b) ACSs, and thigh and shank skin-marker trajectories (represented in blue and red, respectively). The axes of the ACSs are represented in red, green, and blue for the x (antero/posterior, div = 50 mm), y (superior/inferior, div = 50 mm), and z (right/left, div = 20 mm) directions, respectively.

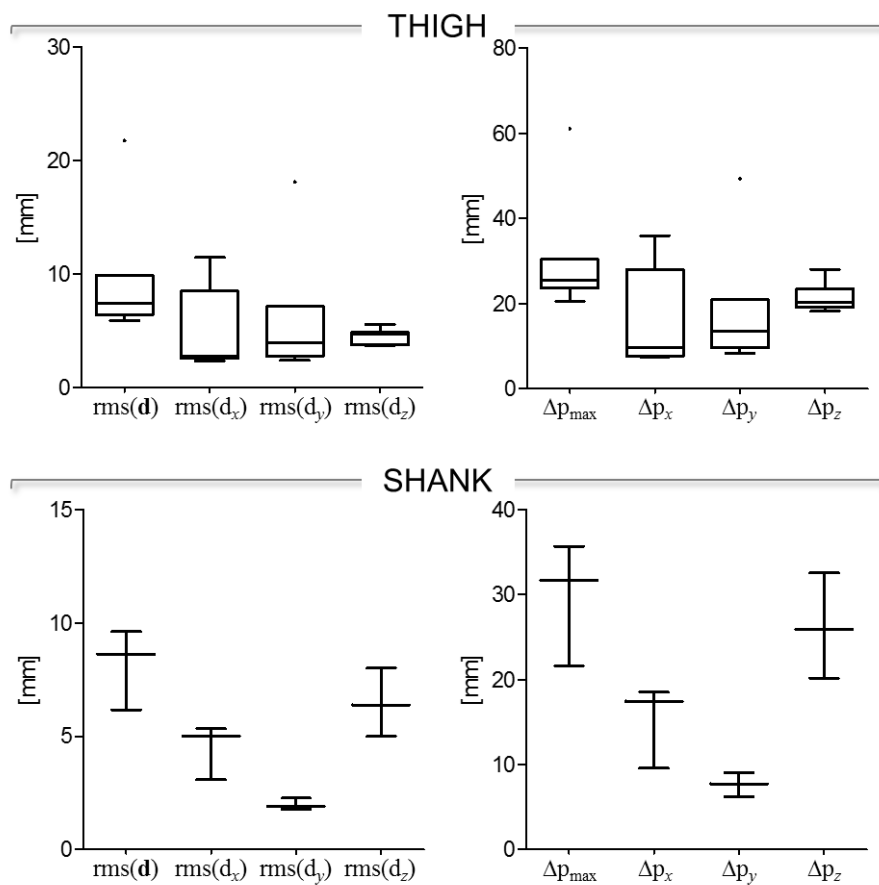


Figure 57 – OPEN-CHAIN KNEE FLEXION. Box-plots of the eight parameters (rms(**d**), rms(d_x), rms(d_y), and rms(d_z), in the left panel; Δp_{\max} , Δp_x , Δp_y , and Δp_z , in the right panel) that describe the STA affecting the six and three skin-markers on the thigh and shank, respectively, during the movement. Outliers are also depicted.

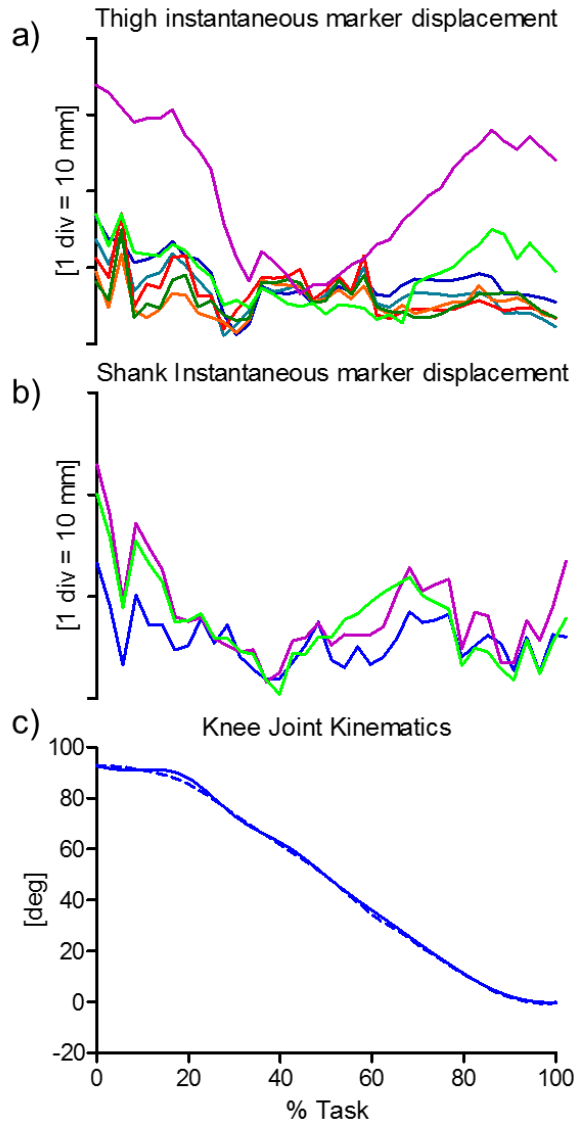


Figure 58 – OPEN-CHAIN KNEE FLEXION. Magnitude of the instantaneous displacement of the six and three skin-markers glued on the thigh (a) and shank (b) represented in the relevant ACS. c) Relevant knee joint kinematics computed according to the convention proposed by Grood and Suntay (1983) (flexion/extension in blue, with flexion as positive – fluoro kinematics in continuous line and the best performing marker-based kinematic in dotted line).

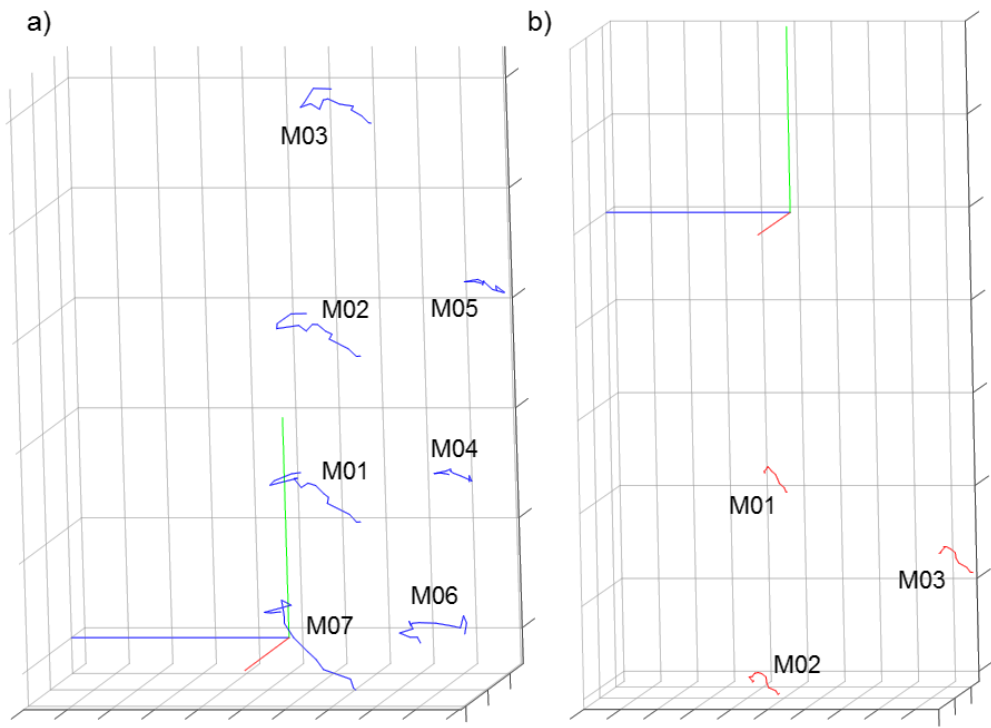


Figure 59 – WALKING ON A TREADMILL. Femur (a) and tibial (b) ACSs, and thigh and shank skin-marker trajectories (represented in blue and red, respectively). The axes of the ACSs are represented in red, green, and blue for the x (antero/posterior, div = 50 mm), y (superior/inferior, div = 50 mm), and z (right/left, div = 20 mm) directions, respectively.

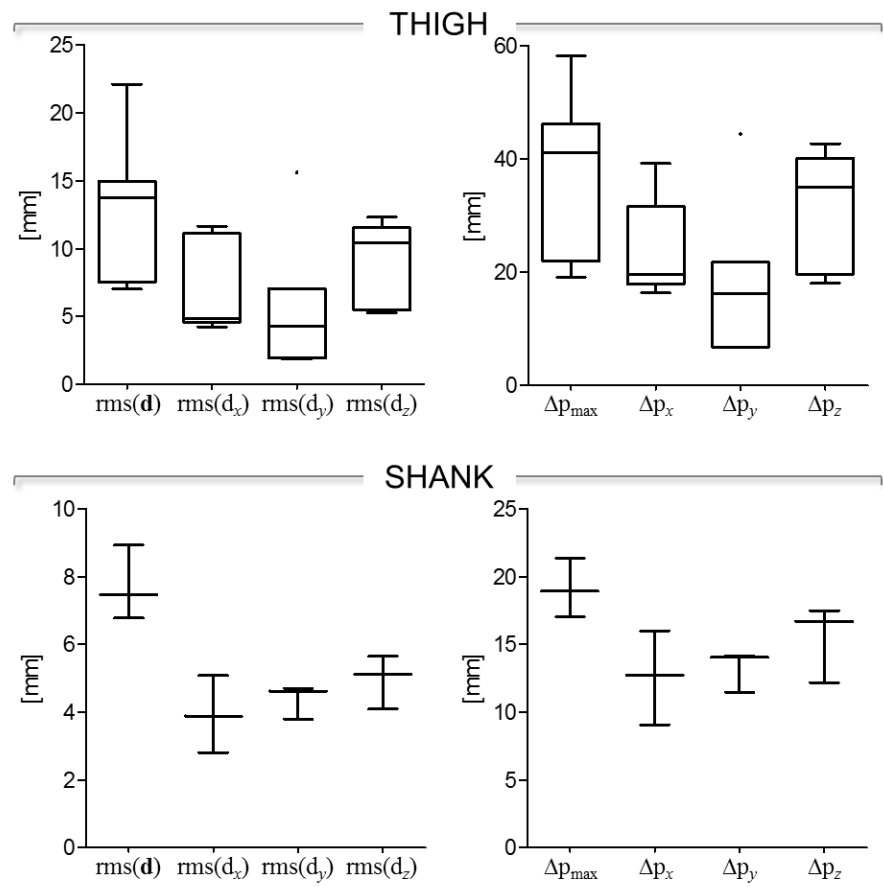


Figure 60 – WALKING ON A TREADMILL. Box-plots of the eight parameters ($\text{rms}(\mathbf{d})$, $\text{rms}(\mathbf{d}_x)$, $\text{rms}(\mathbf{d}_y)$, and $\text{rms}(\mathbf{d}_z)$, in the left panel; Δp_{\max} , Δp_x , Δp_y , and Δp_z , in the right panel) that describe the STA affecting the six and three skin-markers on the thigh and shank, respectively, during the movement. Outliers are also depicted.

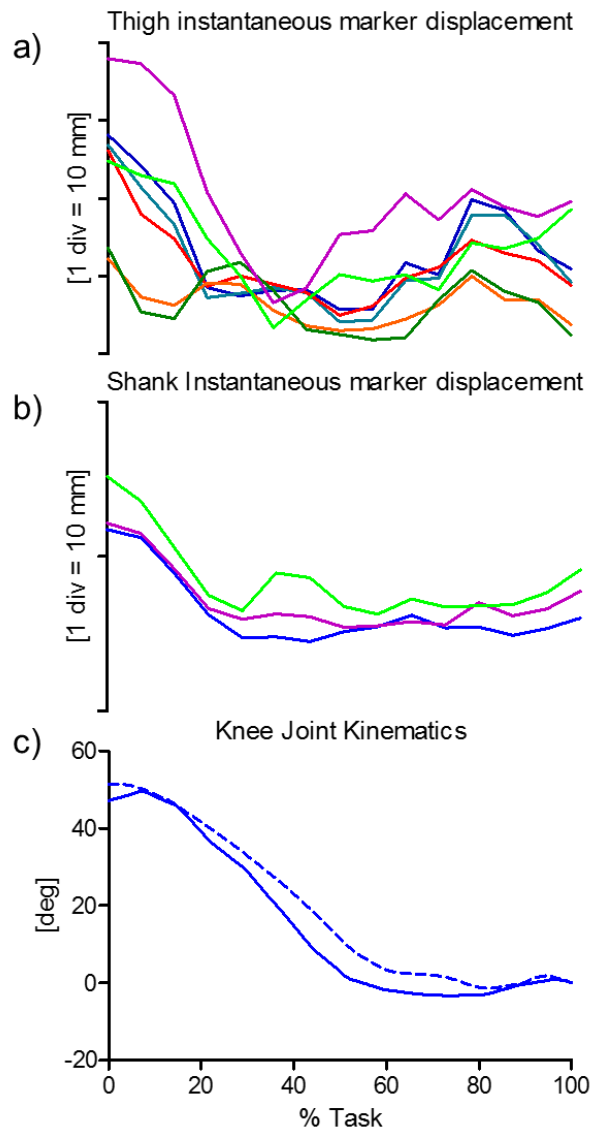


Figure 61 – WALKING ON A TREADMILL. Data were visible only from mid-swing to mid-stance. Magnitude of the instantaneous displacement of the six and three skin-markers glued on the thigh (a) and shank (b) represented in the relevant ACS. c) Relevant knee joint kinematics computed according to the convention proposed by Grood and Suntay (1983) (flexion/extension in blue, with flexion as positive – fluoro kinematics in continuous line and the best performing marker-based kinematic in dotted line).

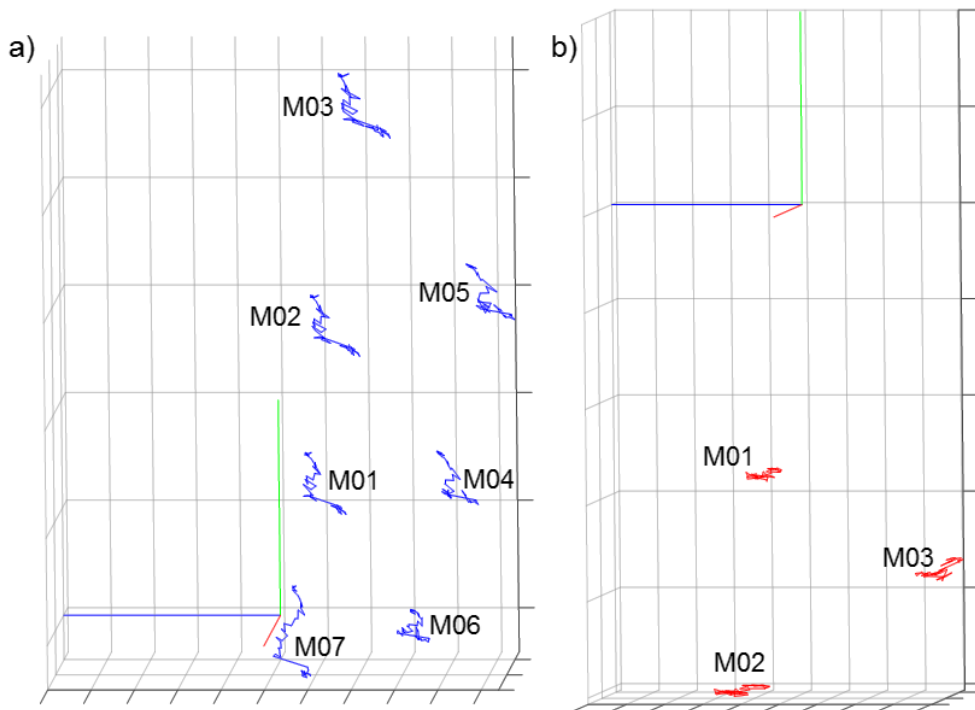


Figure 62 – STEP-UP. Femur (a) and tibial (b) ACSs, and thigh and shank skin-marker trajectories (represented in blue and red, respectively). The axes of the ACSs are represented in red, green, and blue for the x (antero/posterior, div = 50 mm), y (superior/inferior, div = 50 mm), and z (right/left, div = 20 mm) directions, respectively.

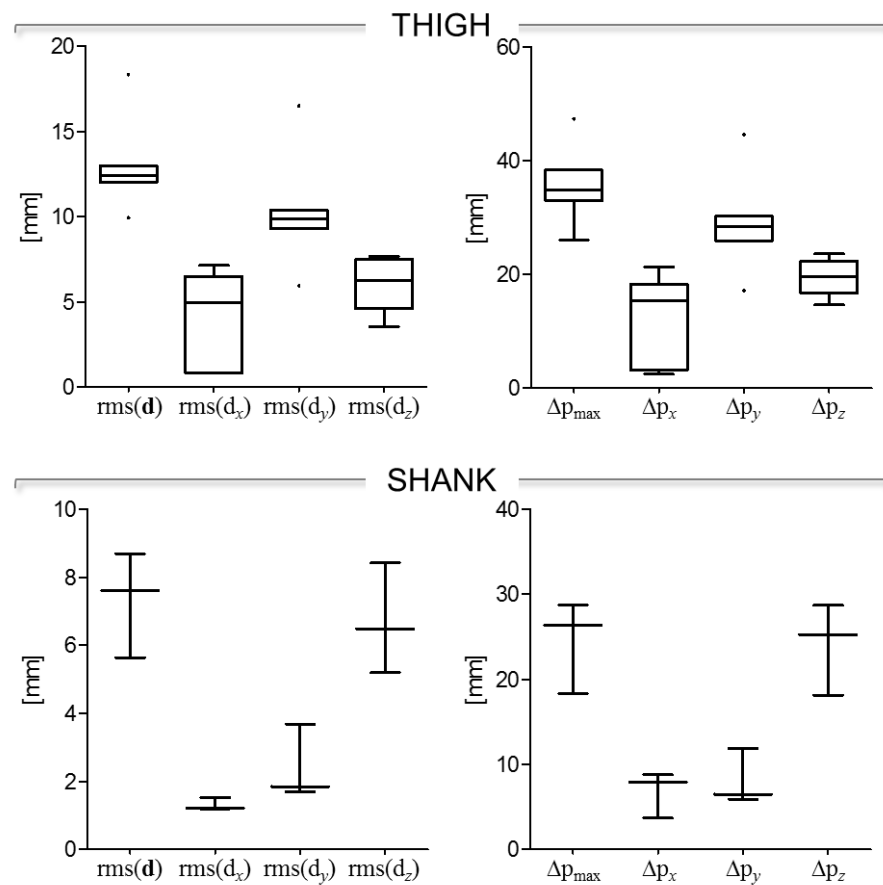


Figure 63 – STEP-UP. Box-plots of the eight parameters ($\text{rms}(\mathbf{d})$, $\text{rms}(d_x)$, $\text{rms}(d_y)$, and $\text{rms}(d_z)$, in the left panel; Δp_{\max} , Δp_x , Δp_y , and Δp_z , in the right panel) that describe the STA affecting the six and three skin-markers on the thigh and shank, respectively, during the movement. Outliers are also depicted.

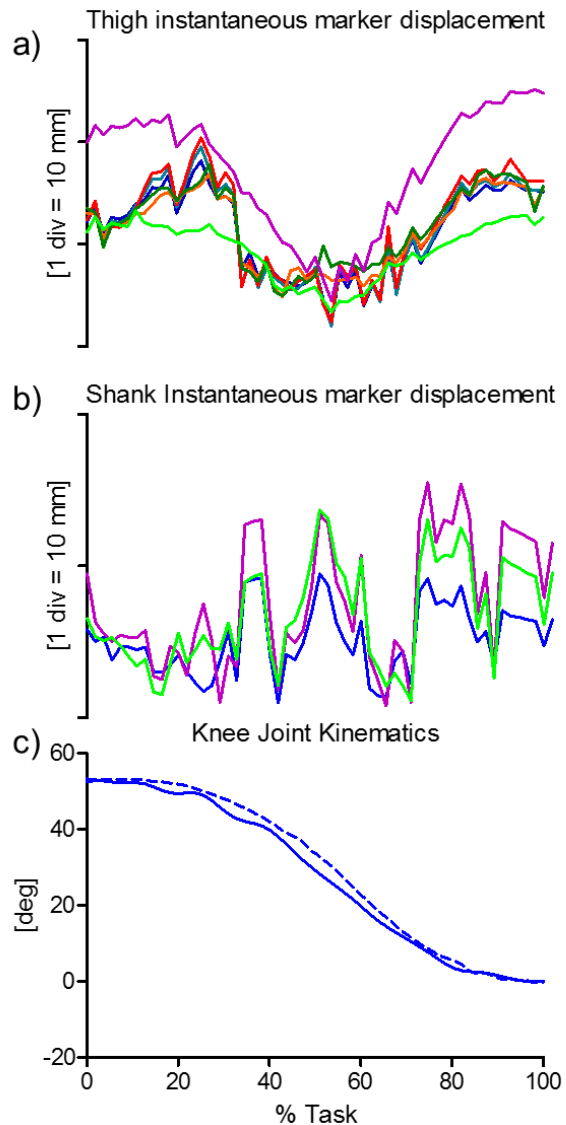


Figure 64 – STEP-UP. Magnitude of the instantaneous displacement of the six and three skin-markers glued on the thigh (a) and shank (b) represented in the relevant ACS. c) Relevant knee joint kinematics computed according to the convention proposed by Grood and Suntay (1983) (flexion/extension in blue, with flexion as positive – fluoro kinematics in continuous line and the best performing marker-based kinematic in dotted line).

2.8. *In-vivo data from S2M*

Scientific articles of reference - A detailed description of the original data set can be found in Dal Maso et al., (2014) and Dal Maso et al., (2015).

Experimental data description - Seven and eight markers were attached on the humeral and scapular regions, respectively. This included two markers on the humerus ALs (EL, EM, the third “AL marker” was the gleno-humeral joint centre optimally located via a functional approach (Begon et al., 2007)), three markers on the scapular ALs (AI, TS, AA), and seven and eight technical markers on the arm and over the region of the scapula, respectively. (Fig. 65).

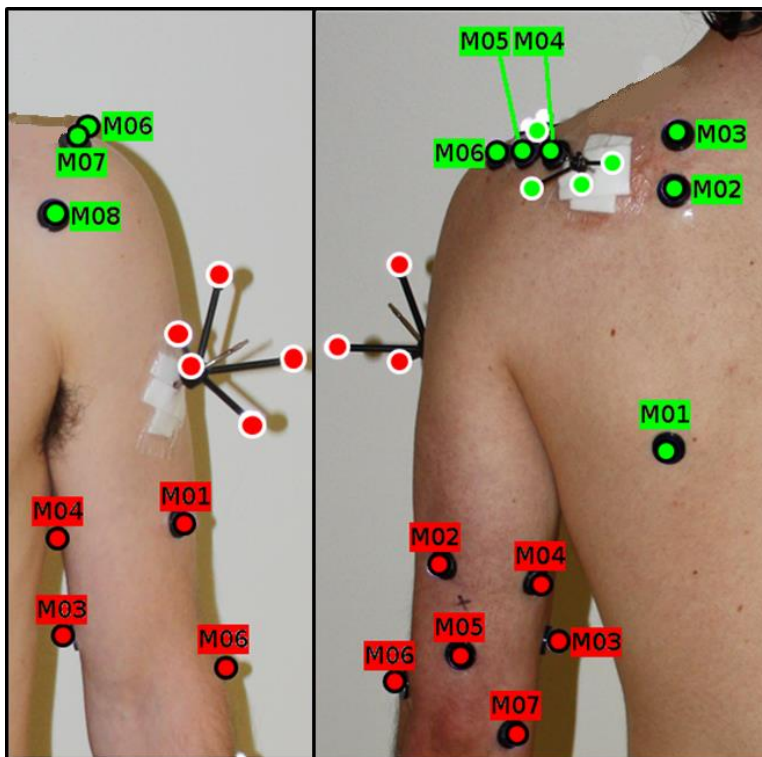


Figure 65 – Marker placement including both pin- and skin-marker clusters (over anatomical landmarks and in technical positions). Only the markers included in the data samples 20,21,23-31 are shown, for the scapula (in green, M02 = TS, M06 = AA, M01 = AI) and for the arm (in red, M06=EL, M07=EM).

Anatomical coordinate system definitions - Both humeral and scapular ACSs were determined according to the definitions proposed in Wu et al. (2005).

Measurement specifications - The instantaneous markers position was reconstructed using an 18-camera stereophotogrammetric system (VICON; Oxford Metrics Ltd., Oxford, UK; 5 cameras T20S and 13 cameras T40S) acquiring at 300 sample/s. The measurement volume was a 2.5-m-sided square, 1.6-m-height. A rigid stick was used to perform a spot-check of the stereophotogrammetric system accuracy and revealed an accuracy of 0.5 mm (min-max range).

Ground truth - Intracortical pins were inserted into the first third of the scapular spine and on the lateral aspect of the humerus just below the attachment of the middle deltoid of the participants' left side. Clusters of four and five reflective markers were secured on scapular and humeral pins, respectively. Pin locations were chosen to avoid muscles and the rigidity of the montage was manually checked.

2.8.1. Data samples 20,21,23,25: Arm elevations

Subject characteristics - A healthy male subject 27 y.o. Height = 1.65 m, mass = 57 kg.

Motor task description - The trial started with the arm relaxed at the side with thumb pointing forward referred to as neutral axial rotation. The following shoulder motions were analyzed: one arm elevation at their maximum range of motion in four planes of elevation adduction, abduction, flexion, and extension. The subject was asked to elevate his arm at his own pace without changing its axial rotation from the relaxed position. The elbow was kept extended throughout the elevations.

STA characteristics - Skin-marker trajectories in the scapula and arm ACSs are depicted in Figs. 66, 69, 72, 75, for arm elevations during adduction, abduction, flexion, and extension, respectively. Unfiltered data were used. Statistical data describing the STAs are shown in Figs. 67, 70, 73, 76, for arm elevations during adduction, abduction, flexion, and extension, respectively. For each motor task, the magnitude of the instantaneous displacement of scapula and arm skin-markers along with the shoulder joint angular kinematics are depicted in Figs. 68, 71, 74, 77, for arm elevations during adduction, abduction, flexion, and extension, respectively.

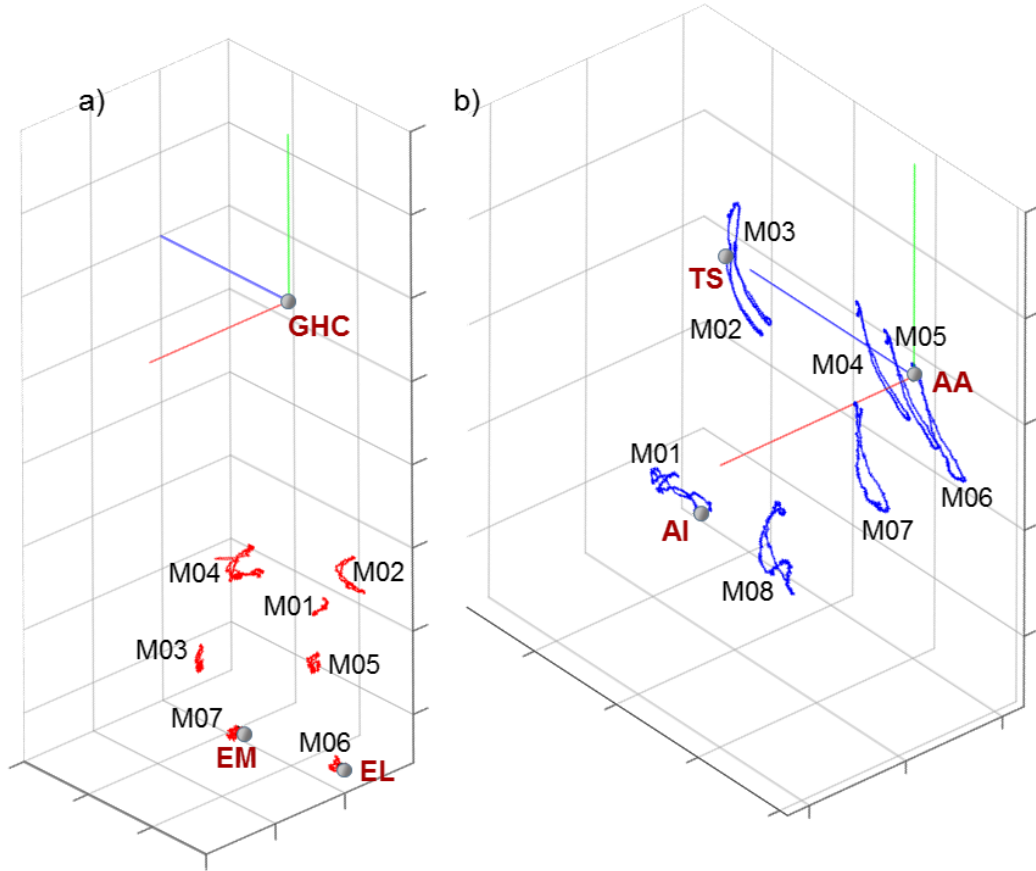


Figure 66 – ADDUCTION. Humeral (a) and scapular (b) ACSs, relevant ALs, and arm and scapula skin-marker trajectories (represented in red and blue, respectively). The axes of the ACSs are represented in red, green, and blue for the x (antero/posterior, div = 50 mm), y (superior/inferior, div = 50 mm), and z (right/left, div = 50 mm) directions, respectively.

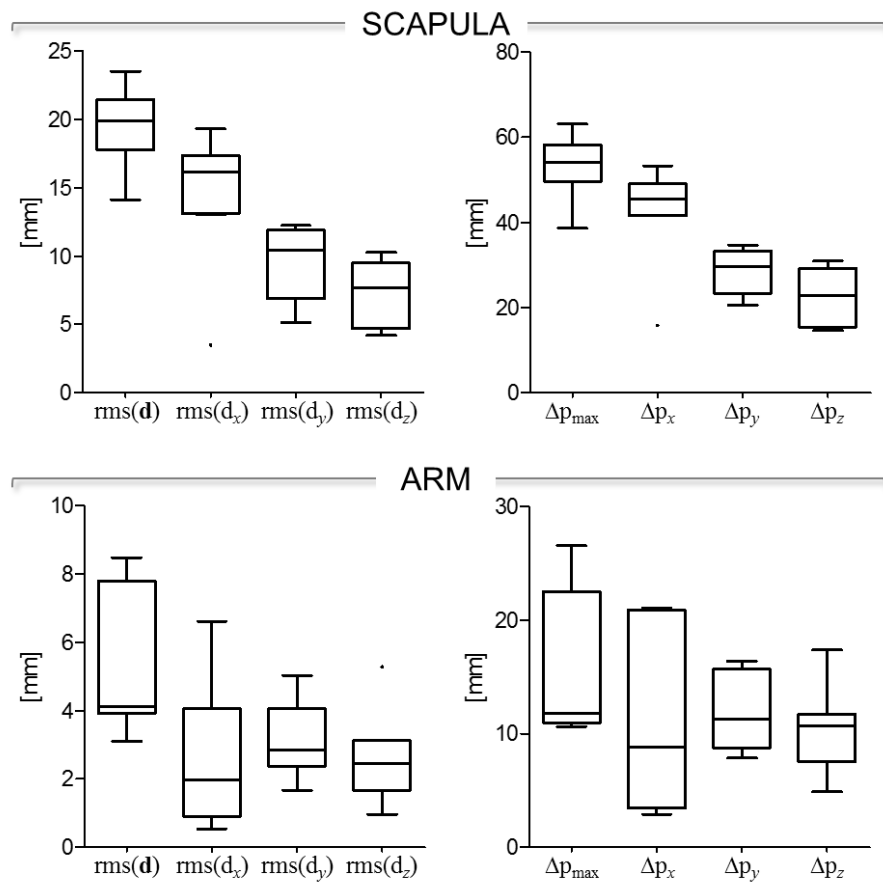


Figure 67 – ADDUCTION. Box-plots of the eight parameters (rms(d), rms(d_x), rms(d_y), and rms(d_z), in the left panel; Δp_{\max} , Δp_x , Δp_y , and Δp_z , in the right panel) that describe the STA affecting the eight and seven skin-markers on the scapula and arm, respectively, during the movement. Outliers are also depicted.

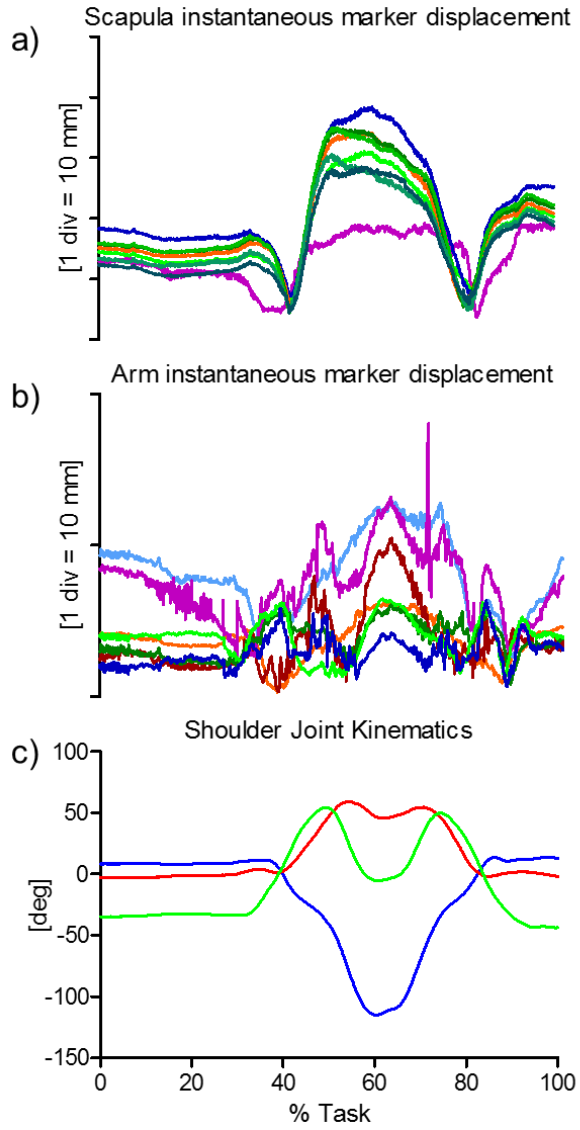


Figure 68 – ADDUCTION. Magnitude of the instantaneous displacement of the eight and seven skin-markers glued on the scapula (a) and arm (b) represented in the relevant ACS. c) Relevant shoulder kinematics calculated using the $X_t Z_f' Y_h''$ sequence (Bonnefoy-Mazure et al., 2012): rotation around the X_t axis of the thorax corresponding to the shoulder elevation (blue); rotation around the floating Z_f' axis corresponding to the shoulder flexion/extension (red); rotation around the Y_h'' axis of the humerus corresponding to the shoulder axial rotation (green). Superior elevation, flexion and internal rotations are positive.

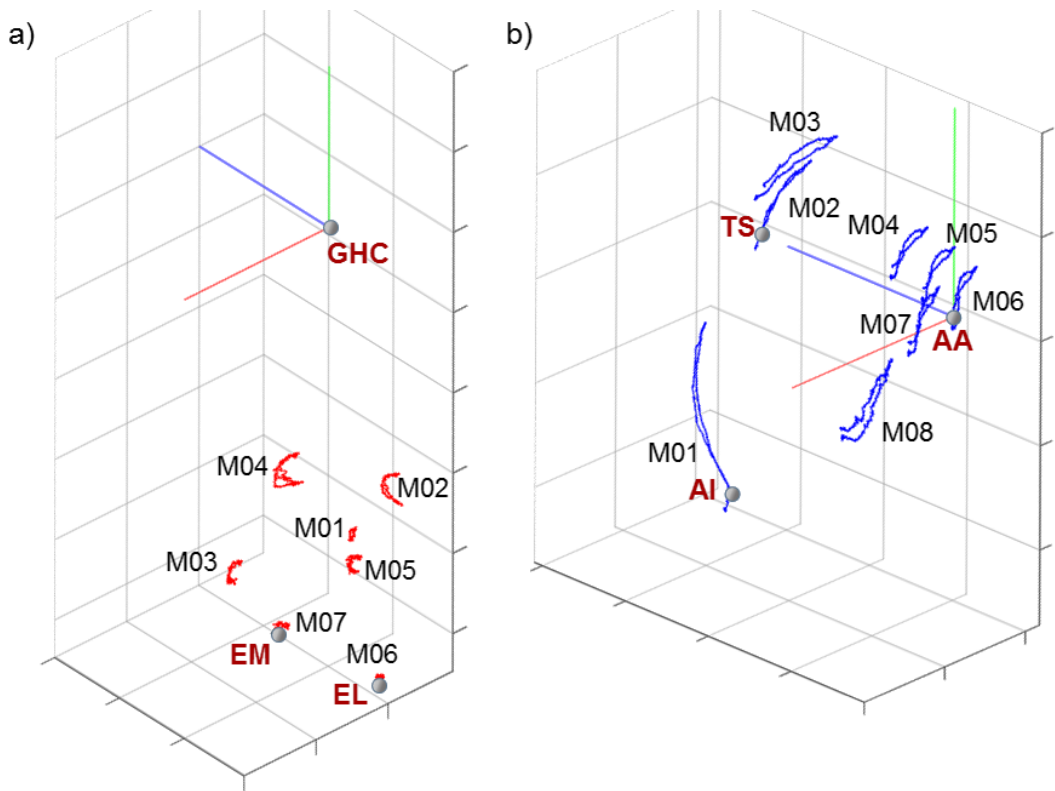


Figure 69 – ABDUCTION. Humeral (a) and scapular (b) ACSs, relevant ALs, and arm and scapula skin-marker trajectories (represented in red and blue, respectively). The axes of the ACSs are represented in red, green, and blue for the x (antero/posterior, div = 50 mm), y (superior/inferior, div = 50 mm), and z (right/left, div = 50 mm) directions, respectively.

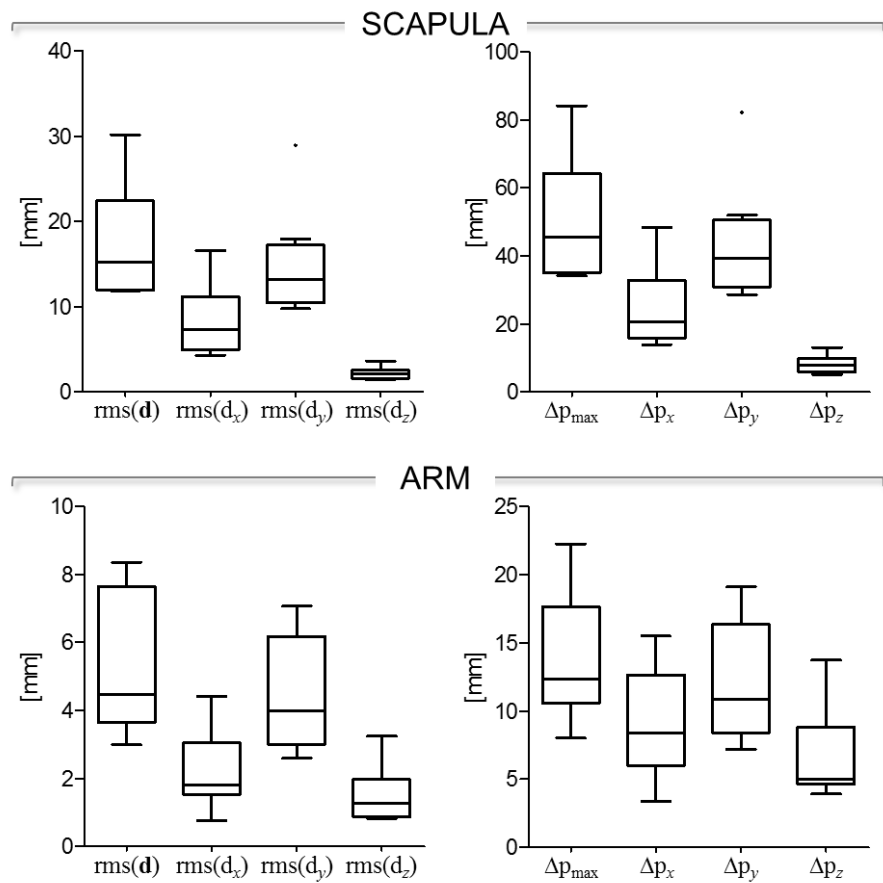


Figure 70 – ABDUCTION. Box-plots of the eight parameters ($\text{rms}(\mathbf{d})$, $\text{rms}(\mathbf{d}_x)$, $\text{rms}(\mathbf{d}_y)$, and $\text{rms}(\mathbf{d}_z)$, in the left panel; Δp_{\max} , Δp_x , Δp_y , and Δp_z , in the right panel) that describe the STA affecting the eight and seven skin-markers on the scapula and arm, respectively, during the movement. Outliers are also depicted.

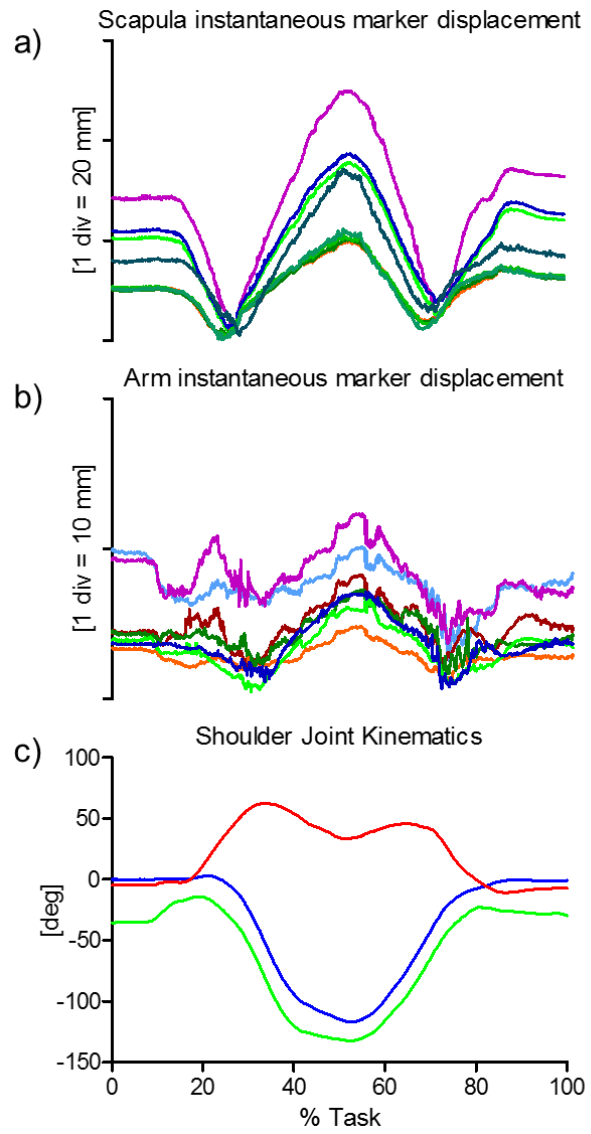


Figure 71 – ABDUCTION. Magnitude of the instantaneous displacement of the eight and seven skin-markers glued on the scapula (a) and arm (b) represented in the relevant ACS. c) Relevant shoulder kinematics calculated using the X_t Z_f' Y_h'' sequence (Bonnefoy-Mazure et al., 2012): rotation around the X_t axis of the thorax corresponding to the shoulder elevation (blue); rotation around the floating Z_f' axis corresponding to the shoulder flexion/extension (red); rotation around the Y_h'' axis of the humerus corresponding to the shoulder axial rotation (green). Superior elevation, flexion and internal rotations are positive.

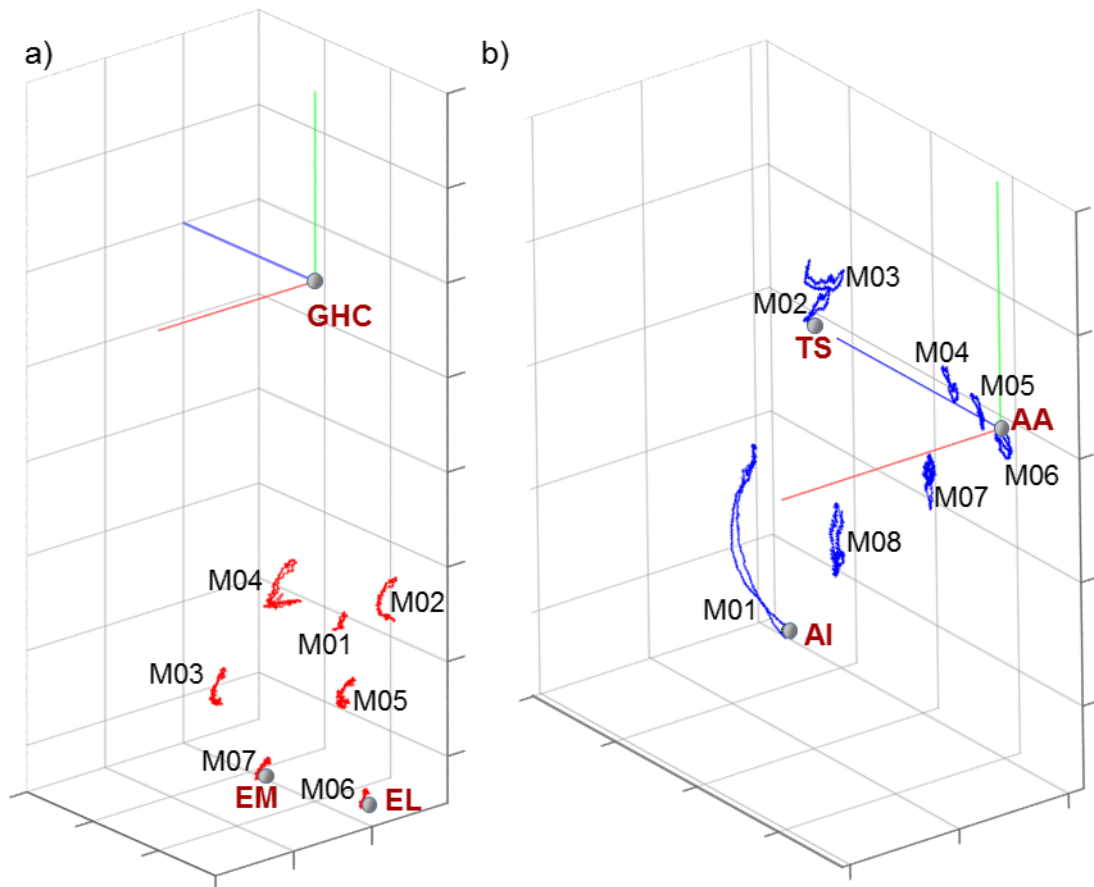


Figure 72 – FLEXION. Humeral (a) and scapular (b) ACSs, relevant ALs, and arm and scapula skin-marker trajectories (represented in red and blue, respectively). The axes of the ACSs are represented in red, green, and blue for the x (antero/posterior, div = 50 mm), y (superior/inferior, div = 50 mm), and z (right/left, div = 50 mm) directions, respectively.

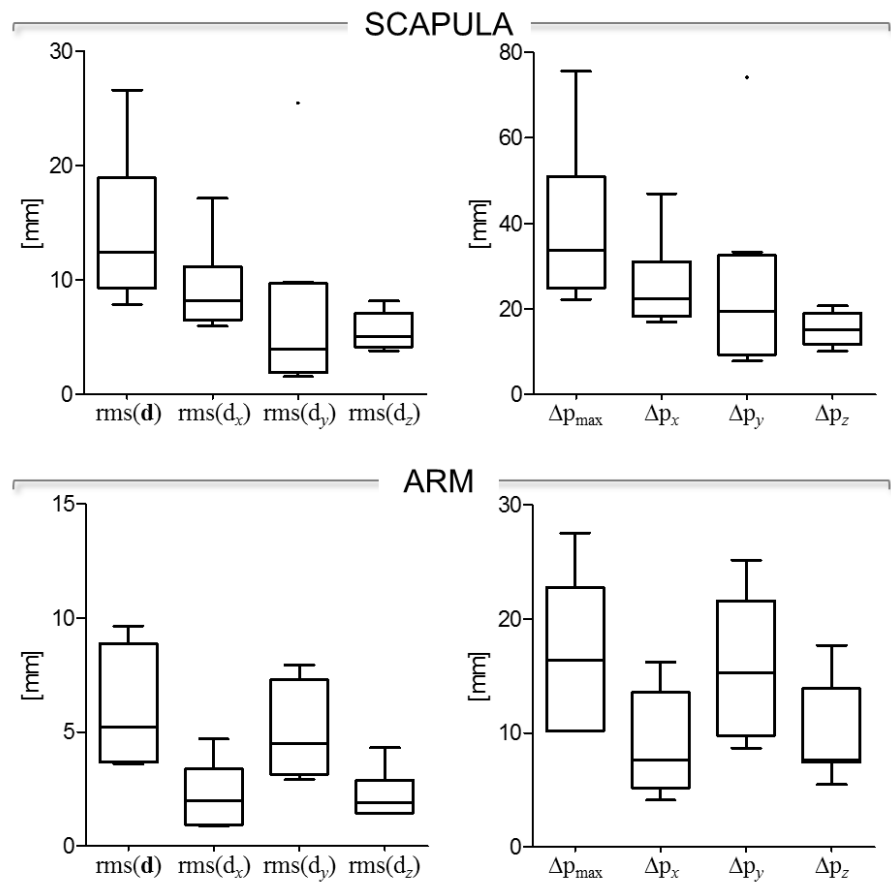


Figure 73 – FLEXION. Box-plots of the eight parameters ($\text{rms}(\mathbf{d})$, $\text{rms}(\mathbf{d}_x)$, $\text{rms}(\mathbf{d}_y)$, and $\text{rms}(\mathbf{d}_z)$, in the left panel; Δp_{\max} , Δp_x , Δp_y , and Δp_z , in the right panel) that describe the STA affecting the eight and seven skin-markers on the scapula and arm, respectively, during the movement. Outliers are also depicted.

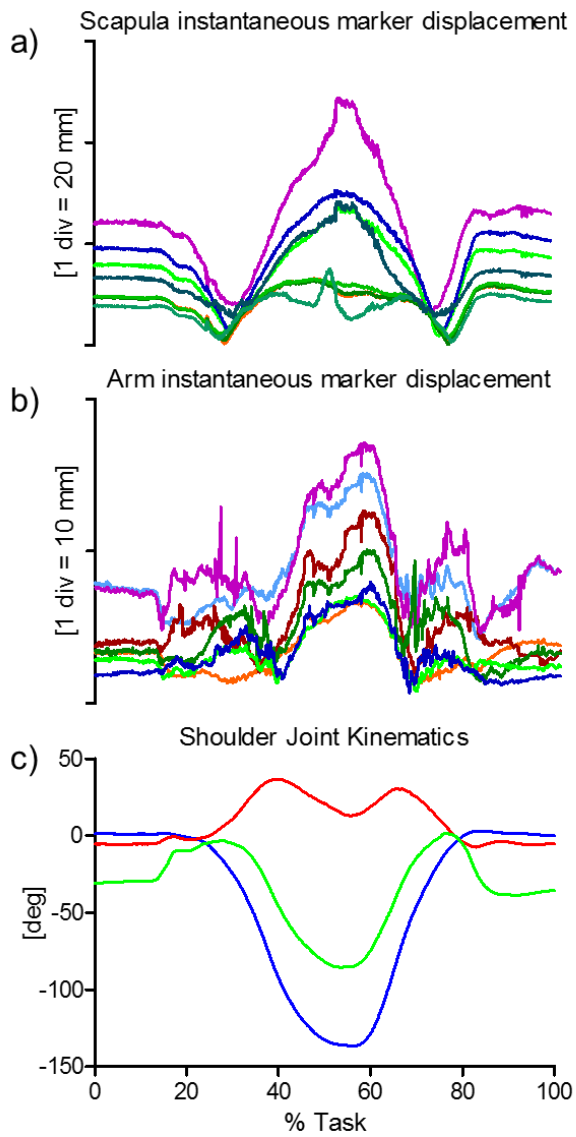


Figure 74 – FLEXION. Magnitude of the instantaneous displacement of the eight and seven skin-markers glued on the scapula (a) and arm (b) represented in the relevant ACS. c) Relevant shoulder kinematics calculated using the $X_t Z_f' Y_h''$ sequence (Bonnefoy-Mazure et al., 2012): rotation around the X_t axis of the thorax corresponding to the shoulder elevation (blue); rotation around the Z_f' axis corresponding to the shoulder flexion/extension (red); rotation around the Y_h'' axis of the humerus corresponding to the shoulder axial rotation (green). Superior elevation, flexion and internal rotations are positive.

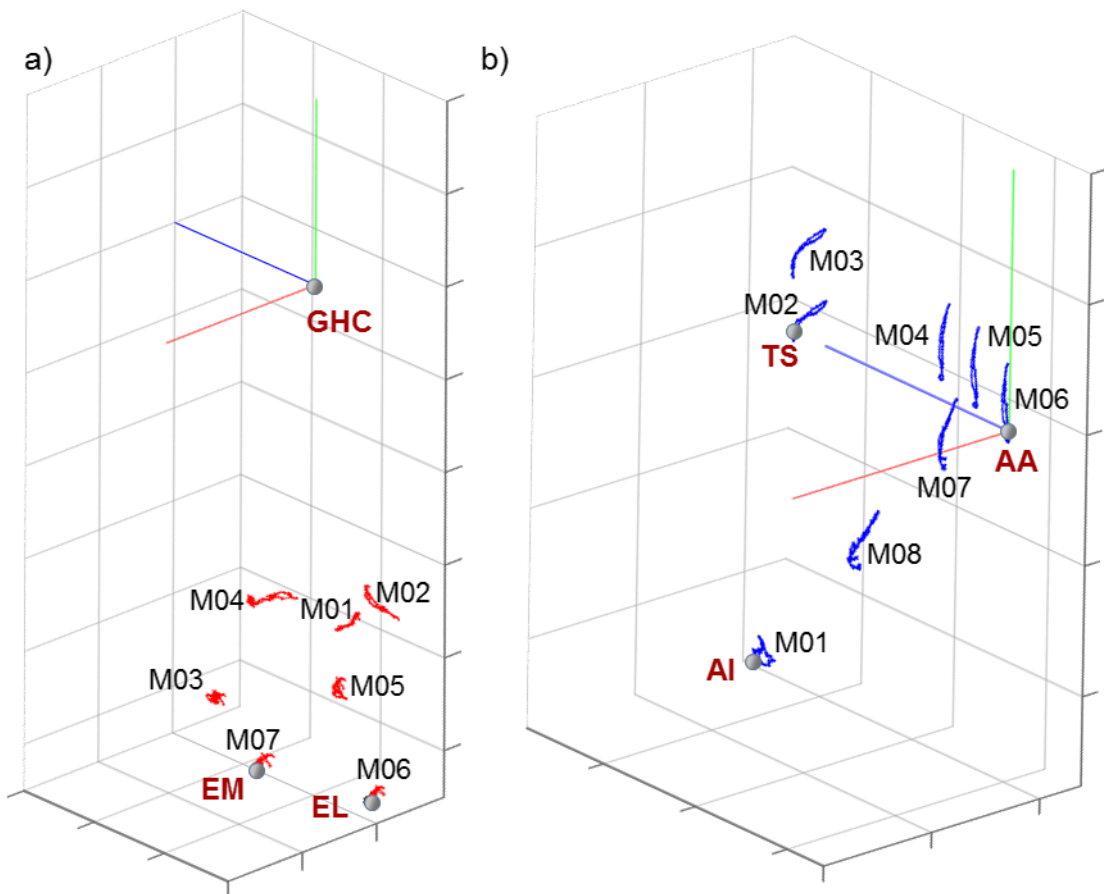


Figure 75 – EXTENSION. Humeral (a) and scapular (b) ACSs, relevant ALs, and arm and scapula skin-marker trajectories (represented in red and blue, respectively). The axes of the ACSs are represented in red, green, and blue for the x (antero/posterior, div = 50 mm), y (superior/inferior, div = 50 mm), and z (right/left, div = 50 mm) directions, respectively.

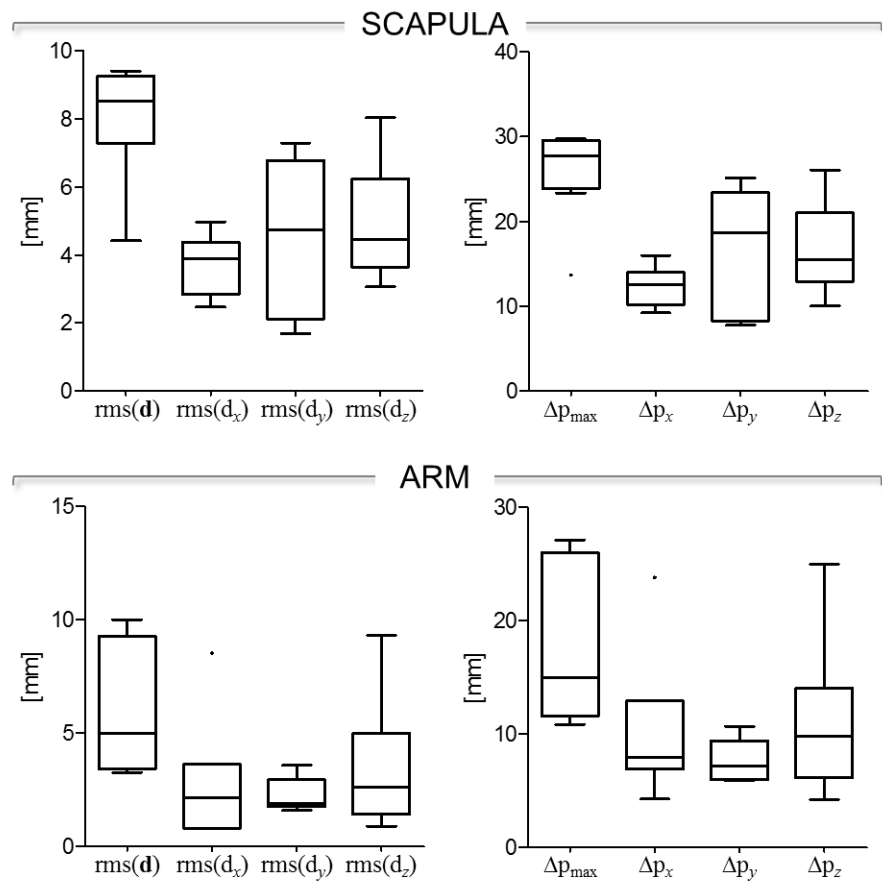


Figure 76 – EXTENSION. Box-plots of the eight parameters ($\text{rms}(\mathbf{d})$, $\text{rms}(\mathbf{d}_x)$, $\text{rms}(\mathbf{d}_y)$, and $\text{rms}(\mathbf{d}_z)$, in the left panel; Δp_{\max} , Δp_x , Δp_y , and Δp_z , in the right panel) that describe the STA affecting the eight and seven skin-markers on the scapula and arm, respectively, during the movement. Outliers are also depicted.

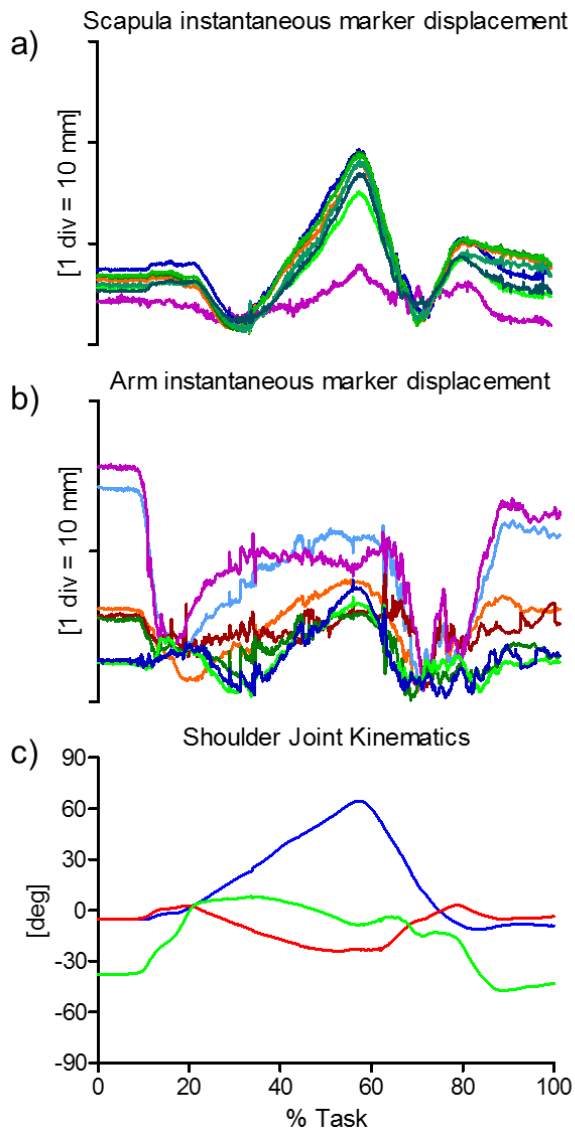


Figure 77 – EXTENSION. Magnitude of the instantaneous displacement of the eight and seven skin-markers glued on the scapula (a) and arm (b) represented in the relevant ACS. c) Relevant shoulder kinematics calculated using the $X_t Z_f' Y_h''$ sequence (Bonnefoy-Mazure et al., 2012): rotation around the X_t axis of the thorax corresponding to the shoulder elevation (blue); rotation around the floating Z_f' axis corresponding to the shoulder flexion/extension (red); rotation around the Y_h'' axis of the humerus corresponding to the shoulder axial rotation (green). Superior elevation, flexion and internal rotations are positive.

2.8.2. Data samples 26-31: daily living activities

Subject characteristics - A healthy male subject 27 y.o. Height = 1.65 m, mass = 57 kg.

Motor task description - All trials started with the arm relaxed at the side with thumb pointing forward referred to as neutral axial rotation. The subject was asked to mimic hair combing, ball throwing, eating, gleno-humeral functional movements, punching in a bag, reaching back. The gleno-humeral functional movements consisted of successive maximum arm elevations, circumductions and arm sweeping.

STA characteristics - Skin-marker trajectories in the scapula and arm ACSs are depicted in Fig. 78, 81, 84, 87, 90, 93, for hair combing, ball throwing, eating, gleno-humeral functional movements, punching, and reaching with the hand the middle of the opposite side of the back, respectively. Unfiltered data were used. Statistical data describing the STAs are shown in Figs. 79, 82, 85, 88, 91, 94, for hair combing, ball throwing, eating, gleno-humeral functional movements, punching, and reaching back, respectively. For each motor task, the magnitude of the instantaneous displacement of scapula and arm skin-markers along with the shoulder joint angular kinematics are depicted in Figs. 80, 83, 86, 89, 92, 95, for hair combing, ball throwing, eating, gleno-humeral functional movements, punching, and reaching back, respectively.

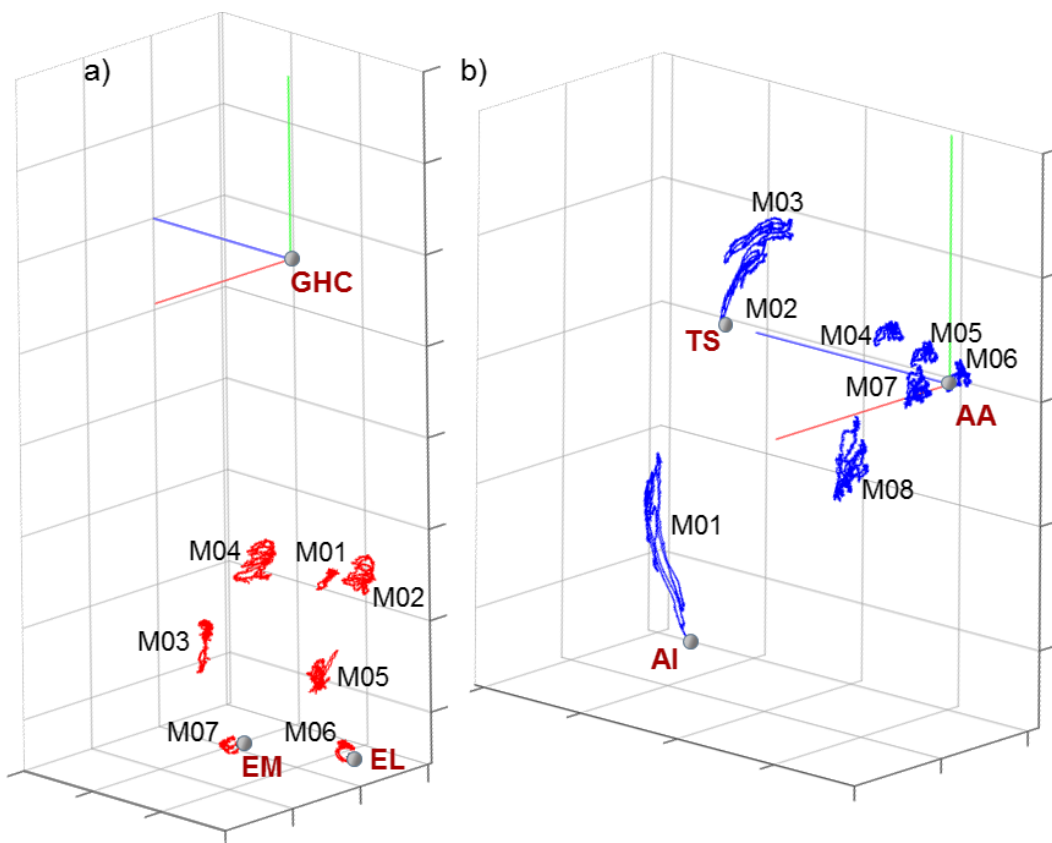


Figure 78 – HAIR COMBING. Humeral (a) and scapular (b) ACSs, relevant ALs, and arm and scapula skin-marker trajectories (represented in red and blue, respectively). The axes of the ACSs are represented in red, green, and blue for the x (antero/posterior, div = 50 mm), y (superior/inferior, div = 50 mm), and z (right/left, div = 50 mm) directions, respectively.

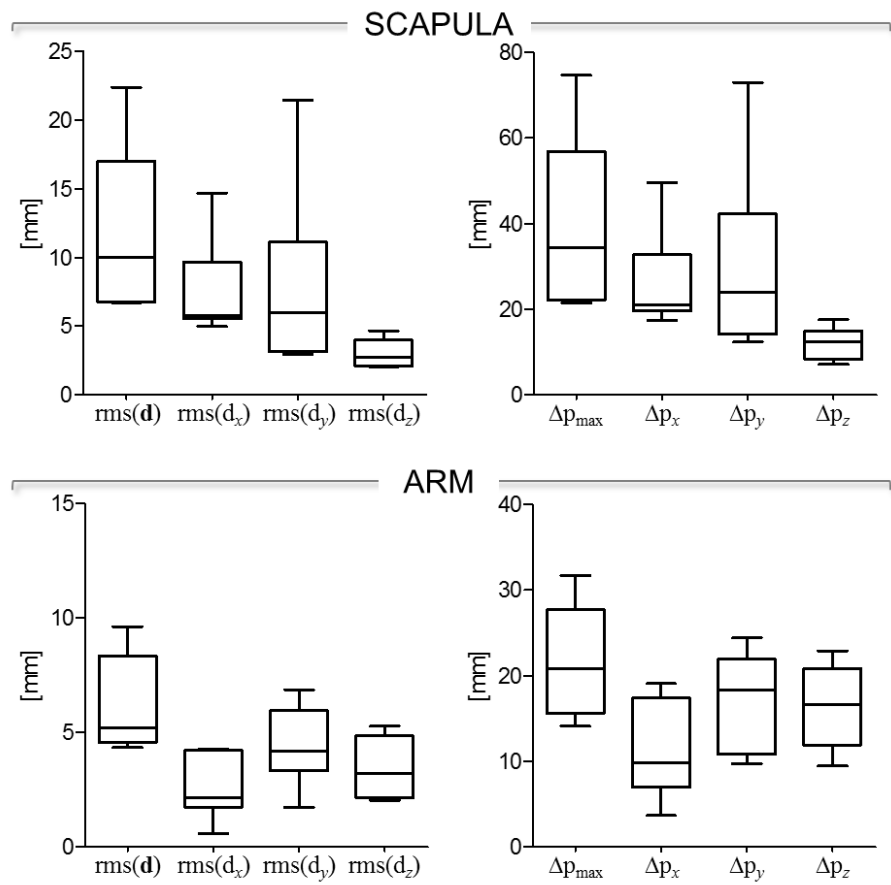


Figure 79 – HAIR COMBING. Box-plots of the eight parameters ($\text{rms}(\mathbf{d})$, $\text{rms}(\mathbf{d}_x)$, $\text{rms}(\mathbf{d}_y)$, and $\text{rms}(\mathbf{d}_z)$, in the left panel; Δp_{\max} , Δp_x , Δp_y , and Δp_z , in the right panel) that describe the STA affecting the eight and seven skin-markers on the scapula and arm, respectively, during the movement. Outliers are also depicted.

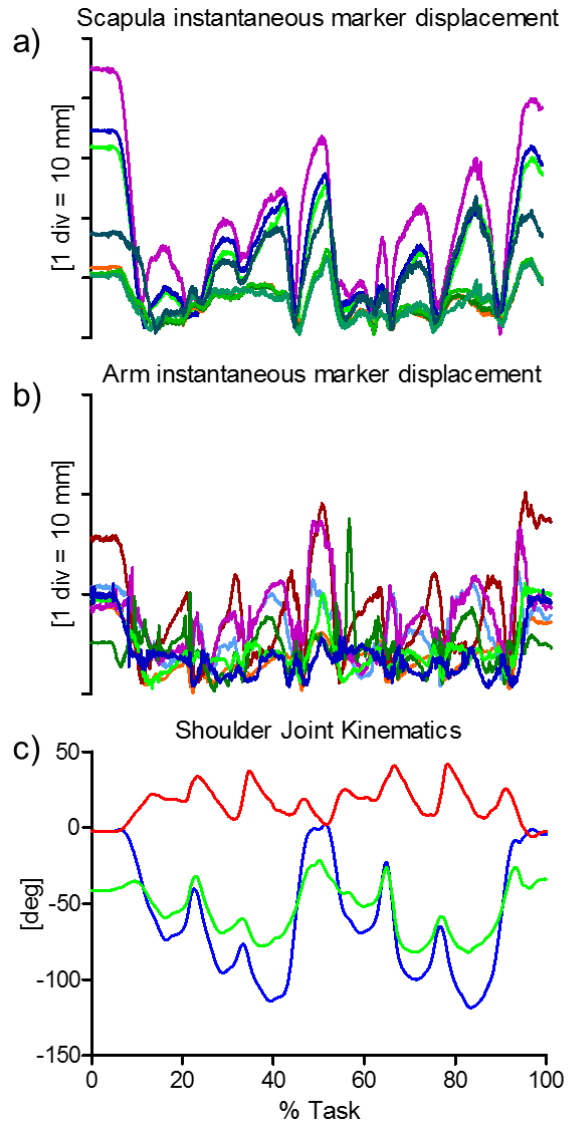


Figure 80 – HAIR COMBING. Magnitude of the instantaneous displacement of the eight and seven skin-markers glued on the scapula (a) and arm (b) represented in the relevant ACS. c) Relevant shoulder kinematics calculated using the $X_t Z_f' Y_h''$ sequence (Bonnefoy-Mazure et al., 2012): rotation around the X_t axis of the thorax corresponding to the shoulder elevation (blue); rotation around the floating Z_f' axis corresponding to the shoulder flexion/extension (red); rotation around the Y_h'' axis of the humerus corresponding to the shoulder axial rotation (green). Superior elevation, flexion and internal rotations are positive.

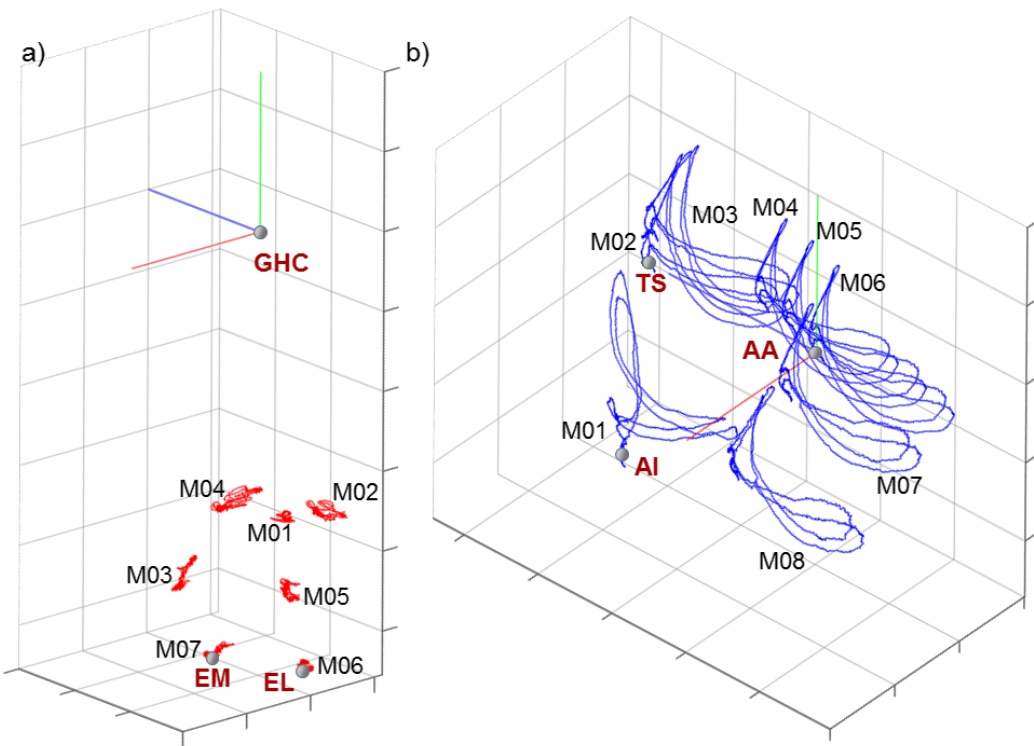


Figure 81 – BALL THROWING. Humeral (a) and scapular (b) ACSs, relevant ALs, and arm and scapula skin-marker trajectories (represented in red and blue, respectively). The axes of the ACSs are represented in red, green, and blue for the x (antero/posterior, div = 50 mm), y (superior/inferior, div = 50 mm), and z (right/left, div = 50 mm) directions, respectively.

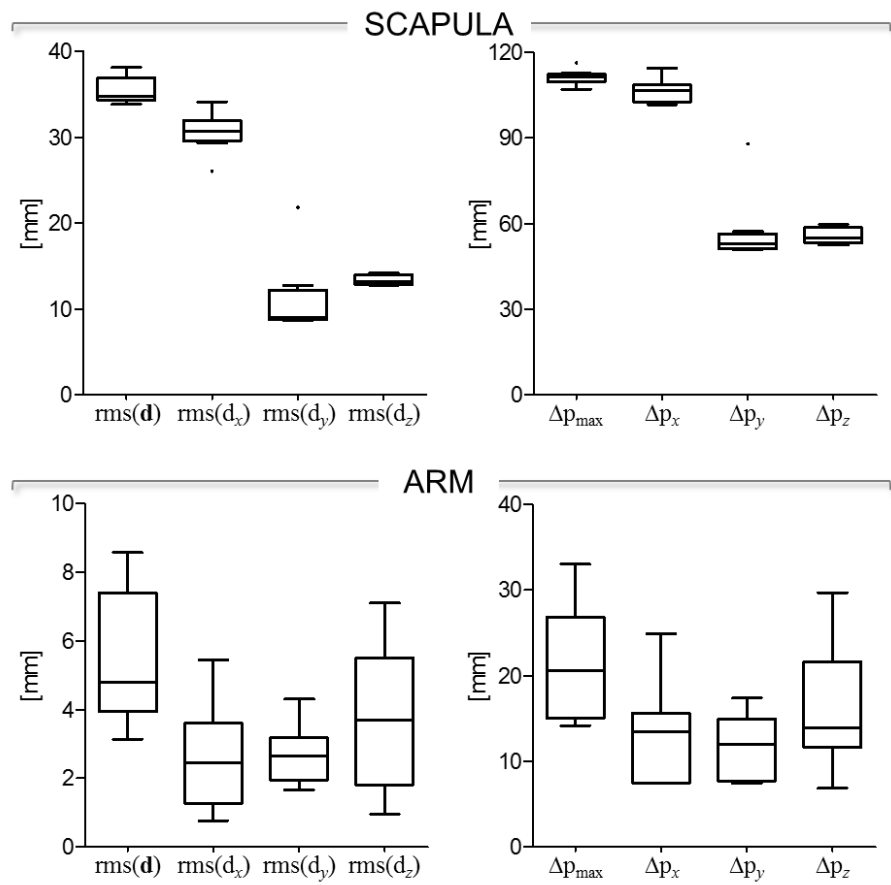


Figure 82 – BALL THROWING. Box-plots of the eight parameters ($\text{rms}(\mathbf{d})$, $\text{rms}(\mathbf{d}_x)$, $\text{rms}(\mathbf{d}_y)$, and $\text{rms}(\mathbf{d}_z)$, in the left panel; Δp_{max} , Δp_x , Δp_y , and Δp_z , in the right panel) that describe the STA affecting the eight and seven skin-markers on the scapula and arm, respectively, during the movement. Outliers are also depicted.

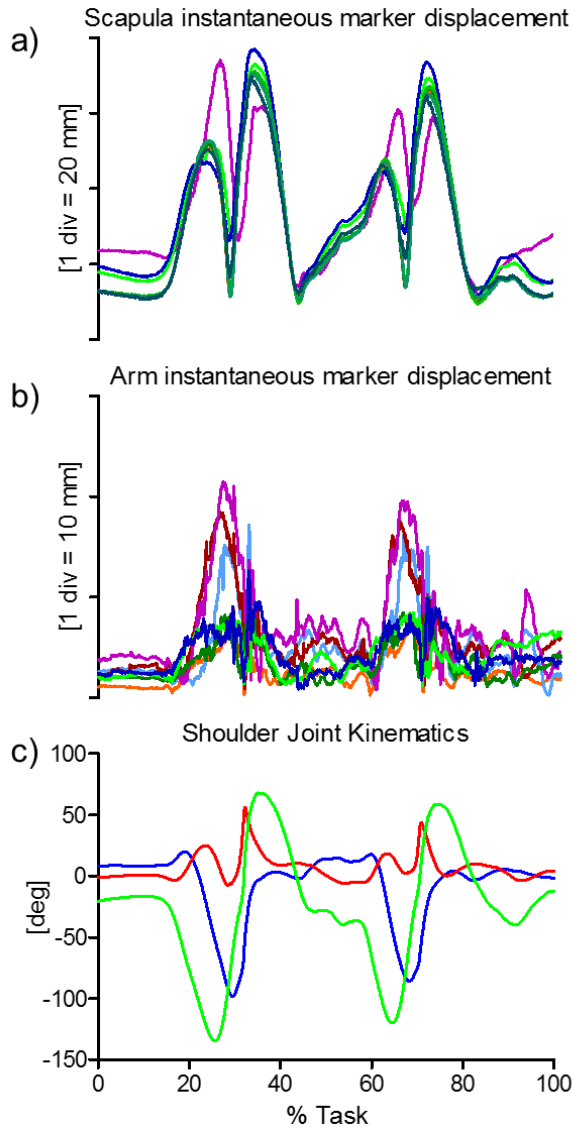


Figure 83 – BALL THROWING. Magnitude of the instantaneous displacement of the eight and seven skin-markers glued on the scapula (a) and arm (b) represented in the relevant ACS. c) Relevant shoulder kinematics calculated using the $X_t Z_f' Y_h''$ sequence (Bonnefoy-Mazure et al., 2012): rotation around the X_t axis of the thorax corresponding to the shoulder elevation (blue); rotation around the floating Z_f' axis corresponding to the shoulder flexion/extension (red); rotation around the Y_h'' axis of the humerus corresponding to the shoulder axial rotation (green). Superior elevation, flexion and internal rotations are positive.

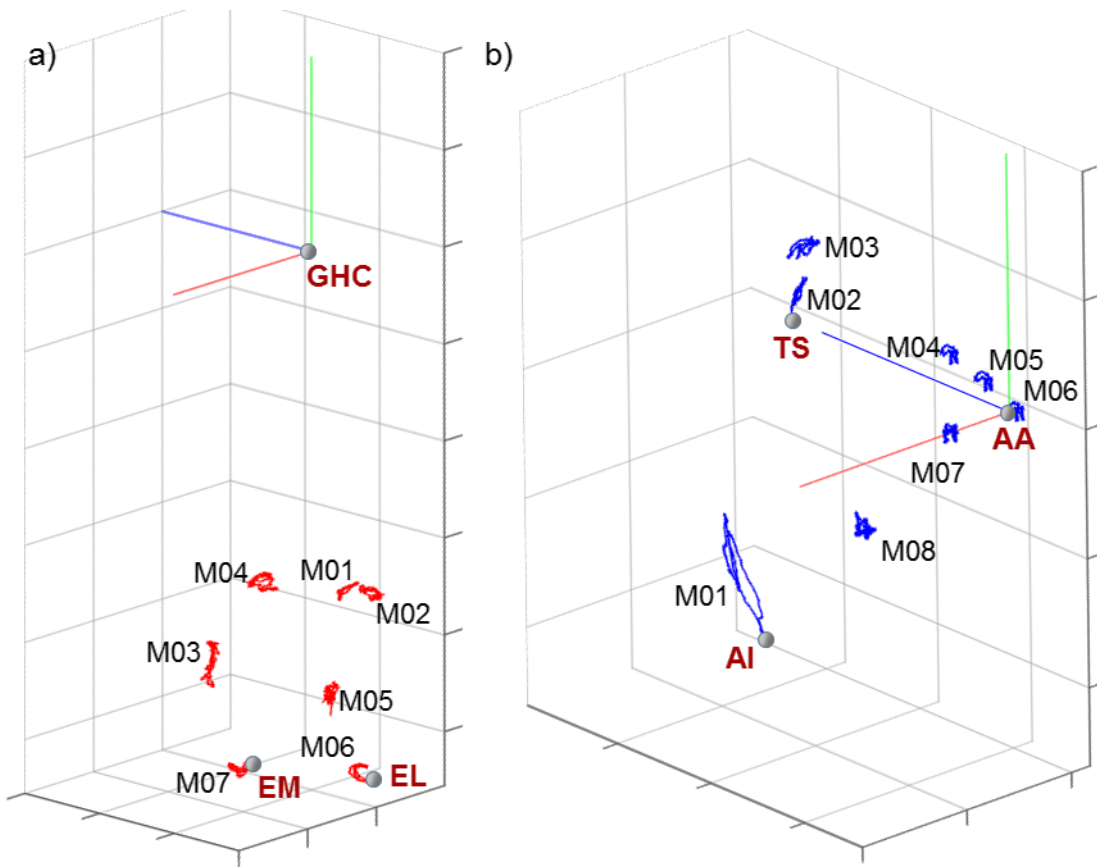


Figure 84 – EATING. Humeral (a) and scapular (b) ACSs, relevant ALs, and arm and scapula skin-marker trajectories (represented in red and blue, respectively). The axes of the ACSs are represented in red, green, and blue for the x (antero/posterior, div = 20 mm), y (superior/inferior, div = 50 mm), and z (right/left, div = 50 mm) directions, respectively.

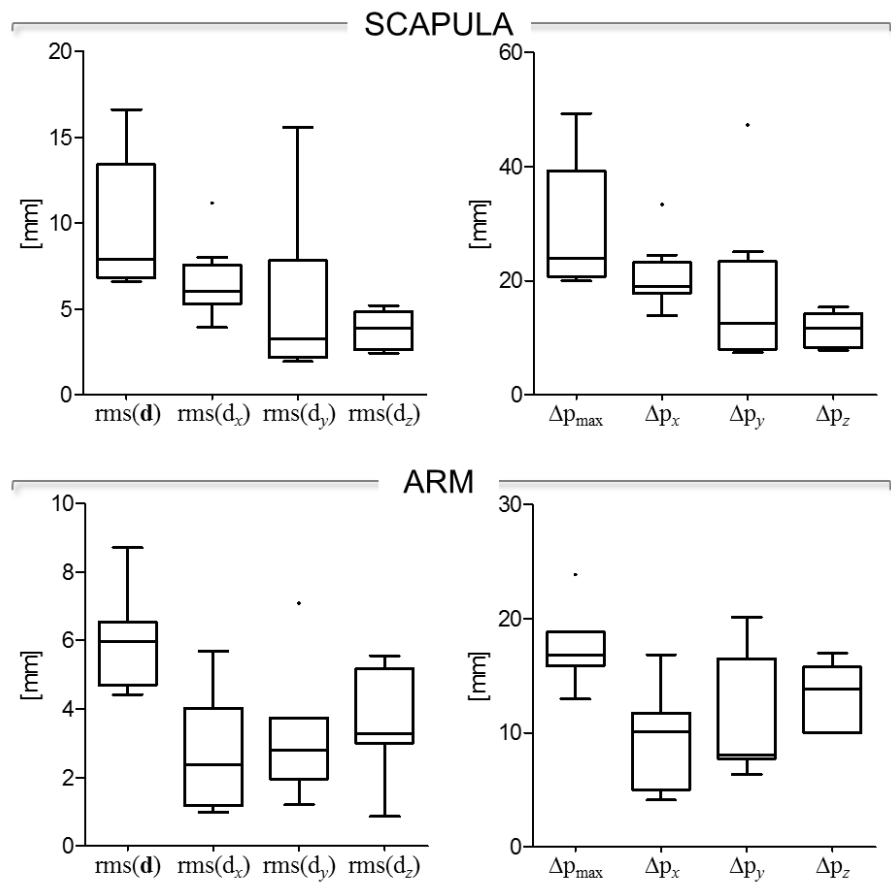


Figure 85 – EATING. Box-plots of the eight parameters ($\text{rms}(\mathbf{d})$, $\text{rms}(\mathbf{d}_x)$, $\text{rms}(\mathbf{d}_y)$, and $\text{rms}(\mathbf{d}_z)$, in the left panel; Δp_{\max} , Δp_x , Δp_y , and Δp_z , in the right panel) that describe the STA affecting the eight and seven skin-markers on the scapula and arm, respectively, during the movement. Outliers are also depicted.

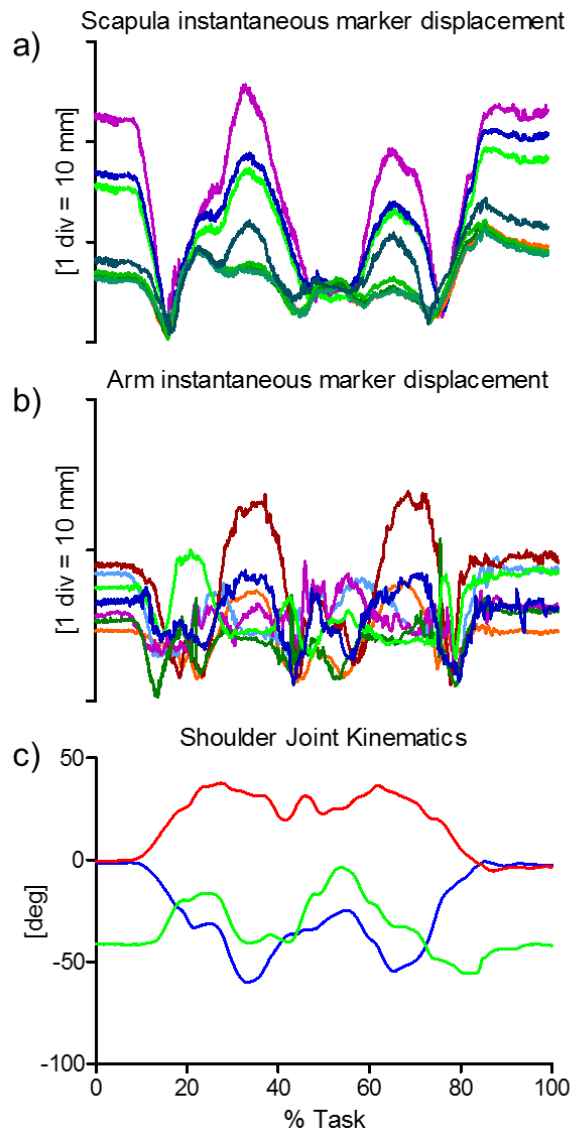


Figure 86 – EATING. Magnitude of the instantaneous displacement of the eight and seven skin-markers glued on the scapula (a) and arm (b) represented in the relevant ACS. c) Relevant shoulder kinematics calculated using the X_t Z_f' Y_h'' sequence (Bonnefoy-Mazure et al., 2012): rotation around the X_t axis of the thorax corresponding to the shoulder elevation (blue); rotation around the floating Z_f' axis corresponding to the shoulder flexion/extension (red); rotation around the Y_h'' axis of the humerus corresponding to the shoulder axial rotation (green). Superior elevation, flexion and internal rotations are positive.

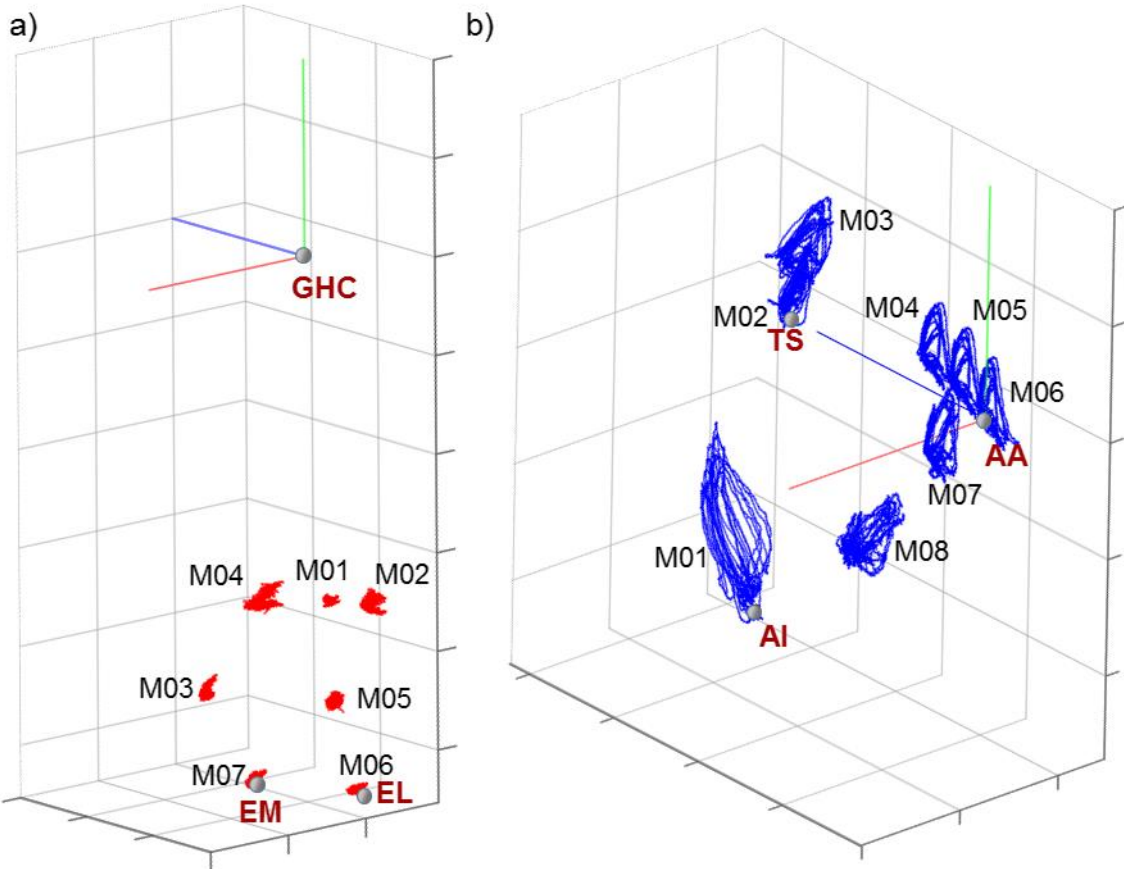


Figure 87 – GLENO-HUMERAL FUNCTIONAL MOVEMENTS. Humeral (a) and scapular (b) ACSs, relevant ALS, and arm and scapula skin-marker trajectories (represented in red and blue, respectively). The axes of the ACSs are represented in red, green, and blue for the x (antero/posterior, div = 50 mm), y (superior/inferior, div = 50 mm), and z (right/left, div = 50 mm) directions, respectively.

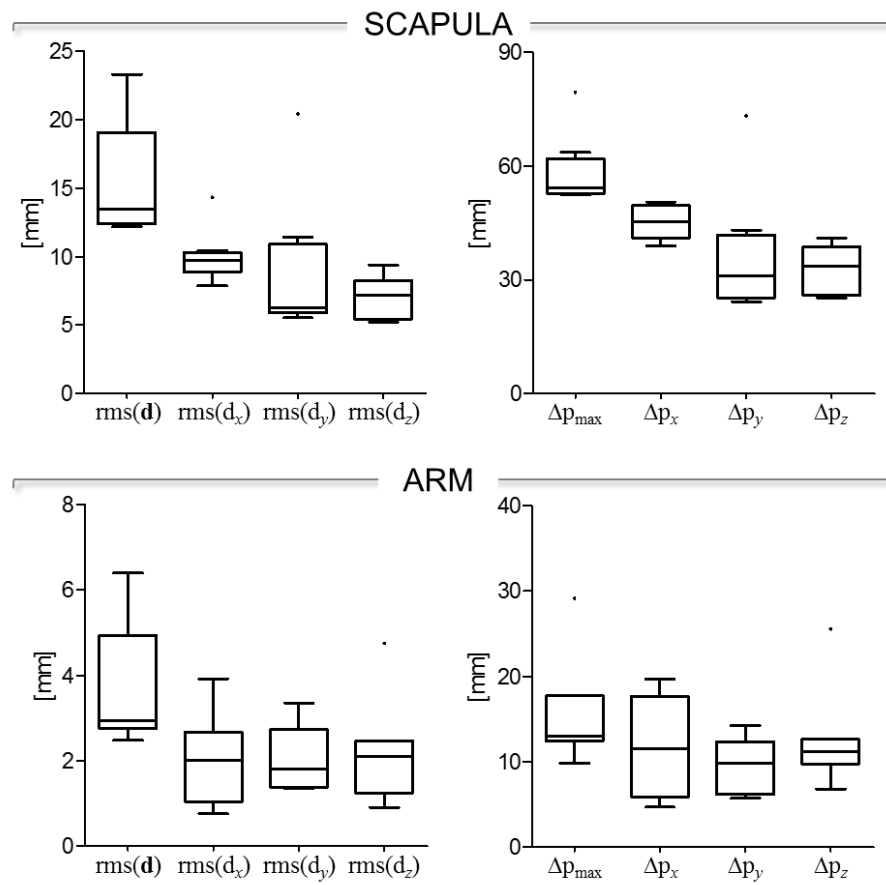


Figure 88 – GLENO-HUMERAL FUNCTIONAL MOVEMENTS. Box-plots of the eight parameters ($\text{rms}(\mathbf{d})$, $\text{rms}(\mathbf{d}_x)$, $\text{rms}(\mathbf{d}_y)$, and $\text{rms}(\mathbf{d}_z)$, in the left panel; Δp_{\max} , Δp_x , Δp_y , and Δp_z , in the right panel) that describe the STA affecting the eight and seven skin-markers on the scapula and arm, respectively, during the movement. Outliers are also depicted.

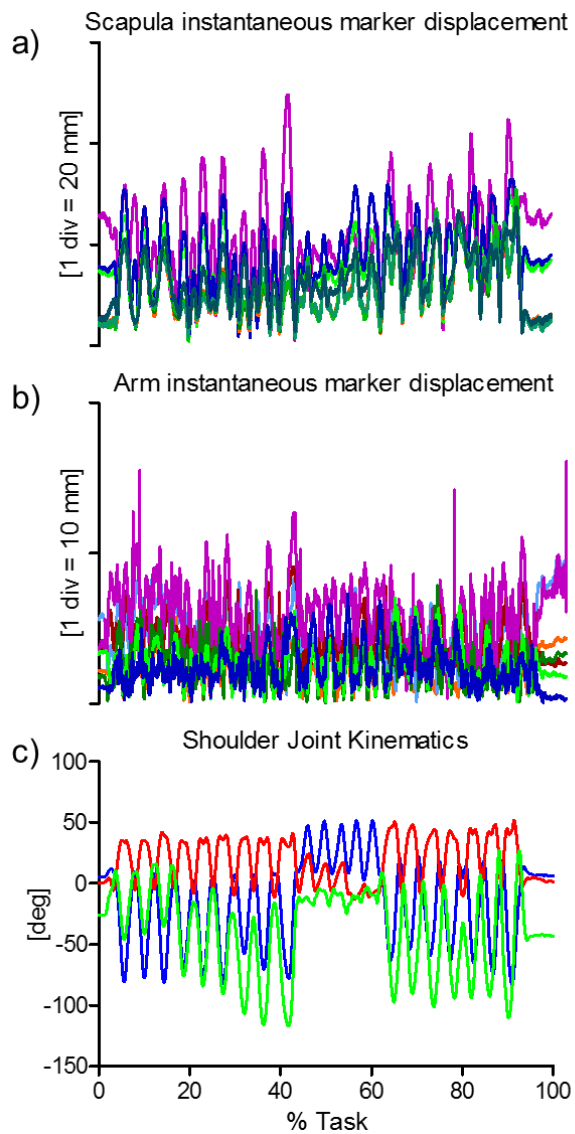


Figure 89 – GLENO-HUMERAL FUNCTIONAL MOVEMENTS. Magnitude of the instantaneous displacement of the eight and seven skin-markers glued on the scapula (a) and arm (b) represented in the relevant ACS. c) Relevant shoulder kinematics calculated using the $X_t Z_f' Y_h''$ sequence (Bonnefoy-Mazure et al., 2012): rotation around the X_t axis of the thorax corresponding to the shoulder elevation (blue); rotation around the floating Z_f' axis corresponding to the shoulder flexion/extension (red); rotation around the Y_h'' axis of the humerus corresponding to the shoulder axial rotation (green). Superior elevation, flexion and internal rotations are positive.

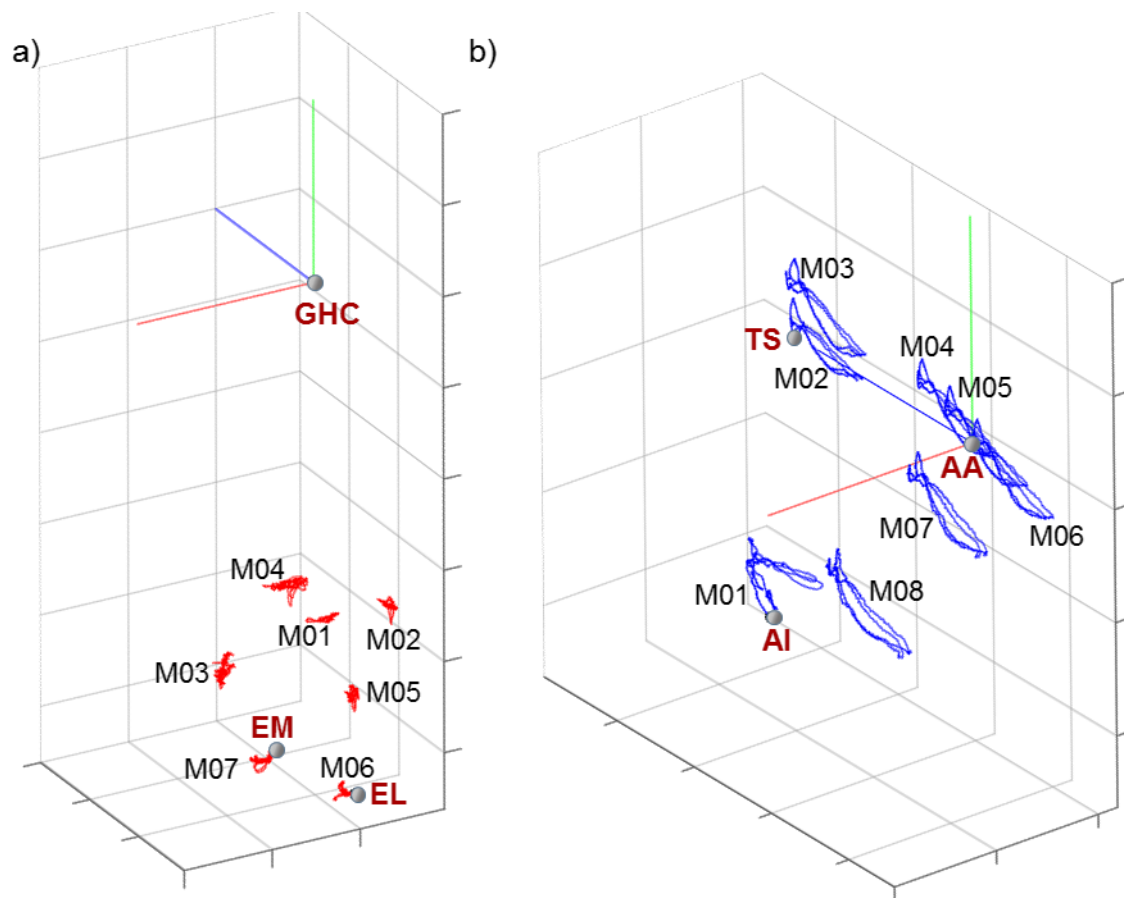


Figure 90 – PUNCHING. Humeral (a) and scapular (b) ACSs, relevant ALs, and arm and scapula skin-marker trajectories (represented in red and blue, respectively). The axes of the ACSs are represented in red, green, and blue for the x (antero/posterior, div = 50 mm), y (superior/inferior, div = 50 mm), and z (right/left, div = 50 mm) directions, respectively.

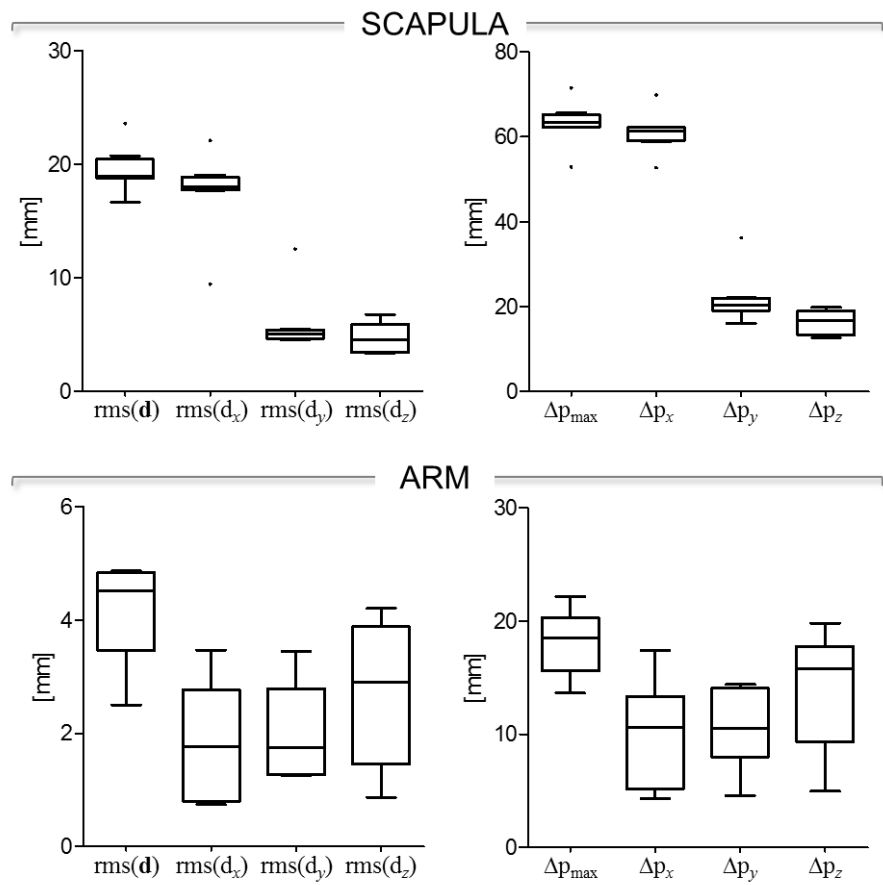


Figure 91 – PUNCHING. Box-plots of the eight parameters ($\text{rms}(\mathbf{d})$, $\text{rms}(\mathbf{d}_x)$, $\text{rms}(\mathbf{d}_y)$, and $\text{rms}(\mathbf{d}_z)$, in the left panel; Δp_{\max} , Δp_x , Δp_y , and Δp_z , in the right panel) that describe the STA affecting the eight and seven skin-markers on the scapula and arm, respectively, during the movement. Outliers are also depicted.

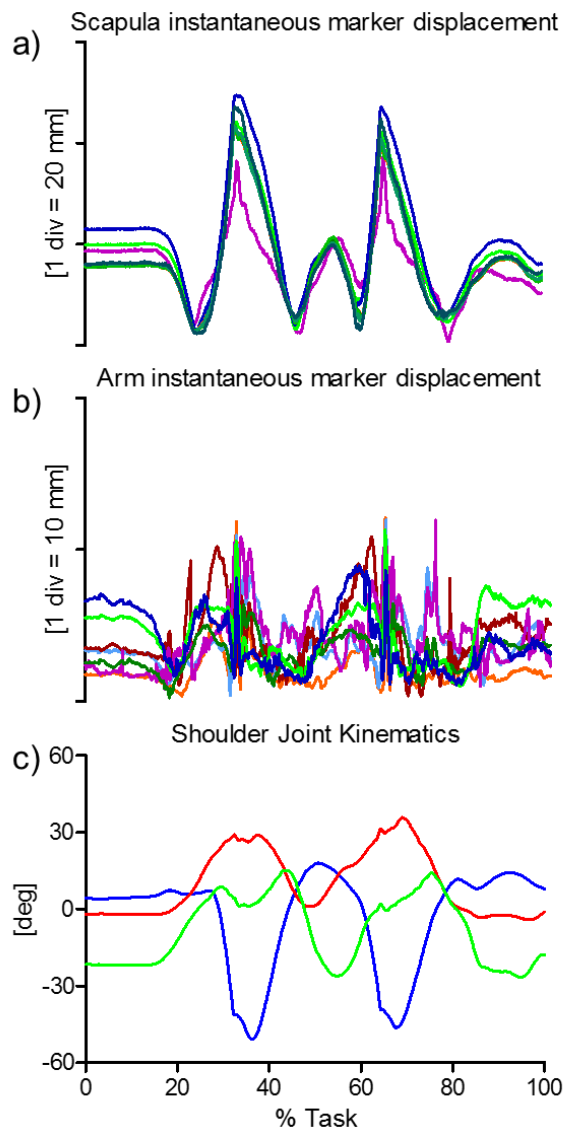


Figure 92 – PUNCHING. Magnitude of the instantaneous displacement of the eight and seven skin-markers glued on the scapula (a) and arm (b) represented in the relevant ACS. c) Relevant shoulder kinematics calculated using the $X_t Z_f' Y_h''$ sequence (Bonnefoy-Mazure et al., 2012): rotation around the X_t axis of the thorax corresponding to the shoulder elevation (blue); rotation around the floating Z_f' axis corresponding to the shoulder flexion/extension (red); rotation around the Y_h'' axis of the humerus corresponding to the shoulder axial rotation (green). Superior elevation, flexion and internal rotations are positive.

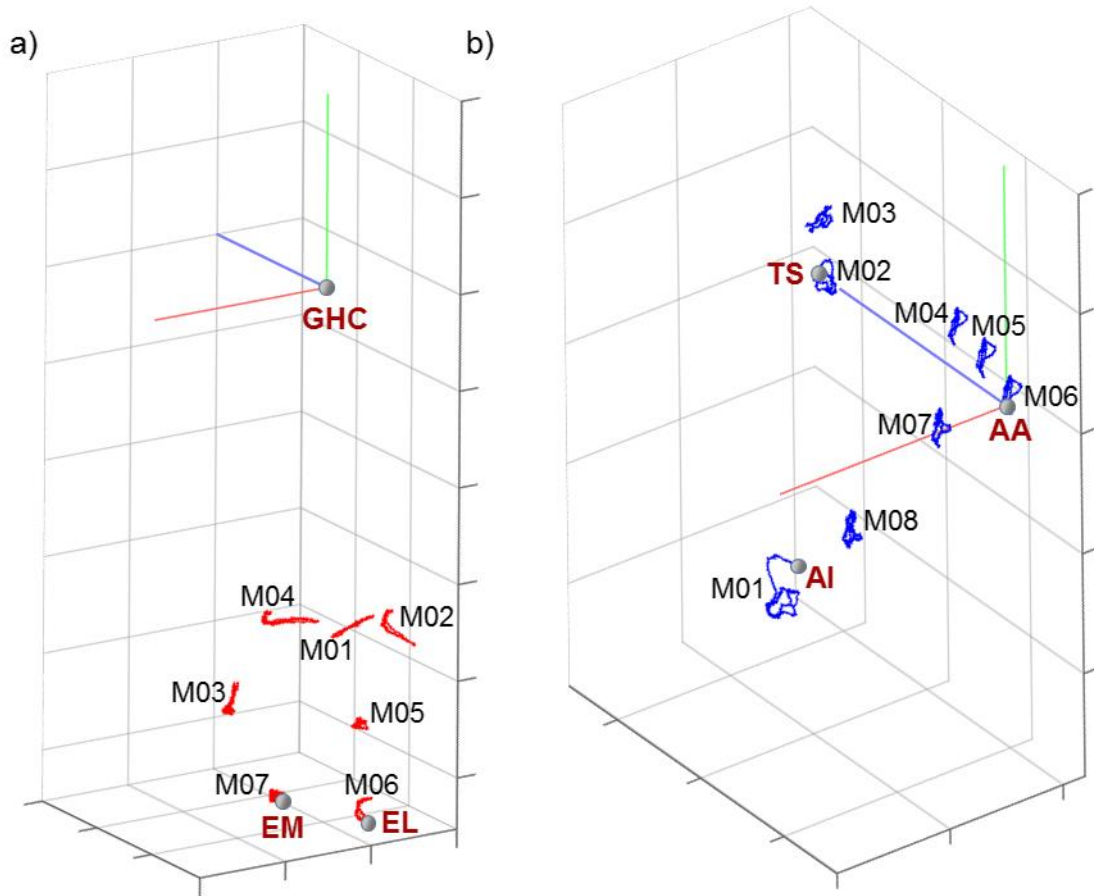


Figure 93 – REACHING BACK. Humeral (a) and scapular (b) ACSs, relevant ALs, and arm and scapula skin-marker trajectories (represented in red and blue, respectively). The axes of the ACSs are represented in red, green, and blue for the x (antero/posterior, div = 50 mm), y (superior/inferior, div = 50 mm), and z (right/left, div = 50 mm) directions, respectively.

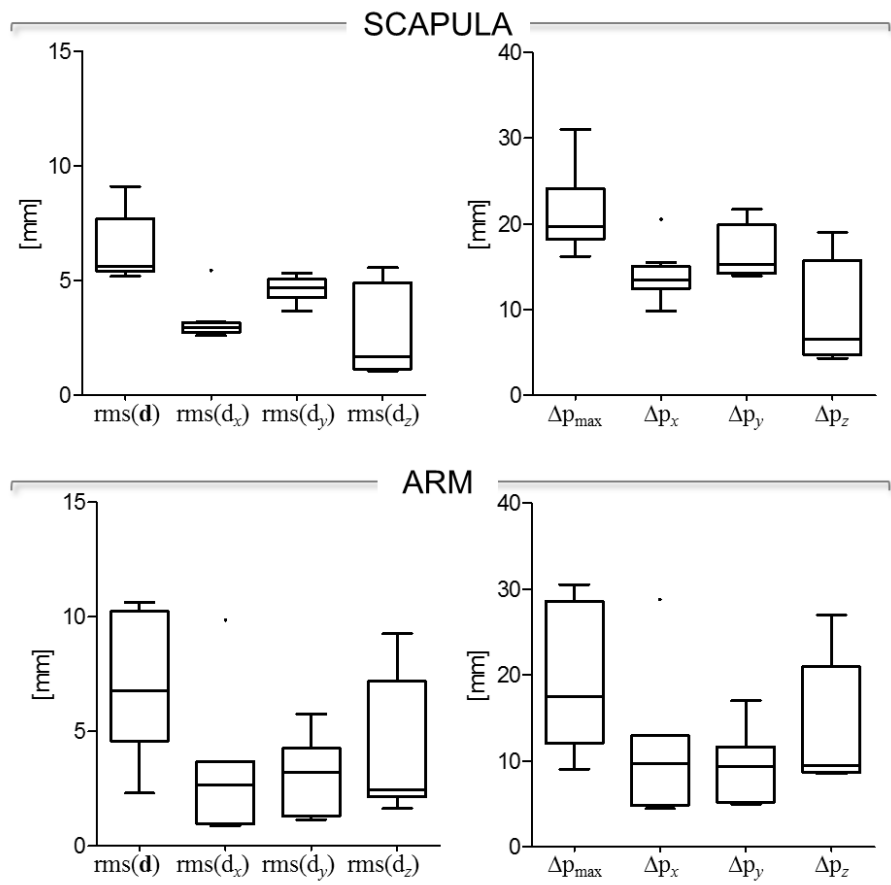


Figure 94 – REACHING BACK. Box-plots of the eight parameters ($\text{rms}(\mathbf{d})$, $\text{rms}(\mathbf{d}_x)$, $\text{rms}(\mathbf{d}_y)$, and $\text{rms}(\mathbf{d}_z)$, in the left panel; Δp_{\max} , Δp_x , Δp_y , and Δp_z , in the right panel) that describe the STA affecting the eight and seven skin-markers on the scapula and arm, respectively, during the movement. Outliers are also depicted.

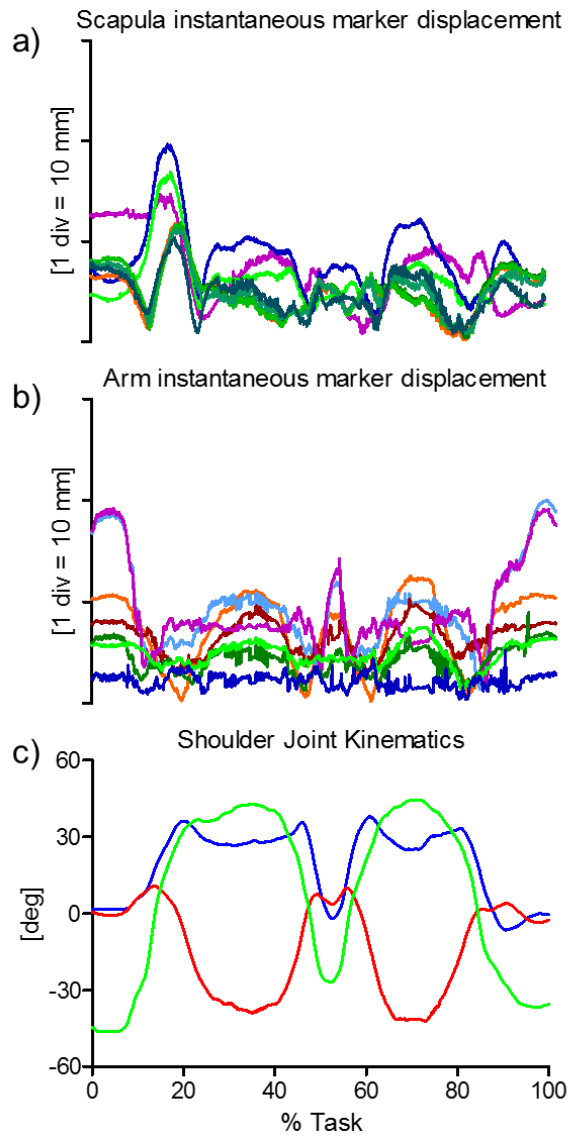


Figure 95 – REACHING BACK. Magnitude of the instantaneous displacement of the eight and seven skin-markers glued on the scapula (a) and arm (b) represented in the relevant ACS. c) Relevant shoulder kinematics calculated using the X_t Z_f' Y_h'' sequence (Bonnefoy-Mazure et al., 2012): rotation around the X_t axis of the thorax corresponding to the shoulder elevation (blue); rotation around the floating Z_f' axis corresponding to the shoulder flexion/extension (red); rotation around the Y_h'' axis of the humerus corresponding to the shoulder axial rotation (green). Superior elevation, flexion and internal rotations are positive.

2.9. In-vivo data from ARTANIM

Scientific articles of reference - A detailed description of the original data set can be found in Charbonnier et al (2014).

Experimental data description - Four markers (\varnothing 14 mm) were attached to the thorax (sternal notch, xiphoid process, C7 and T8 vertebra, and four (\varnothing 14 mm) on the upper arm – two placed on anatomical landmarks (LE_H and ME_H) and two as far as possible from the deltoid. For the scapula, 1 marker (\varnothing 14 mm) was fixed on the acromion. In addition, the scapula was covered with a regular grid of 56 markers (\varnothing 6.5 mm) (Fig. 96).

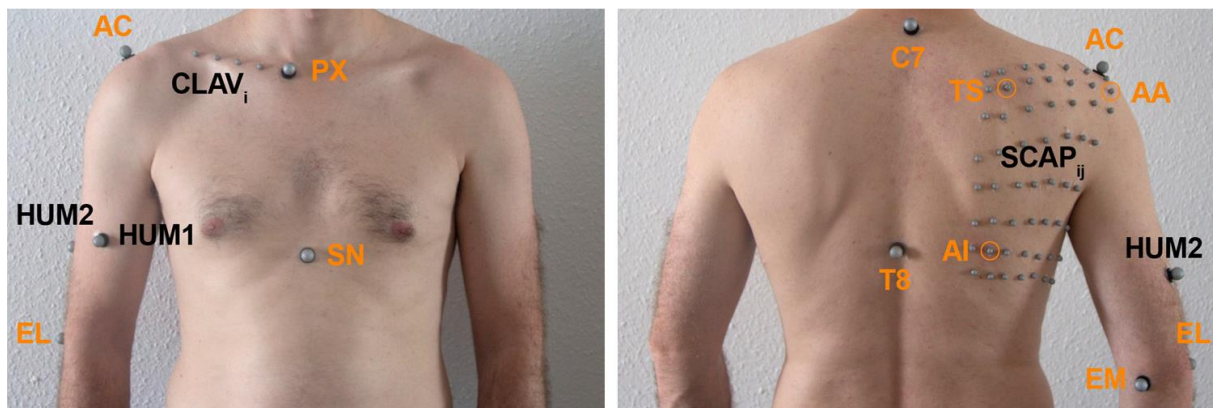


Fig. 2. Marker placement, including markers placed on anatomical landmarks (orange) and technical markers (black). PX = xiphoid process, SN = sternal notch, AC = acromion, TS = trigonum spinae, AA = angulus acromialis, AI = angulus inferior, EL = lateral epicondyle, EM = medial epicondyle.

Figure 96 – Experimental markers setup, including markers placed on anatomical landmarks (orange) and technical markers (black). Landmark names are described in Table 3.3. Markers HUM1 and HUM2 correspond to markers M01 and M02 of the arm segment, markers placed on EL and EM landmarks were named M03 and M04, respectively.

Anatomical coordinate system definitions - Both humerus and scapular ACSs were determined according to the definitions proposed in Wu et al. (2005). The glenohumeral joint centre was calculated using a sphere-fitting method.

Measurement specifications - The instantaneous markers position was reconstructed using a 8-camera stereophotogrammetric system (VICON MX40S) acquiring at 120 sample/s.

Ground truth - Kinematic data were collected using an X-ray fluoroscopy unit (MultiDiagnostEleva, Philips Medical Systems, Netherlands) operating at 30 sample/s. Prior to data collection, the fluoroscopy system was calibrated for image distortion and radiographic projection parameters using a calibration object. A calibration frame was also acquired with 10 non-coplanar retroreflective markers, visible in both systems, to compute the pose of the CS of the stereophotogrammetric system relative to the fluoroscopy CS. The 3D MRI-based model of the scapula and of the humerus were acquired from a 1.5 T HDxT MRI system. The 3D poses of the scapula and humerus were obtained using a 3D-to-2D shape-

matching technique using a custom software. A previous validation study (Moro-Hoka et al., 2007) had shown that best-case accuracy for fluoroscopy measurements was 0.53 mm for in-plane translation (parallel to image plane), 1.6 mm for out-of-plane translation (perpendicular to image plane), and 0.54 deg for rotation in all planes.

2.9.1. Data samples 22,24: Arm flexion and arm elevation in the scapular plane

Subject characteristics - A healthy male subject 25 y.o. Height = 1.80 m, weight = 80 kg.

Motor task description - the following shoulder motions were analyzed: 3 consecutive arm flexions from neutral to maximum flexion, and 3 consecutive elevation from neutral to maximum abduction in the scapular plane.

STA characteristics - Skin-marker trajectories in the scapula and arm ACSs are depicted in Fig. 97, 100, for arm flexion and arm elevation in the scapular plane, respectively. Stereophotogrammetric data were acquired at 120 Hz and then down-sampled to 30 Hz. Statistical data describing the STAs are shown in Figs. 98, 101, for arm flexion and arm elevation in the scapular plane, respectively. For each motor task, the magnitude of the instantaneous displacement of scapula and humerus skin-markers along with the shoulder joint angular kinematics is depicted in Figs. 99, 102, for arm flexion and arm elevation in the scapular plane, respectively.

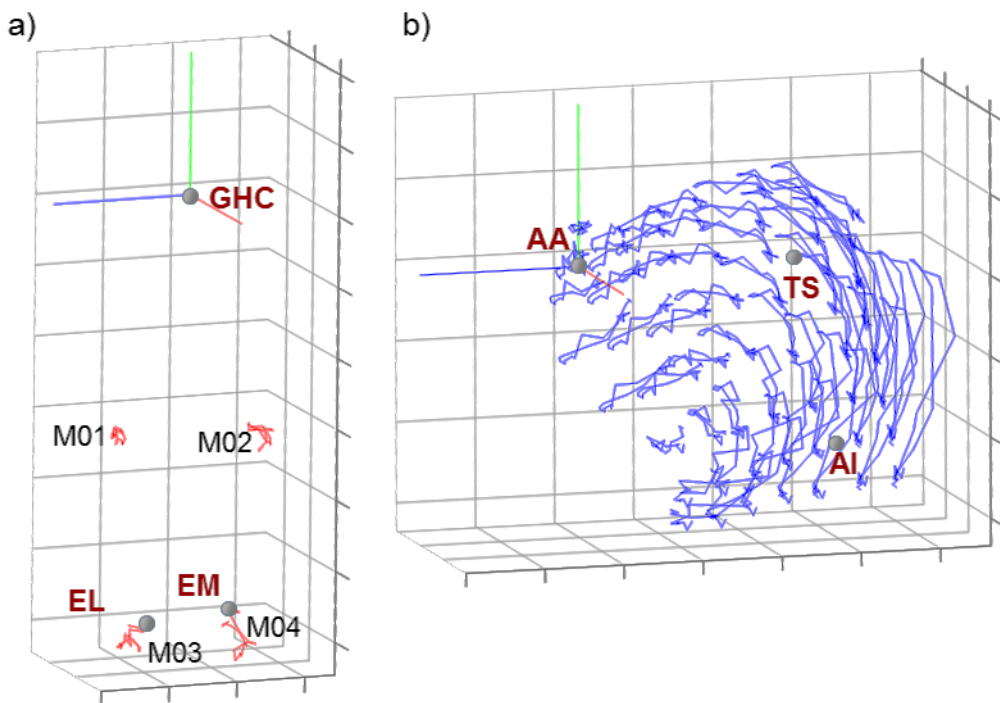


Figure 97 – FLEXION. Humerus (a) and scapular (b) ACSs, relevant ALs, and arm and scapula skin-marker trajectories (represented in red and blue, respectively). The axes of the ACSs are represented in red, green, and blue for the x (antero/posterior, div = 50 mm), y (superior/inferior, div = 50 mm), and z (right/left, div = 50 mm) directions, respectively.

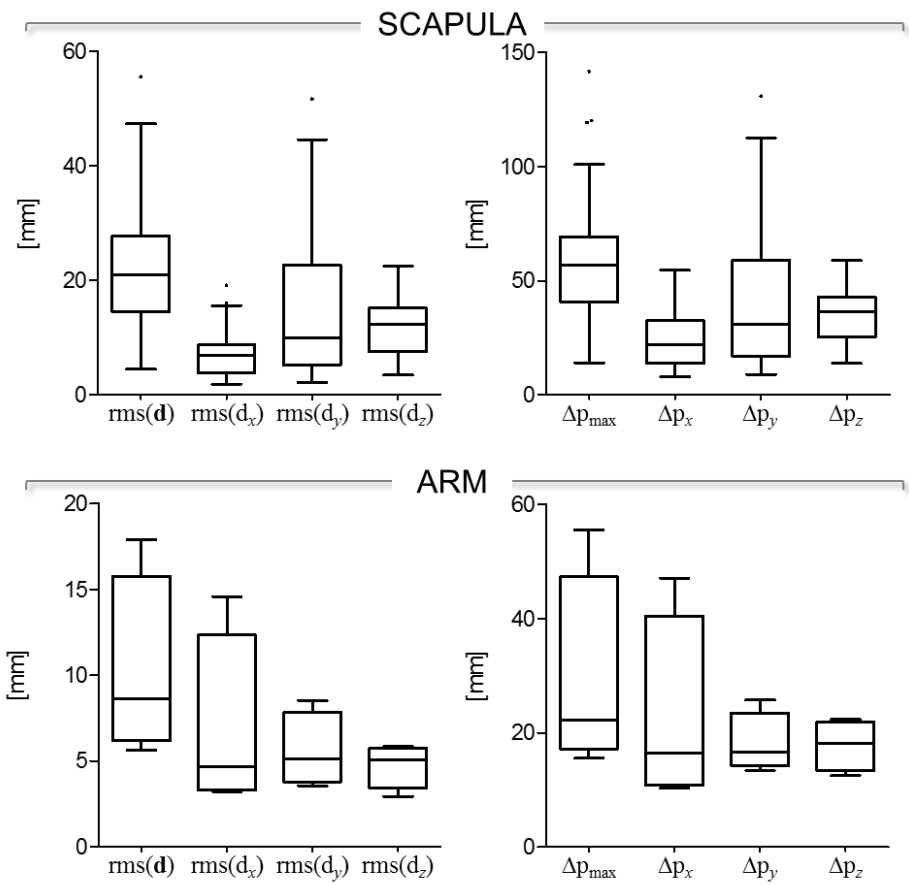


Figure 98 – FLEXION. Box-plots of the eight parameters ($\text{rms}(\mathbf{d})$, $\text{rms}(\mathbf{d}_x)$, $\text{rms}(\mathbf{d}_y)$, and $\text{rms}(\mathbf{d}_z)$, in the left panel; Δp_{max} , Δp_x , Δp_y , and Δp_z , in the right panel) that describe the STA affecting the fifty-seven and four skin-markers on the scapula and arm, respectively, during the movement. Outliers are also depicted.

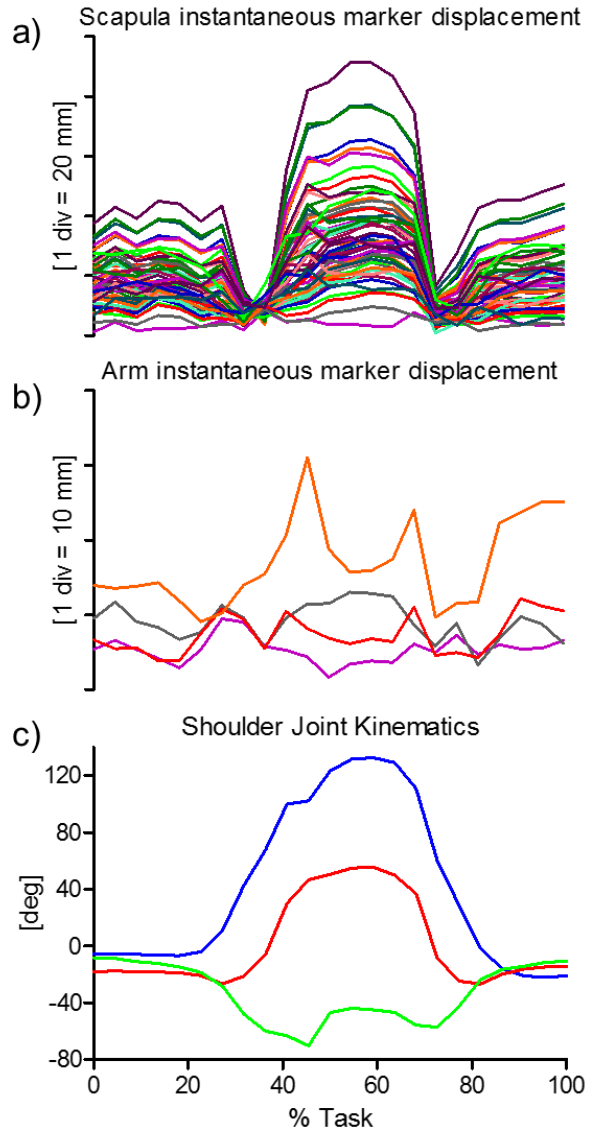


Figure 99 – FLEXION. Magnitude of the instantaneous displacement of the fifty-seven and four skin-markers glued on the scapula (a) and arm (b) represented in the relevant ACS. c) Relevant shoulder kinematics calculated using the $X_t Z_f Y_h''$ sequence (Bonnefoy-Mazure et al., 2012): rotation around the X_t axis of the thorax corresponding to the shoulder elevation (blue); rotation around the floating Z_f axis corresponding to the shoulder flexion/extension (red); rotation around the Y_h'' axis of the humerus corresponding to the shoulder axial rotation (green). Superior elevation, flexion and internal rotations are positive.

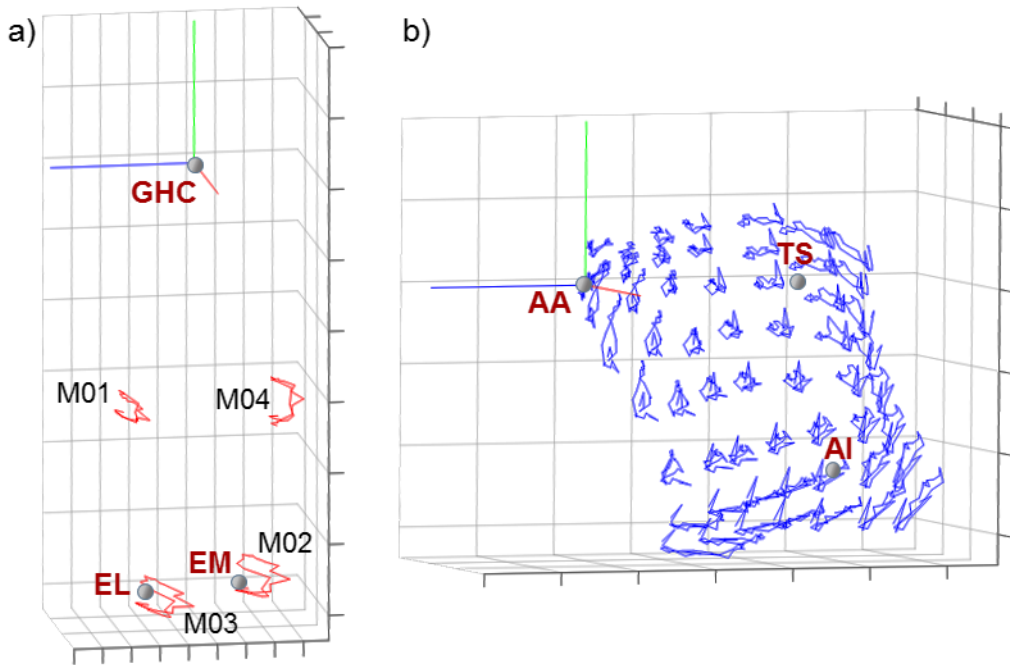


Figure 100 – ABDUCTION. Humerus (a) and scapular (b) ACSs, relevant ALs, and arm and scapula skin-marker trajectories (represented in red and blue, respectively). The axes of the ACSs are represented in red, green, and blue for the x (antero/posterior, div = 50 mm), y (superior/inferior, div = 50 mm), and z (right/left, a) div = 20 mm; b) div = 50 mm) directions, respectively.

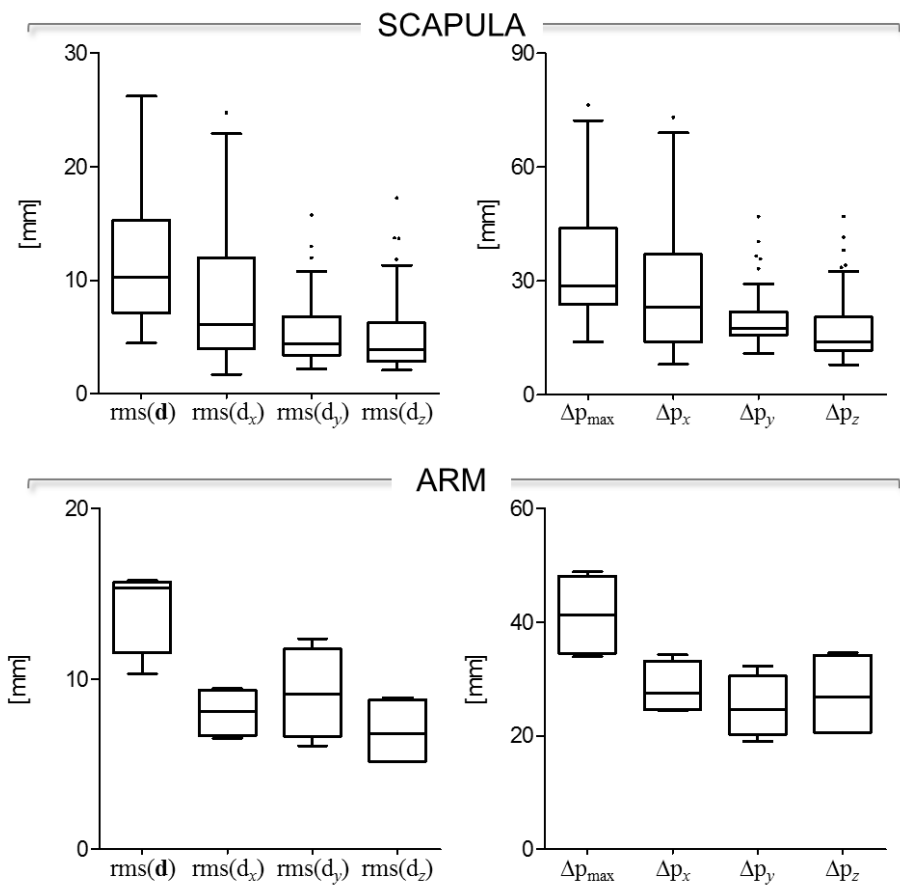


Figure 101 – ABDUCTION. Box-plots of the eight parameters ($\text{rms}(\mathbf{d})$, $\text{rms}(d_x)$, $\text{rms}(d_y)$, and $\text{rms}(d_z)$, in the left panel; Δp_{\max} , Δp_x , Δp_y , and Δp_z , in the right panel) that describe the STA affecting the fifty-seven and four skin-markers on the scapula and arm, respectively, during the movement. Outliers are also depicted.

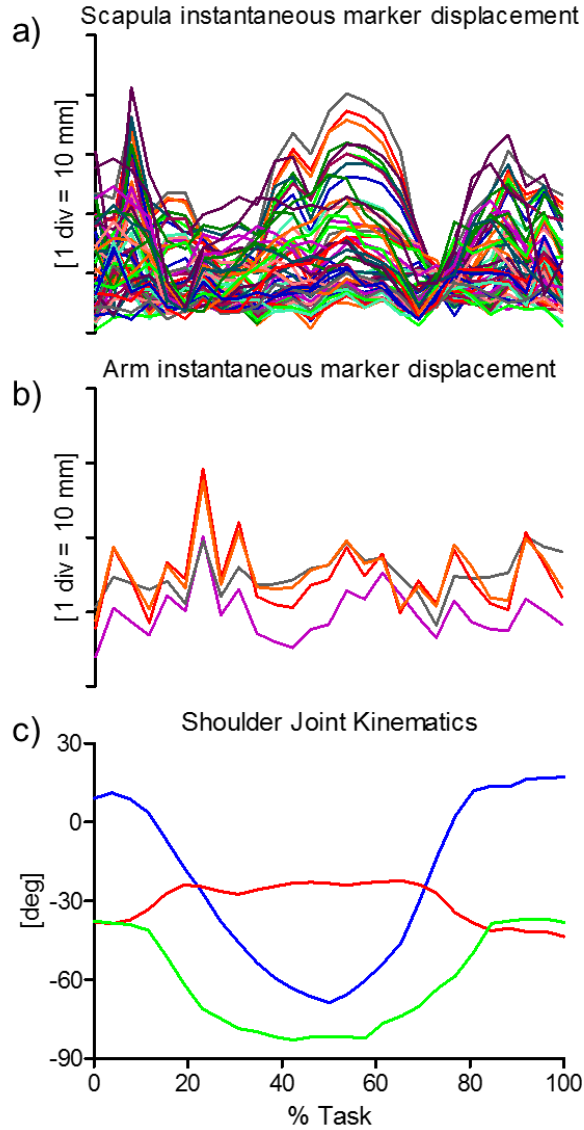


Figure 102 – ABDUCTION. Magnitude of the instantaneous displacement of the fifty-seven and four skin-markers glued on the scapula (a) and arm (b) represented in the relevant ACS. c) Relevant shoulder kinematics calculated using the $X_t Z_f' Y_h''$ sequence (Bonnefoy-Mazure et al., 2012): rotation around the X_t axis of the thorax corresponding to the shoulder elevation (blue); rotation around the floating Z_f' axis corresponding to the shoulder flexion/extension (red); rotation around the Y_h'' axis of the humerus corresponding to the shoulder axial rotation (green). Superior elevation, flexion and internal rotations are positive.

3. Data storing and exchange: the lexicon

3.1. Dataset description

Data were stored according to the same lexicon into Matlab structures, named datasets, each consisting of:

1. an *info* field, of type text, which contains general information concerning the experiment, the experimental set up, possible problems in the dataset, and on the subject/trial/task characteristics
2. several *subject* fields, one for each subject, containing specific subject information and numeric data

3.1.1. Dataset name

The dataset name has the following format:

dataset_provider name_motor task name

where:

provider name	indicates the institution owner of the data (see Table {owner})
motor task name	can assume one of the values listed in the Table {motortask}

Example:

dataset_FOROIT_hipFunct

3.1.2. Data information

The information listed below were included, when available, in the *info* field. These information are general to the dataset, specific problems relative to specific subjects are detailed at the subject level.

The following format was used:

contact person	person who acquired/organized the data
experiment day	day/month/year of original data acquisition
experiment location	location of original data acquisition

motor task description	details on the task under analysis (e.g. speed; tread and rise when step or seat are used; type of footwear, see relevant Table).
number of subjects	
number of trials per subject	
body segments	
number of markers per segment	indicating the number decided in the experiment design
marker location	a general description of the location (frontal, distal, etc)
reference data source	short details on how bone pose was determined (pin, fluoroscopy, sampling frequency of the reference data, etc.)
subject/specimen	stating if it was <i>in-vivo</i> or <i>ex-vivo</i>
anatomical coordinate system	definition adopted for each segment (to be brief reference to literature can be used)
measurement errors	if experiments were carried out to assess measurement errors, information on them is provided here.
data processing	if normalized data are provided as supplementary trials, information on normalization is provided here. Similarly, if interpolated data are provided to cope with occlusions, on interpolation is provided here.
sampling frequency	indicating the sampling frequency of the system providing the skin kinematics (sampling frequency of the reference data source are indicated along with other information on the relevant measurement system).

Example:

[dataset_FOROIT_hipFunct.info](#)

CONTACT PERSON: VALENTINA CAMOMILLA; EXPERIMENT DATE AND LOCATION: NIZZA 2006; MOTOR TASK DESCRIPTION: STAR-ARC MOVEMENT; NUMBER OF SUBJECTS: 1; NUMBER OF TRIALS PER SUBJECT: 1; TYPE OF SEGMENTS: RIGHT LOWER LIMB AND PELVIS; NUMBER OF MARKERS PER SEGMENT: 12 ON THE THIGH AND 4 ON THE SHANK; MARKER

LOCATION: THIGH AND SHANK ANTERIOR ASPECT; REFERENCE DATA SOURCE: PIN MARKERS;
EX-VIVO; ANATOMICAL COORDINATE SYSTEM DEFINITION ADOPTED FOR EACH SEGMENT:
CAPPozzo 1995 ET AL.

3.1.3. Measurement units

The default assumption for the units of measurement used to report data is the reported in the following section. Any difference with respect to this standard should be state in the *info* section of each dataset.

Time Unit s

Linear Kinematic Unit mm for lengths

Angular Kinematic Unit rad for angles

Mass Inertia Unit kg for body mass

3.2. Subject description

3.2.1. Subject name

The subject name has the following format:

subjNumber

where only the number can sequentially change. Each number is described by two characters (e.g., please specify 01 instead of 1). The root “subj” must be used for all subjects. Additional information on a possible subject identifier is to be included in the *info* field.

3.2.2. Subject information

The information listed below were included, when available, in the *info* field, to provide an identification for the subject in addition to basic anthropometric measures and age and sex. These information are general to the subject, specific problems relative to specific trials are detailed at the trial level.

The following format was used:

ref_code	is an string uniquely identifying the patient within the institution of the creator of the file
pathology	identifies a patient pathology, if any (see Table {pathology})
age	is the patient's age (in years) at the date of the experiment

sex	is the patient's gender (M or F)
body_mass	is the patient's body mass
stature	is the patient's stature
other	Other information. For example: anatomical measures available for the subject. Supplementary details if the patient wears a prosthesis or an orthosis.

Example:

```

dataset_FOROIT_hipFunct.subj01.info.ref_code
'2301'

dataset_FOROIT_hipFunct.subj01.info.pathology
'abled body'

dataset_FOROIT_hipFunct.subj01.info.age
6

dataset_FOROIT_hipFunct.subj01.info.sex
'M'

dataset_FOROIT_hipFunct.subj01.info.body_mass
70

dataset_FOROIT_hipFunct.subj01.info.stature
1750

dataset_FOROIT_hipFunct.subj01.info.other
'segment geometry: diameters of the proximal, median, and distal sections of the thigh  
are 161, 123, 105 mm, respectively'

```

3.2.3. Warning

A brief description of the experimental problems, if any, should be reported with reference to the trial numbers. Write "none" if the subject is complete.

Example:

```

dataset_FOROIT_hipFunct.subj03.warning
'For trial03, no markers are available for the shank.'

```

3.2.4. Subject data

The trials available for each specific subject are included in the subject field. For the posture trial, if available, use the number 00.

Example:

dataset_FOROIT_hipFunct.subj03.trial03

In the trial field, each body segment is reported separately and contains both time invariant and time variant data for the specific body segment (use names as in Table {segment}):

warning	A brief description of the experimental problems, if any, at the body segment level. Write "none" if data are complete. If there are missing fields, state it here.
mrk.Mxx	This field contains a set of subfields, one for each marker M01, M02, M03 etc. Marker coordinates are provided in the anatomical coordinate system (antero-posterior, x; superior-inferior, y; left-right, z). Data dimension for each marker: [Nx3]
(mrk_raw.Mxx)	Optional. This field contains a set of subfields, one for each marker M01, M02, M03 etc. When skin-marker trajectories presented gaps smaller than 0.35 s that were filled using a partial Procrustes superimposition approach (Grimpampi et al., 2014) or larger gaps that were not filled, original marker coordinates are also provided in this field. The latter coordinates are provided in the anatomical coordinate system (antero-posterior, x; superior-inferior, y; left-right, z). Data dimension for each raw marker: [Nx3]
ALs.ALnames	Anatomical landmarks named as in Cappozzo 1995/ISB convention reported in Table {anat_landmk} (antero-posterior, x; superior-inferior, y; right-left, z). Data dimension for each landmark: [3x1]
gRa	Rotation matrix of the segment anatomical coordinate system with respect to the global coordinate system. Each row contains

the 3x3-matrix element reported colon-wise for a given instant of time (r11, r12,r13,r21,r22,r23,...). Data dimension: [Nx9]

gta Translation vector of the anatomical coordinate system with respect to the global coordinate system. Each row contains the 3 vector elements reported colon-wise for a given instant of time (t11, t12,t13). Data dimension: [Nx3]

A supplementary field is also provided for each trial to store sample indices related to specific events useful, for example, to normalize data afterwards: for a gait task, it can be the foot strike events or the toe off. This information can be used to average or determine the variability of processed data.

evt.xxx The field contains subfields, each of them specific to a kind of event. There is no table with standardized event's name. Data dimension: [Mx1] where M is the number of time the event was detected.

Example:

dataset_FOROIT_hipFunct.subj01.trial03.L_thigh.warning

None

dataset_FOROIT_hipFunct.subj01.trial03.L_thigh.mrk

M01 [2423x3]

M02 [2423x3]

M03 [2423x3]

M04 [2423x3]

dataset_FOROIT_hipFunct.subj01.trial03.L_thigh.ALs

HJC [0 396.24 0]

LE [0 -2.44 59.80]

ME [1.64 2.44 -59.80]

dataset_FOROIT_hipFunct.subj01.trial03.L_thigh.gRa

[2423x9]

dataset_FOROIT_hipFunct.subj01.trial03.L_thigh.gta

[2423x3]

In case vast portions of the dataset were interpolated due to occlusion problems, raw data were stored using NaN as missed frame identifier. However, interpolated data can be stored as supplementary field in the subject data structure. Information on interpolation procedures must be stored in the data processing field of the data information.

Example:

dataset_FOROIT_hipFunct.subj01.trial03.L_thigh.gRa_int

[2423x9]

dataset_FOROIT_hipFunct.subj01.trial03.L_thigh.gta_int

[2423x3]

dataset_FOROIT_hipFunct.subj01.trial03.L_thigh.mrk_int

[2423x3]

3.3. Tables

Table {owner}

<i>Ecole Polytechnique Fédérale de Lausanne, Laboratory of Movement Analysis and Measurement</i>	LMAM
<i>Fondation Artanim</i>	ARTANIM
<i>National Taiwan University</i>	NTU
<i>Simulation et Modélisation du Mouvement</i>	S2M
<i>Università degli Studi di Roma "Foro Italico"</i>	FOROIT
<i>University of Bologna</i>	UNIBO
<i>University of Melbourne</i>	UNIMELB
<i>University of Ohio</i>	CSUOHIO
<i>University of Ottawa</i>	OTTAWA

Table {motortask}

<i>walking:</i>	walking
<i>cutting:</i>	cutting
<i>hopping:</i>	hopping
<i>treadmill walking:</i>	treadmillWalking
<i>step up & down:</i>	stepUp
<i>functional hip joint centre determination:</i>	hipFunct
<i>hip axial rotation:</i>	hipAxialRot
<i>hip and knee flexion & extension:</i>	hipKneeFlex
<i>knee extension against gravity:</i>	kneeAgainstGravity
<i>sit-to-stand:</i>	sit2stand
<i>knee flexion & extension:</i>	kneeFlex
<i>running:</i>	running
<i>arm adduction:</i>	armAdd
<i>arm abduction (scapular plane):</i>	armAbd
<i>arm flexion:</i>	armFlex
<i>arm extension:</i>	armExt
<i>hair combing:</i>	hairComb
<i>ball throwing:</i>	ballThrowing
<i>eating:</i>	eating
<i>punching:</i>	punching
<i>reach the back:</i>	behindBackReach
<i>functional gleno-humeral centre determination:</i>	glenoHumeralFunct

Table {footwear}

<i>barefoot:</i>	BF
<i>training shoes:</i>	TS
<i>other:</i>	OT

Table {pathology}

<i>able-bodied:</i>	AB
joint implant	
<i>hip:</i>	IH
<i>knee:</i>	IK
<i>ankle:</i>	IA
joint disease	
<i>hip:</i>	JH
<i>knee:</i>	JK
<i>ankle:</i>	JA
amputee	
<i>hip disarticulation:</i>	HD
<i>above-knee:</i>	AK
<i>through knee:</i>	TK
<i>below-knee:</i>	BK
<i>through ankle:</i>	TA
<i>foot:</i>	FO
<i>other:</i>	OT

Table {side}

<i>left:</i>	L
<i>irrelevant:</i>	I
<i>right:</i>	R

Table {segment}

<i>Thorax</i>	
<i>L_clavicle</i>	
<i>L_scapula</i>	
<i>L_humerus</i>	
<i>R_clavicle</i>	
<i>R_scapula</i>	
<i>R_humerus</i>	
<i>pelvis</i>	
<i>L_thigh</i>	
<i>L_shank</i>	
<i>L_foot</i>	
<i>R_thigh</i>	
<i>R_shank</i>	
<i>R_foot</i>	

Table {anat_landmk}

<i>Thorax</i>	
<i>incisura jugularis:</i>	IJ

<i>xiphoid process:</i>	PX
<i>spinous process of the 8th thoracic vertebra:</i>	T8
<i>spinous process of the 7th cervical vertebra:</i>	C7
<i>sternal notch:</i>	SN
Clavicle	
<i>sternal extremity of the clavicle:</i>	SC
<i>acromial extremity of the clavicle:</i>	AC
Scapula	
<i>angulus inferior:</i>	AI
<i>trigonum spinae:</i>	TS
<i>angulus acromialis:</i>	AA
Humerus	
<i>glenohumeral joint centre:</i>	GHC
<i>lateral epicondyle of the humerus:</i>	EL
<i>medial epicondyle of the humerus:</i>	EM
Pelvis	
<i>right anterior superior iliac spine:</i>	RASIS
<i>left anterior superior iliac spine:</i>	LASIS
<i>right posterior superior iliac spine:</i>	RPSIS
<i>left posterior superior iliac spine:</i>	LPSIS
Femur	
<i>centre of the femoral head:</i>	FH
<i>greater trochanter external surface:</i>	GT
<i>medial epicondyle:</i>	ME
<i>lateral epicondyle:</i>	LE
<i>antero-lateral apex of the patellar surface ridge:</i>	LP
<i>antero-medial apex of the patellar surface ridge:</i>	MP
<i>adductor tubercle:</i>	AT
<i>most distal point of the lateral condyle:</i>	LC
<i>most distal point of the medial condyle:</i>	MC
TibiaFibula	
<i>prominence of the tibial tuberosity:</i>	TT
<i>apex of head of the fibula:</i>	HF
<i>most medial ridge of the medial tibial plateau:</i>	MR
<i>most lateral ridge of the medial lateral plateau:</i>	LR
<i>Gerdy's tubercle:</i>	YT
<i>distal apex of the medial malleolus:</i>	MM
<i>distal apex of the lateral malleolus:</i>	LM
Foot	
<i>upper ridge of the calcaneus posterior surface:</i>	CA
<i>sustentaculum tali:</i>	ST

<i>tuberosity of navicular bone:</i>	TN
<i>dorsal aspect of first metatarsal head:</i>	FM
<i>dorsal aspect of second metatarsal head:</i>	SM
<i>dorsal aspect of fifth metatarsal head:</i>	VM
<i>tuberosity of fifth metatarsal bone:</i>	VT
<i>peroneal trochlea:</i>	PT

4. MATLAB code example

4.1. Main script

```
% -----
%% Reference:
% Cereatti et al. (2017). Standardization proposal of soft tissue artefact
% description and data exchange for data sharing in
% human motion measurements. To be published
%
% Grimpampi et al. (2014). Metrics for describing soft-tissue artefact and
% its effect on pose, size, and shape of marker
% clusters. IEEE Trans. Biomed. Eng. 61, 362-367.
%
%%
%
% Version: 1.1
% Tecla Bonci
% Life and Health Sciences, Aston University, Birmingham, UK
%
% Interuniversity Centre of Bioengineering of the Human
Neuromusculoskeletal
% system, University of Rome "Foro Italico", Rome, Italy
%
% 2016 Dec 29
% -----
```

```
clear all
close all
clc

% select the dataSample_*.mat of interest
[a,b] = uigetfile ('*.mat');
data = load([b,a]);
dataSample = fieldnames(data);
disp(strcat('Load data: ',dataSample))
Seg = fieldnames(data.(dataSample{1}).subj01.trial01);

%% 3D Skin marker trajectories - ACS and ALs - PLOTS
t = [0 0 0]';
R = eye(3);
scale = 100; % scale factor for the axes dimension
linewidth = 2;

% A graph is created for each segment in the structure
for seg = 1:size(Seg,1)

    % Skin-marker trajectories in the ACS
    % Check that mrk coordinates are available
    check =
strcmp(fieldnames(data.(dataSample{1}).subj01.trial01.(Seg{seg})), 'mrk');
    if find(check)
        figure('Name',strcat((Seg{seg}),' mrk + ALs -
ARF'), 'NumberTitle','off')
        set3Dview
        hold on
        mrk =
fieldnames(data.(dataSample{1}).subj01.trial01.(Seg{seg}).mrk);
```

```

    for i =1:size(mrk,1)
        hold on
        mrkNow =
data.(dataSample{1}).subj01.trial01.(Seg{seg}).mrk.(mrk{i});
        plot3d_tb(mrkNow,'b',5)
    end
end

% ACS
my3Dplot(t,R,scale,linewidth)

% Check that AL coordinates are available
check =
strcmp(fieldnames(data.(dataSample{1}).subj01.trial01.(Seg{seg})), 'ALs');
if find(check)
    mrk =
fieldnames(data.(dataSample{1}).subj01.trial01.(Seg{seg}).ALs);
    for i =1:size(mrk,1)
        mrkNow =
data.(dataSample{1}).subj01.trial01.(Seg{seg}).ALs.(mrk{i});
        plot3d_tb(mrkNow,'.k',30)
        text(mrkNow(1,1),mrkNow(2,1),mrkNow(3,1),...
            strcat('\leftarrow -',(mrk{i})), 'FontSize',10)
    end
end
axis equal
end

%% STA Parameters for each segment calculated as detailed in the manuscript
for seg = 1:size(Seg,1)
    check =
strcmp(fieldnames(data.(dataSample{1}).subj01.trial01.(Seg{seg})), 'mrk');
    if find(check)
        mrk =
fieldnames(data.(dataSample{1}).subj01.trial01.(Seg{seg}).mrk);
        [rmsd, deltap, d] =
STA_Parameters(data.(dataSample{1}).subj01.trial01.(Seg{seg}).mrk,mrk');

        figure('Name',strcat('rms(d) and delta p - '
',(Seg{seg})), 'NumberTitle', 'off')
        subplot(121)
        boxplot([rmsd.mod,rmsd.x, rmsd.y, rmsd.z],
'Labels',{'rms(d)', 'rms(d_x)', 'rms(d_y)', 'rms(d_z)'})
        title('rms(d)', 'fontWeight','bold', 'FontSize', 14);
        ylabel('[mm]', 'FontSize', 12);

        subplot(122)
        boxplot([deltap.max, deltap.x, deltap.y,
deltap.z], 'Labels',{'deltap_max','deltap_x','deltap_y','deltap_z'})
        title('delta p', 'fontWeight','bold', 'FontSize', 14);
        ylabel('[mm]', 'FontSize', 12);

        figure('Name', 'Instantaneous displacement
vector', 'NumberTitle', 'off')
        title(strcat('Instantaneous displacement vector -
',(Seg{seg})), 'fontWeight','bold', 'FontSize', 14);
        set3Dview
        hold on
        mrk = fieldnames(d);

```

```

cc = hsv(size(mrk,1));
for i =1:size(mrk,1)
    hold on
    plot3(d.(mrk{i}) (:,1),d.(mrk{i}) (:,2),d.(mrk{i}) (:,3), '-',
'MarkerSize',2,'color',cc(i,:))

end
xlabel('x [mm]')
ylabel('y [mm]')
zlabel('z [mm]')
end

```

4.2. Functions

```

% -----
%% STA Parameters for each segment calculated as detailed in the Cereatti
et al.(2017)
% INPUT
%      STA (Structure)      Skin-marker trajectories (M01, M02,...)
represented in the relevant ACS
%                           Each marker trajectory is [nx3]
%      mrk (3x3)           Name of the skin-markers
%
% OUTPUT
%      d                  Instantaneous displacement vector
%      rmsd               Root mean square amplitude (rmsd.mod) and its
%                           components (rmsd.x, rmsd.y, rmsd.z)
%      deltap             Peak-to-peak amplitude, maximum value (deltap.max)
%                           and relevant components (deltap.x, deltap.y,
deltap.z)
% -----
%%

function [rmsd, deltap, d] = STA_Parameters(STA, mrk)

for j = 1:size(mrk,2)
STAnow = STA.(mrk{j});
n = size(STAnow,1);
for k = 1:n
    STAvect (k,:) = STAnow(k,:);
    STAvectx (k,1) = STAnow(k,1);
    STAvecty (k,1) = STAnow(k,2);
    STAvectz (k,1) = STAnow(k,3);
end

pmeanx = mean(STAvectx);
pmeany = mean(STAvecty);
pmeanz = mean(STAvectz);

for k = 1:n
D(k,1) = norm(STAvect(k,:) - mean(STAnow));
d.(mrk{j})(k,:) = STA vect(k,:) - mean(STAnow);

dx(k,1) = STA vectx(k,1) - pmeanx;
dy(k,1) = STA vecty(k,1) - pmeany;

```

```

dz(k,1) = STAveclz(k,1) - pmeanz;
end

rmsd.mod(j,1) = rms(D);
rmsd.x(j,1) = rms(dx);
rmsd.y(j,1) = rms(dy);
rmsd.z(j,1) = rms(dz);

% Deltap max
P = STAnow;
[M N] = size(P); % Number of points and number of dimensions

% METHOD 1 (quick, without loops)

if M < 500
    % Distances between pairs of points
    P = shiftdim(P, -1); % (1×M×N)
    P2 = reshape(P, [M 1 N]); % (M×1×N)
    dd = bsxfun(@minus, P, P2); % Distance vectors (M×M×N)
    dd = magn(dd, 3); % Scalar distances (M×M)

    % Row and column containing maximum value in DD
    [dd, rows] = max(dd); % (1×M)
    [Deltap, column] = max(dd); % (1×1)

% METHOD 2 (slower, but requires a much smaller amount of memory)
else
    dd = zeros(M-1, 1);
    ii2 = zeros(M-1, 1);
    for i = 1 : (M-1)
        next = (i+1) : M;
        Deltap = bsxfun(@minus, P(i,:), P(next,:)); % Distances (M-i1×N)
        Deltap = magn(Deltap, 2); % Scalar distances (M-i1×1)
        [dd(i), j] = max(Deltap);
        ii2(i) = i + j;
    end

    [Deltap, i1] = max(dd);
end

deltap.max(j,1) = Deltap;

deltap.x(j,1) = (max(STAnow(:,1))- min(STAnow(:,1)));
deltap.y(j,1) = (max(STAnow(:,2))- min(STAnow(:,2)));
deltap.z(j,1) = (max(STAnow(:,3))- min(STAnow(:,3)));
end

```

```

% -----
%% Plotting 3-D reference frame axes defined by t and R
%   t (3x1)          Origin position
%   R (3x3)          Orientation of the axes (each column of the
%                     matrix represents an axis)
%   scale (1x1)       Scale factor for axes dimension
%
% The axes are plotted using the following convention:
%   x-axis --> red line
%   y-axis --> green line
%   z-axis --> blue line
% -----
%%
function my3Dplot(t,R,scale,linewidth)
e = t*ones(1,3)+scale*R;

    plot3([t(1),e(1,1)], [t(2),e(2,1)], [t(3),e(3,1)], 'r-
', 'Linewidth', linewidth);
    plot3([t(1),e(1,2)], [t(2),e(2,2)], [t(3),e(3,2)], 'g-
', 'Linewidth', linewidth);
    plot3([t(1),e(1,3)], [t(2),e(2,3)], [t(3),e(3,3)], 'b-
', 'Linewidth', linewidth);
end

```

References

- Abdel-Aziz, Y.I., Karara, H.M., 1971. Direct linear transformation from comparator coordinates into object space coordinates in close range photogrammetry. In ASP Symp. Close Range Photogrammetry, pp. 1-19. American Society of Photogrammetry, Falls Church.
- Akbarshahi, M., Schache, A.G., Fernandez, J.W., Baker, R., Banks, S., Pandy, M.G., 2010. Non-invasive assessment of soft-tissue artifact and its effect on knee joint kinematics during functional activity. *J Biomech* 43, 1292–301.
- Andersen, M.S., Damsgaard, M., Rasmussen, J., Ramsey, D.K., Benoit, D.L., 2012. A linear soft tissue artefact model for human movement analysis: proof of concept using in vivo data. *Gait Posture* 35, 606-11.
- Baltzopoulos, V., 1995. A video fluoroscopy method for optical distortion correction and measurement of knee-joint kinematics, *Clin Biomech* 10, 85–92.
- Banks, S.A., Hodge, W.A., 1996. Accurate measurement of three dimensional knee replacement kinematics using single-plane fluoroscopy. *IEEE Trans. Biomed. Eng.* 43, 638–649.
- Barré, A., Thiran, J.-P., Jolles, B.M., Theumann, N., Aminian, K., 2013. Soft tissue artifact assessment during treadmill walking in subjects with total knee arthroplasty. *IEEE Trans Biomed Eng* 60, 3131–3140.
- Barré A., Jolles B.M., Theumann N., Aminian, K., 2015. Soft tissue artifact distribution on lower limbs during treadmill gait: Influence of skin markers' location on cluster design. *J Biomech* 48, 1965-71.
- Begon, M., Monnet, T., Lacouture, P., 2007. Effects of movement for estimating the hip joint centre. *Gait Posture* 25, 353-359.
- Benoit, D.L., Ramsey, D.K., Lamontagne, M., Xu, L., Wretenberg, P., Renström, P., 2006. Effect of skin movement artifact on knee kinematics during gait and cutting motions measured in vivo. *Gait Posture*. 24, 152-64.
- Besl, P.J., McKay, H.D., 1992. A method for registration of 3-D shapes. *IEEE Trans PAMI* 14, 239–256.
- Bonci, T., Camomilla, V., Dumas, R., Chèze, L., & Cappozzo, A., 2014. A soft tissue artefact model driven by proximal and distal joint kinematics. *J Biomech* 47(10), 2354-2361.

Bonnefoy-Mazure, A., Slawinski, J., Riquet, A., Lévèque, J. M., Miller, C., & Cheze, L., 2010. Rotation sequence is an important factor in shoulder kinematics. Application to the elite players' flat serves. *J Biomech*, 43(10), 2022-2025.

Cappozzo, A., Della Croce, U., Catani F, Leardini, A., 1994a. Anatomical Frame Definition and Determination. CAMARC II Internal Report.

Charbonnier, C., Chagué, S., Kolo, F.C., Chow, J.C.K., Lädermann, A., 2014. A patient-specific measurement technique to model shoulder joint kinematics. *Orthop Traumatol Surg Res* 100, 715–719.

Dal Maso, F., Raison, M., Lundberg, A., Arndt, A., Begon, M., 2014. Coupling between 3D displacements and rotations at the glenohumeral joint during dynamic tasks in healthy participants. *Clin Biomech* 29, 1048–55.

Dal Maso F., Blache Y., Raison M., Lundberg A., Begon, M., 2016. Glenohumeral joint kinematics measured by intracortical pins, reflective markers, and computed tomography: A novel technique to assess acromiohumeral distance. *J Electromyog Kinesiol* 29, 4-1

Della Croce, U., Cappozzo, A., 2000. A spot check for estimating stereophotogrammetric errors. *Med. Biol. Eng. Comput.* 38, 260-266.

Eckhoff, D.G., Bach, J.M., Spitzer, V.M., Reinig, K.D., Bagur, M.M., Baldini, T.H., Flannery, N.M.P., 2005. Three-dimensional mechanics, kinematics, and morphology of the knee viewed in virtual reality. *J Bone Joint Surg.* 87, 71–80.

Gronenschild, E., 1997. The accuracy and reproducibility of a global method to correct for geometric image distortion in the X-ray imaging chain. *Med Phys* 24, 1875–1888.

Hatze, H., 1988. High-precision three-dimensional photogrammetric calibration and object space reconstruction using a modified DLT approach. *J. Biomech* 21, 533-538.

Lu, T.W., Tsai, T.Y., Kuo, M.Y., Hsu, H.C., Chen, H.L., 2008. In vivo three-dimensional kinematics of the normal knee during active extension under unloaded and loaded conditions using single-plane fluoroscopy. *Med Eng Phys* 30, 1004–1012.

Miranda, D.L., Rainbow, M.J., Leventhal, E.L., Crisco, J.J., Fleming, B.C., 2010. Automatic determination of anatomical coordinate systems for three-dimensional bone models of the isolated human knee. *J Biomech* 43, 1623-6.

Moro-oka, T.A., Hamai, S., Miura, H., Shimoto, T., Higaki, H., Fregly, B.J., Iwamoto, Y., Banks, S.A., 2007. Can magnetic resonance imaging-derived bone models be used for accurate motion measurement with single-plane three-dimensional shape registration. *J Ortho Res* 25, 867–72.

Paul, J.P., 1992. Terminology and Units. Deliverable n. 4, C.E.C. Program AIM, Project A-2002, CAMARC-II.

Penney, G.P., Weese, J., Little, J.A., Desmedt, P., Hill, D.L.G., Hawkes, D.J. 1998. A comparison of similarity measures for use in 2D–3D medical image registration, IEEE T Med Imaging, 17, 586–595.

Ramsey, D.K., Wretenberg, P.F., Benoit, D.L., Lamontagne, M., Nemeth, G., 2003. Methodological concerns using intra-cortical pins to measure tibiofemoral kinematics. Knee Surg Sport Tr A 11, 344–9.

Soderkvist, I. and Wedin, P.A., 1993. Determining the movements of the skeleton using well-configured markers. J. Biomech 26, 1473-1477.

Winter, D.A., 1990. Biomechanics and Motor Control of Human Movement. J. Wiley, New York.

Wood, G.A. and Marshall, R.N., 1986. The accuracy of DLT extrapolation in three-dimensional film analysis. J. Biomech 9, 781-785.

Wu, G., van der Helm, F.C.T., Veeger, H.E.J., Makhsous, M., Van Roy, P., Anglin, C., Nagels, J., Karduna, A.R., McQuade, K., Wang, X., Wernerl, F.W., Buchholz, B., 2005. ISB recommendation on definitions of joint coordinate systems of various joints for the reporting of human joint motion—Part II: shoulder, elbow, wrist and hand. J. Biomech 38, 981–992